SELECTED APPLICATIONS OF OPTOACOUSTIC SPECTROMETRY TO THE EXAMINATION OF SOLIDS

by

KANISSERIL RADHAKRISHNA MENON M.Sc(Lond) C.Chem., MRIC, AIFST

A thesis submitted for the Degree of
DOCTOR OF PHILOSOPHY
of the University of London

Department of Chemistry
Imperial College of Science & Technology
London SW7 2AY

ABSTRACT

Studies of laser mirrors have been made which relate the spectra obtained using optoacoustic spectroscopy to those obtained using conventional absorption, transmission and reflectance spectroscopic techniques. The use of optoacoustic spectroscopy as a calorimetric technique is described. Scattering phenomena occurring when highly reflective samples are examined have been investigated by studying some photochromic materials.

Theoretical predictions made by Rosencwaig and Gersho for the cases of optically opaque, thermally thin and optically opaque, thermally thick samples have been demonstrated experimentally by making studies of polymer film samples.

A preliminary investigation of the effect of particle size of the sample upon the magnitude of the optoacoustic signal has been made.

Quantitative results are reported for the determination of moisture in single cell protein and for the presence of polyvinylacetate in vinylchloride/vinylacetate copolymer. The results obtained employing optoacoustic spectroscopy have been compared with the results obtained using the alternative techniques of wide-line nuclear magnetic resonance spectroscopy and diffuse reflectance spectroscopy.

The application of optoacoustic spectroscopy to a number of different sample types is described.

CONTENTS

ACKNOWLEDGEMENTS

The work in this thesis was carried out in the Chemistry Department of the Imperial College of Science and Technology between October 1977 and September 1979. It is entirely original, except where due reference is made and no part has been submitted for any other degree.

I wish to express my thanks to my supervisor, Dr G.F. Kirkbright, for providing me with the opportunity to conduct this work and for the help and encouragement during the course.

I also wish to thank Dr M.J. Adams (1977-1978) and Dr S.L. Castleden (1978-1979) who were my immediate supervisors for their invaluable help and guidance throughout my research and preparation of this thesis.

I wish to express my gratitude to the Science Research Council and Imperial Chemical Industries Ltd. for their financial support, during the SRC/CASE Studentship.

Gratitude is also expressed to Dr J.K. Becconsall my industrial supervisor and Dr H.A. Willis and other staff in the Spectroscopy Department of ICI at Welwyn Garden City for their help rendered during my industrial project.

Acknowledgement is due to my colleagues in the Analytical Section : Mr J.G. Highfield, Dr B.C. Beadle, Dr R.D. Snook, Mr D.E.M. Spillane, Mrs C.M. Ashworth and Mr P.K.P. Drew for their help and discussions. My thanks also to Miss T. Richardson for her patience in typing this thesis.

Last, but not least, I would like to thank my wife Ganga for her enormous encouragement, to my children for their endurance in my preoccupation and also my brothers and sisters for their long distance support.

K.R. Menon

DEDICATION

To my parents
Ram and Janaki

CHAPTER ONE

INTRODUCTION

1.1 OPTICAL SPECTROSCOPY

The science concerned with the propagation and interaction of electromagnetic radiation with matter is termed spectroscopy [1]. Spectroscopic techniques are important for providing information concerning the identity, structure and environment of atoms and molecules by the analysis of the radiation emitted or absorbed by these species.

The history of spectroscopy dates back to the early eighteenth century when Sir Isaac Newton [2] first demonstrated the optical principles necessary for spectroscopic studies. However, spectroscopy did not emerge as a systematic science until the middle of the nineteenth century with the work of Kirchhoff and Bunsen [3,4,5] who defined the principles of spectral analysis and demonstrated that each element exhibits its own characteristic pattern of spectral emission lines which can be used for the identification of the elements. During the nineteenth century knowledge of the electromagnetic spectrum was extended beyond the visible region to encompass the infrared and ultraviolet regions.

The various spectral regions of the electromagnetic spectrum together with their physical phenomena are displayed in Figure 1.1 [6].

Whilst the total energy spectrum of electromagnetic radiation may be employed for spectroscopic studies, the term optical spectroscopy is usually reserved for those spectral regions for which conventional optical

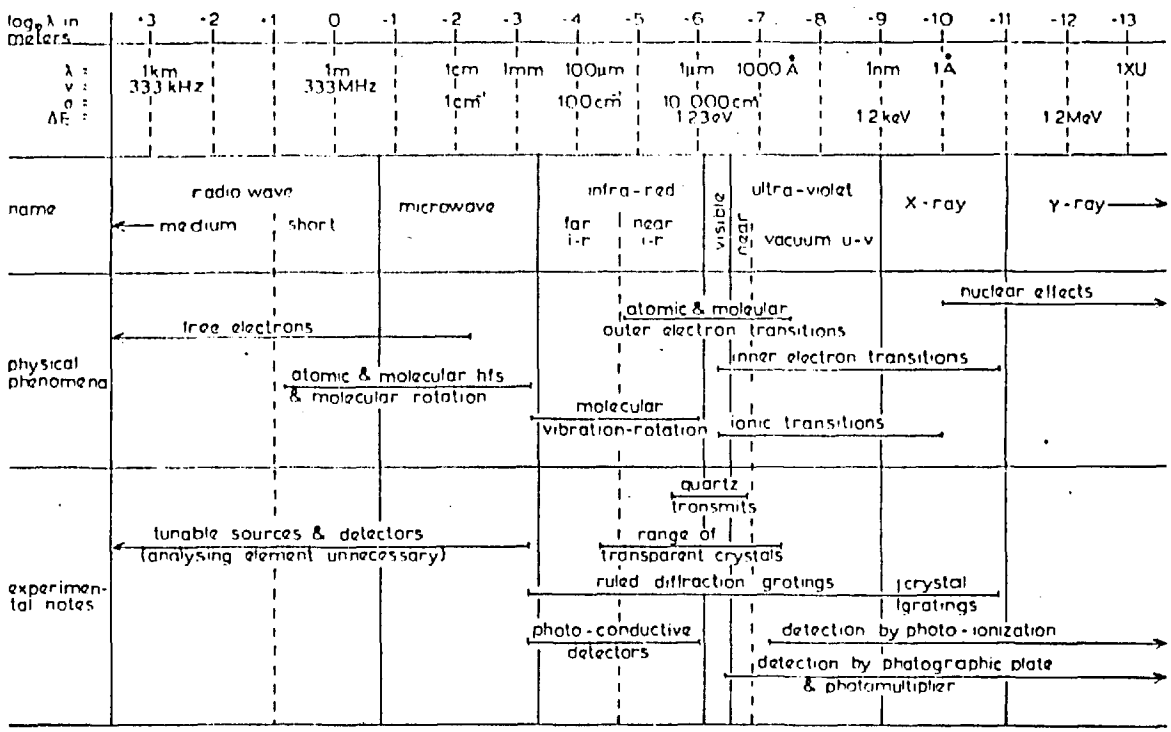

Figure 1.1: The electromagnetic spectrum [6]

materials may be employed to disperse and refract the radiation. In terms of wavelength, therefore, the optical spectral region may be considered as ranging from ca 100 nm in the vacuum ultraviolet to wavelengths of several hundred μm in the far infrared region.

The practical work described in this thesis relates primarily to the relatively small wavelength region of the electromagnetic spectrum from ca. 250 nm to 2.5 μm (the ultraviolet, visible and near-infrared regions).

1.2 ABSORPTION OF OPTICAL RADIATION

1.2.1 Introduction:

The absorption of electromagnetic radiation by a molecular system is complex [7]. The total energy of a molecule is the sum total of electronic, rotational and vibrational energies. For each energy state of the molecule, there are normally several possible vibrational states and for each vibrational state in turn there exist numerous rotational states. Hence the number of possible energy levels that electrons in a molecule may occupy is generally larger than that for an atom. Electronic transitions may be induced by the absorption of highly energetic photons of ultraviolet or visible radiation, vibrational transitions by the lower energy radiation of the middle infrared region whereas rotational transitions require much less energy e.g. wavelengths in the range 10 to 10,000 μm. Changes in the vibrational and rotational levels usually accompany the electronic excitation of a molecule.

A molecule may be excited from any of the vibrational and rotational levels in the ground state to any of a large number of possible vibrational and rotational levels in a given excited state. Because a photon of slightly different energy corresponds to each of the many possible transitions, UV and visible molecular absorption spectra appear usually as broad absorption bands, in contrast to the sharp line structures that characterise atomic spectra. Figure 1.2 depicts the idealised molecular energy levels of electronic, vibrational and rotational transitions.

1.2.2 Absorption Spectroscopy

Molecular absorption spectroscopy has widespread applications to qualitative and quantitative techniques of analysis. The energy (or wavelength) of the absorption provides information concerning the nature of the substance and the magnitude of the absorption provides information about the amount of the substance present in the sample under study. When a beam of radiation is passed through an absorbing substance, the absorbed energy is measured usually by detecting the transmitted radiation i.e. that portion of the incident radiation which is not absorbed by the sample. The principles and laws that govern the absorption of radiation apply for all wavelengths from the x-ray region to the radio frequency range. The law that governs quantitative absorption studies is known as the Beer-Lambert or more commonly as Beer's law.[8]

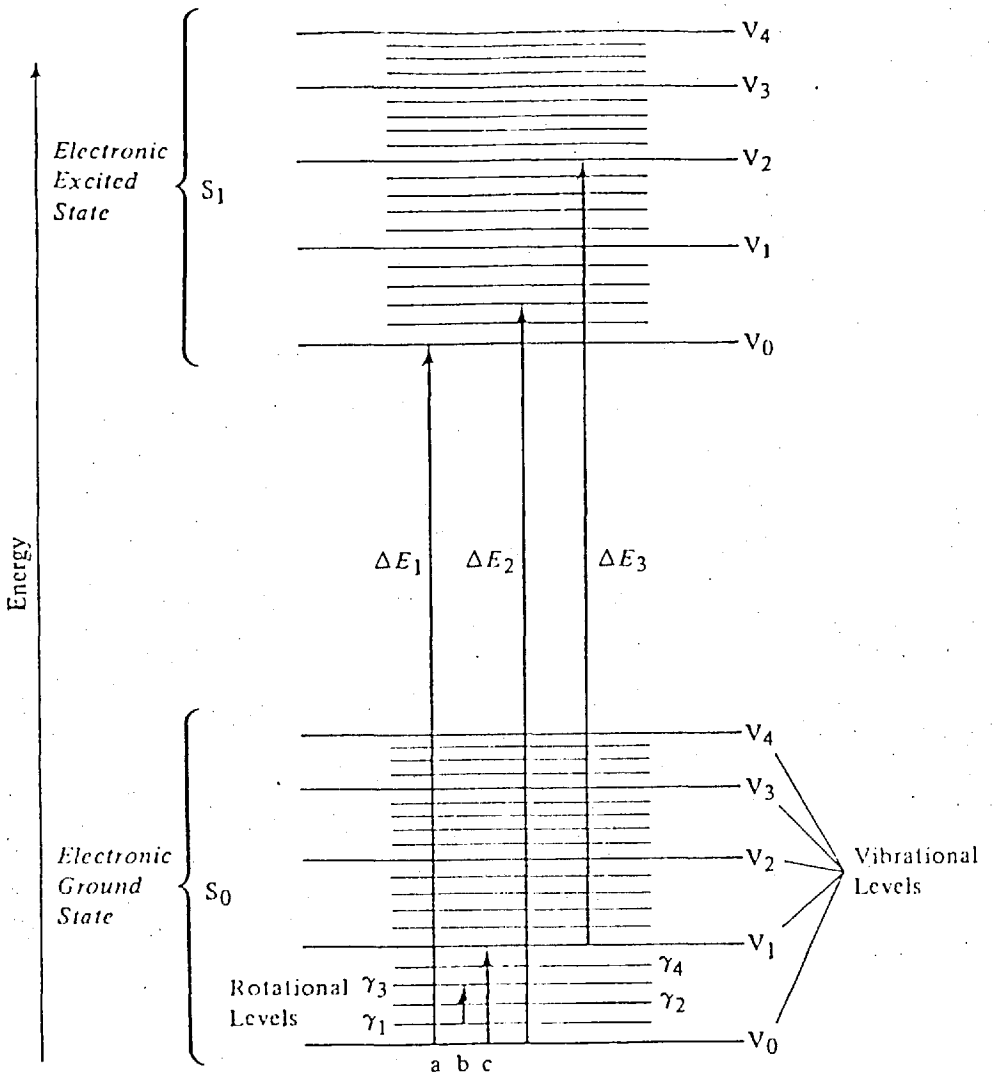

Figure 1.2: Molecular energy levels and (a) electronic, (b) rotational, and (c) vibrational transitions 7

Beer's law

When monochromatic radiation passes through a sample containing an absorbing species, the intensity of the radiation is progressively decreased as more of the energy is absorbed by the particles of that specie . The decrease in the intensity of the incident radiation depends upon the concentration of the absorber and the path length traversed by the radiation. This relationship is expressed by Beer's law.

Let I_o be the intensity of the radiation incident upon a section of the solution that contains c moles of an absorbing substance per unit volume. Let I be the intensity of the transmitted radiation after it has passed through a thickness ℓ of the solution. Beer's law relates the quantities as follows:

$$\log_{10} \frac{I_o}{I} = \varepsilon \ell c \qquad (1.1)$$

where $\log_{10} \frac{I_o}{I}$ is the absorbance and ε the molar absorptivity. Beer's law states that a plot of absorbance versus concentration should be linear. Deviation from Beer's law may be due to instrumental or chemical factors [9]. Instrumental factors includes instability of the radiation source, non-linear response of the detector-amplifier system and the incident radiation being polychromatic. Chemical factors are often due to effects such as dissociation, association, complex formation, polymerization or solvolysis of the solute. Instrumental factors can be studied by plotting absorbance versus cell path

length at a constant absorbant concentration; this plot will be linear if the instrument is working satisfactorily. The variation arising from chemical factors may be observed by changing the concentration of the analyte in solution and keeping the path length constant.

Figure 1.3 shows a diagram of a typical molecular UV, visible and infrared Absorption/Transmission spectrometer.

Transmission measurements become unsuitable for opaque samples, for compounds which dissolve only with difficulty or which react with solvents on dissolution. Such samples can be examined by the technique of reflectance spectroscopy.

1.2.3 Reflectance Spectroscopy

Reflectance spectroscopy is a useful analytical technique which is complementary with the more established techniques of transmission spectroscopy.

In reflectance spectroscopy the radiant intensity reflected from the surface of the sample is monitored. This data is converted to the reflectance, R, using the equations

$$R = \frac{I}{I_o} \qquad (1.2)$$

where I = the intensity of reflected radiation

I_o = the intensity of radiation reflected from standard reflectance surface.

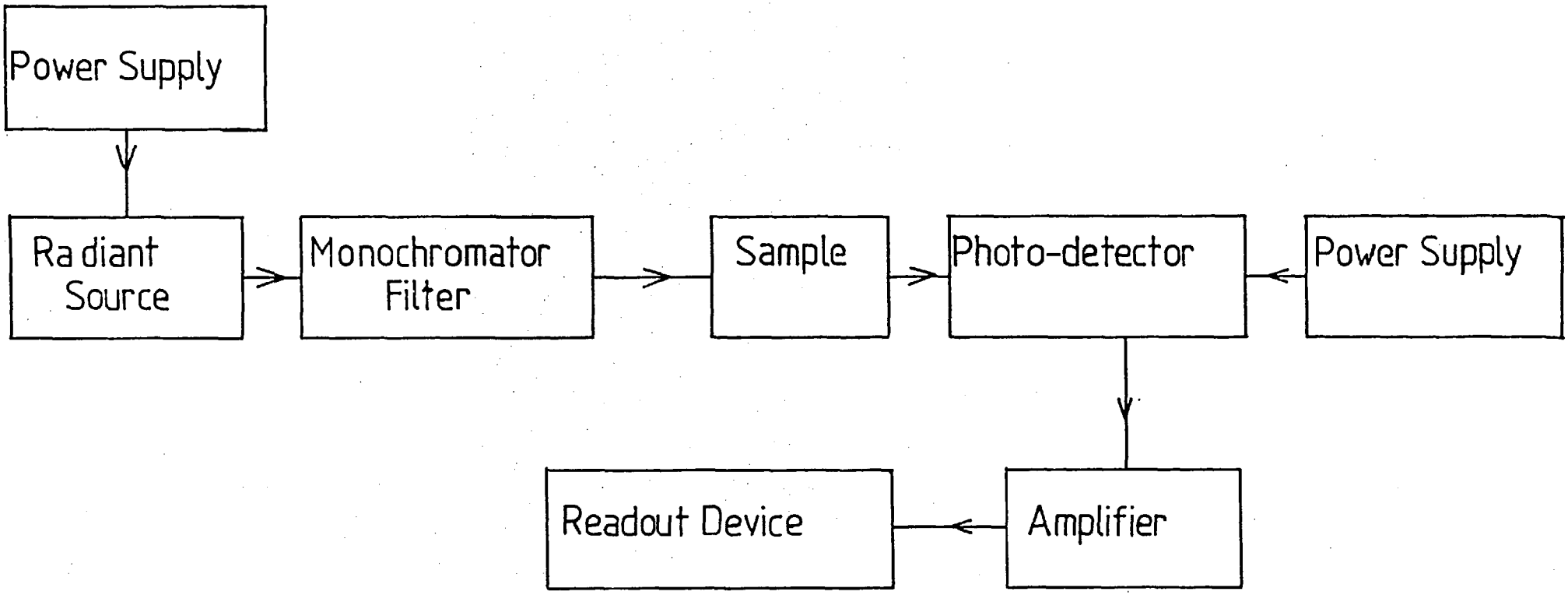

Fig.1.3. The essential components of an absorption/transmission spectrometer.

The reflected radiation from the sample may be considered as comprising of two components resulting from the specular (or regular) reflectance and diffuse reflectance.

In 1961 [10] specular reflectance spectroscopy, also known as internal reflectance or attenuated total reflectance spectroscopy, emerged as an analytical technique of great potential. Specular refers to the mirror-like reflections which occur when incident light is reflected back from a surface. In this case the angles of reflection are well defined and the process is governed by the Fresnel equation [11]:

$$R \equiv \frac{I}{I_o} = \frac{(n-1)^2+n^2\beta^2}{(n+1)^2+n^2\beta^2} \qquad (1.3)$$

where R = specular reflectance
I = reflected radiation intensity
I_o = the intensity of radiation reflected from standard reflecting surface
β = the absorption coefficient
n = refractive index

Diffuse reflectance measurements are employed in most currently available commercial instruments for the study of textiles, paints, plastics, foods, etc. The technique is also used for the examination of absorbed species and surface effects.

Diffuse reflectance is the result of reflected radiant energy that has been partially absorbed and partially scattered by a surface with the angle of reflection being undefined. Initial attempts to use diffuse reflectance spectroscopy as a quantitative

technique date back to 1920 [12,13] and this technique has since become widely employed. The most generally accepted theory of diffuse reflectance is due to Kubelka & Munk [14].

For the case of diffuse reflectance from infinitely thick layers the theory proposes

$$F(R_\infty) = \frac{(1-R_\infty)^2}{2R_\infty} = \beta/s \qquad (1.4)$$

where $F(R_\infty)$ is the Kubelka-Munk function, R_∞ is the absolute reflectance, which is obtained against a standard such as MgO or $BaSO_4$, β is the absorption coefficient and s is the scattering coefficient.

When the reflectance of a sample diluted with a non or low-absorbing powder is measured against the pure powder, the absorption coefficient k may be replaced by the product $2.303_\varepsilon c$ where ε is the molar absorptivity and c is the molar concentration [14]. The Kubelka-Munk equation can be written as,

$$F(R_\infty) = \frac{(1-R_\infty)^2}{2R_\infty} = \frac{c}{k'} \qquad (1.5)$$

where k' is a constant equal to $s/2.303_\varepsilon$. At high enough dilutions, the specular reflection from the sample approximates to that from the standard and is thus cancelled out in any comparison measurement.

A straight-line relationship between $F(R_\infty)$ and c is predicted, however, in practice this is only observed when with weakly absorbing substances are studied and the particle size of the powder sample is restricted to ca 1 μm in diameter. This relation is clearly analogous to

the Beer-Lambert law of absorption spectrophotometry. The non-linear relationship arising between $F(R_\infty)$ and c has been discussed by Kortüm [15].

The measurements of reflectance involves basically the same principles involved in making transmission measurements. The reduction in intensity of radiation reflected by the sample being examined is measured in relation to the intensity reflected by a standard. Figure 1.4 is a diagram of the optical arrangement of a basic instrument, the Beckman DK-A spectroreflectometer [16], which may be used for making diffuse reflectance measurements. The optical diagram indicates the path followed by the radiation as it passes from the tungsten lamp source through the monochromator, into the integrating sphere and alternately on to the sample and reference surfaces from which it is reflected to the sphere walls. The walls reflect the radiation back and forth until it reaches the detector. Before analysing a sample, zero and 100% reflectance are set with magnesium oxide or an alternative appropriate secondary standard at the exit ports.

1.2.4 Luminescence Spectroscopy

The photoluminescent methods of fluorescence and phosphorescence are closely related to molecular absorption spectrophotometry; when a molecule absorbs a photon an electron is raised from a low energy state (ground state) to a higher energy state (excited state). On the electron relaxing and returning to a lower energy state the

1. oscillating mirror
2. sample beam mirror
3. reference beam mirror
4. integrating sphere
5. entrance ports
6. exit ports (sample and reference materials are placed here for reflectance)
7. integrating sphere opening.
8. detector.

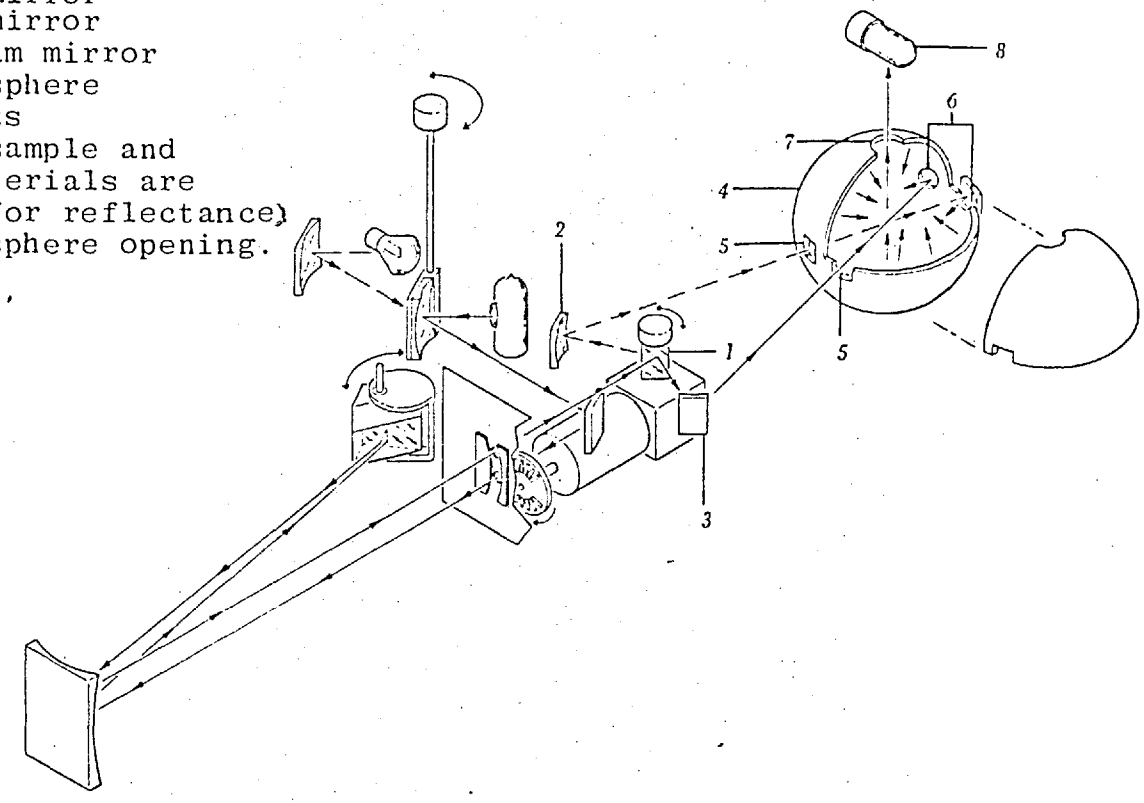

Figure 1.4: Schematic diagram of a diffuse reflectance spectrophotometer [16]

molecule may re-emit a fraction of the previously absorbed radiative energy as a quantum of lower energy. This process constitutes the mechanism describing the phenomena of luminescence and such processes are known to occur in solids, liquids and gases [17].

Many workers [18,19] have described the theoretical and experimental aspects of fluorescence and phosphorescence spectroscopy. The process of absorption and subsequent re-emission of energy is described by reference to Figure 1.5. [20] Upon absorbing the radiant energy, the molecule is raised from a vibrational level in the ground state to one of many vibrational levels in one of the excited electronic levels, usually the first excited singlet state S_1. The absorption step occurs with ca. 10^{-5}s. A number of vibrational levels of the excited state are populated immediately following absorption. After excitation has occured there are several processes which are important in the de-activation of excited states. The radiative parts of de-excitation, are the processes of fluorescence and phosphorescence. The process of fluorescence most commonly occurs between the first excited singlet S_1 and ground state singlet S_0. The process of phosphorescence occurs normally between the lowest triplet state, T_1, and ground state singlet, S_0.

In addition to the radiative de-excitation processes radiationless de-activation may also occur. This is the result of the conversion of electronic energy into vibrational energy within the molecule due to internal conversion and intersystem crossing. Internal conversion occurs between states of like multiplicity (eg singlet to

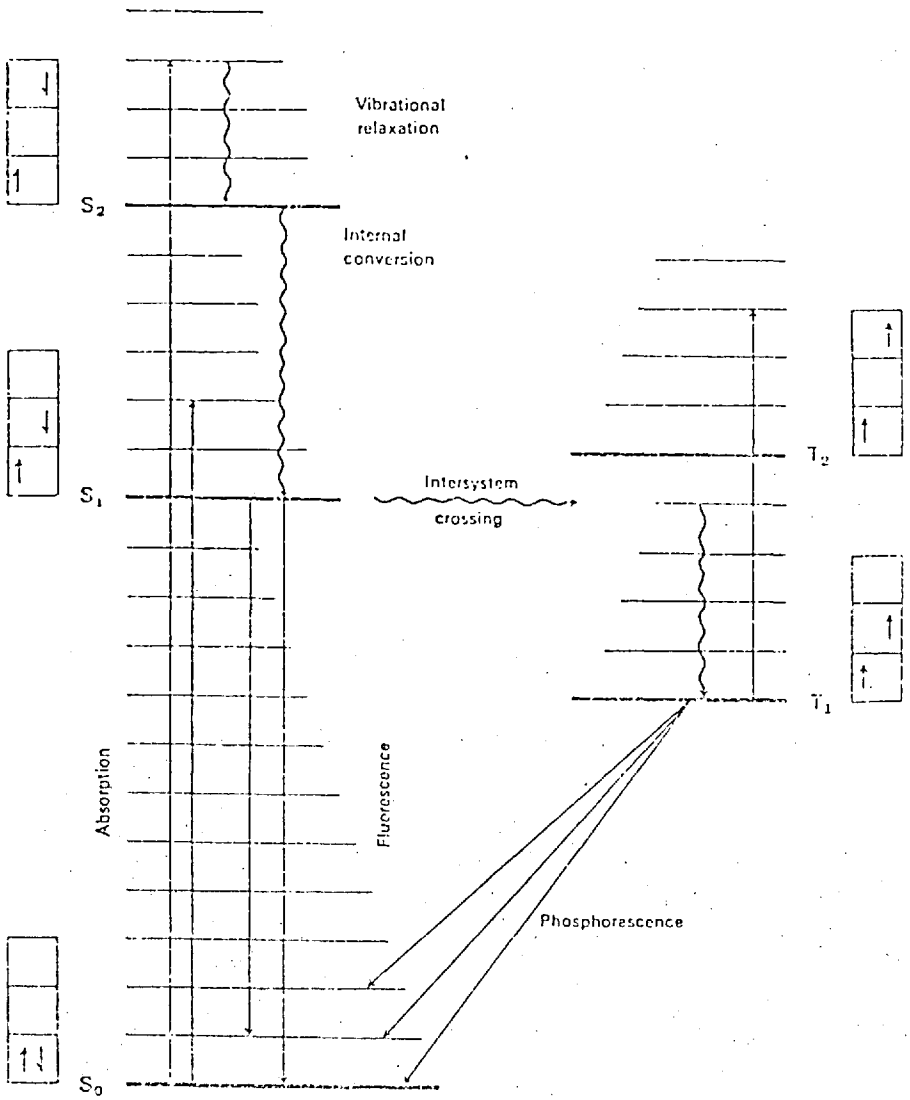

Figure 1.5: Jablonski diagram showing schematic representation of energy levels and photophysical processes which can occur in the excited molecule. Approximate lifetimes of the processes are given below.[19,20]

$S_0 \dashrightarrow S_n$ (absorption)

$S_n \xrightarrow{10^{-11}\text{-}10^{-14}\ \text{sec}} S_1$ (internal conversion)

$S_1 \begin{cases} \xrightarrow{10^{-7}\text{-}10^{-8}\ \text{sec}} S_0 + h\nu & \text{(fluorescence)} \\ \xrightarrow{10^{-8}\ \text{sec}} T_n & \text{(intersystem crossing)} \\ \xrightarrow{10^{-5}\text{-}10^{-7}\ \text{sec}} S_0 & \text{(internal conversion)} \end{cases}$

$T_1 \begin{cases} \xrightarrow{10\text{-}10^{-3}\ \text{sec}} S_0 + h\nu & \text{(phosphorescence)} \\ \xrightarrow{10\text{-}10^{-3}\ \text{sec}} S_0 & \text{(internal conversion)} \end{cases}$

singlet, triplet to triplet).

$$S_2 \rightarrow S_1$$

$$S_1 \rightarrow S_0$$

Intersystem crossing takes place between states of different multiplicity.

$$S_1 \rightarrow T_1$$

$$T_1 \rightarrow S_0$$

Energy separation and conservation of spin are important factors that influence the non-radiative process. The range of a sequential outline of the processes with their approximate lifetimes is given below the Jablonski diagram shown in Figure 1.5.

The luminescence quantum yield of a compound is the fraction of molecules that emit a photon after absorption of energy directly from the radiant source. If all the molecules in the excited state re-emit energy as fluorescence the quantum efficiency of fluorescence is unity. This value is seldom observed, hence, the value is usually less than one. By definition, the intensity of fluorescence emission is equal to the intensity of light absorbed, multiplied by the quantum efficiency of the system.

$$F = I_o(1-10^{-\varepsilon \ell c})\phi \qquad (1.6)$$

where F = Total fluorescence intensity

I_o = Intensity of exciting radiation

ε = Molar absorptivity of substance

c = Molar concentration of the substance

ℓ = Path length of solution in cm

ϕ = Quantum efficiency of fluorescence

However in dilute solution the equation approximates to

$$F = 2.3I_o \varepsilon c\ell \phi \qquad (1.7)$$

Hence it is seen that the intensity of fluorescence is dependent on the intensity of the incident radiation and the concentration of the sample in solution. Thus by increasing the source light intensity the emission intensity may be increased and therefore the sensitivity of the technique is also enhanced. In contrast, the absorption techniques measure $\frac{I_o}{I_t}$ and, hence, an increase in the source intensity has no effect on the absorption, although it may provide for a better signal-to-noise ratio.

In contrast to the absorption spectrophotometry, fluorescence and phosphorescence spectrometry involve the recording of both the excitation and the emission spectra. A schematic diagram of a spectrofluorometer is shown in Figure 1.6. An apparatus for measuring phosphorescence is similar to the fluorometer but the emission is measured following the interruption of the excitation source by a chopper.

1.2.5 Photochemical Effects

Photochemistry is concerned with the chemical (e.g. photosynthesis, bleaching of fabrics, etc.) and related physical effects (e.g. photoluminescence) of electronic

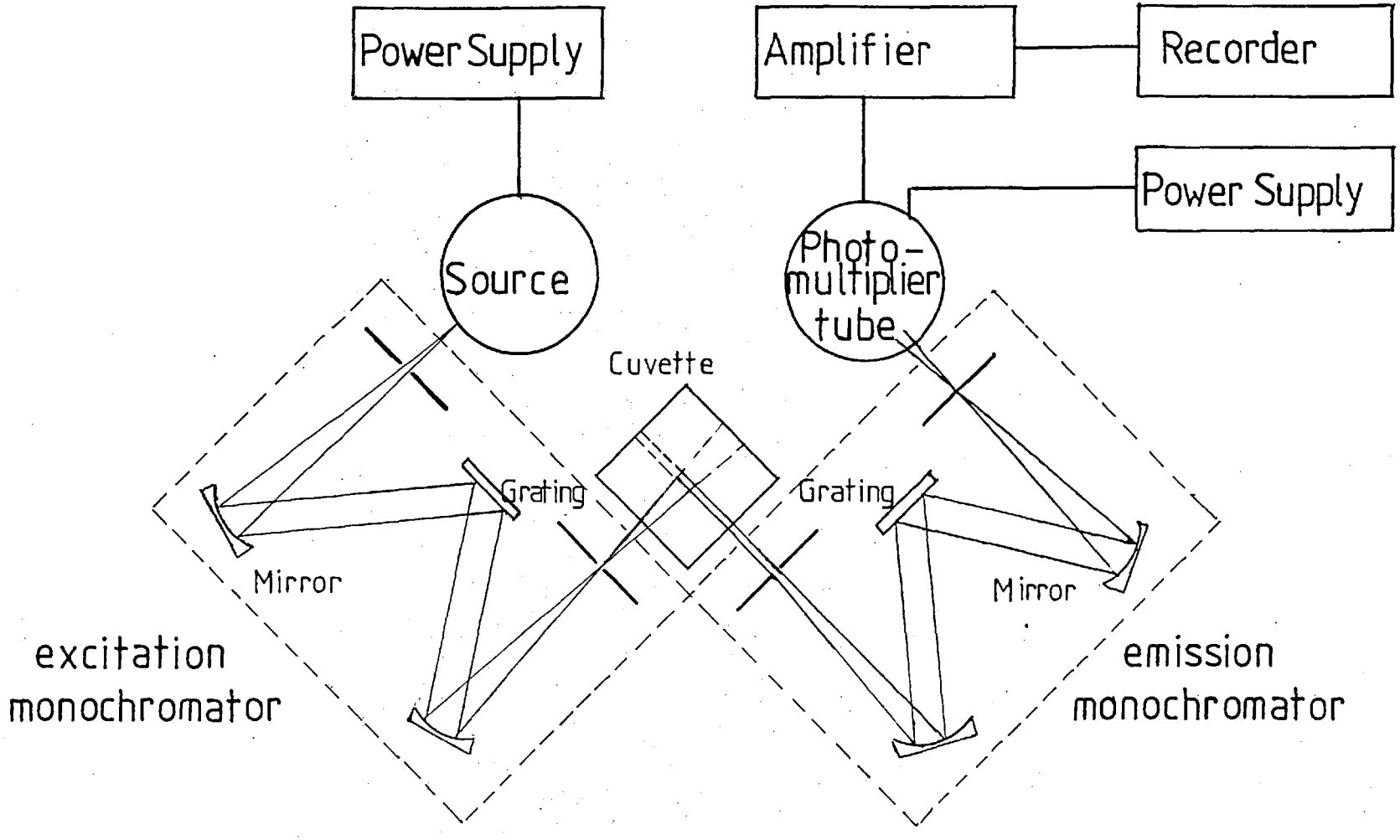

Fig.1.6. Schematic diagram of a fluorescence spectrophotometer[9]

excitation by the interaction of electromagnetic radiation with matter [21]. As photochemical processes are associated with electronic excitation most interest is concerned with the UV-visible regions of the spectrum. A great majority of photochemical reactions occur by the excitation of a molecule to either the first singlet state S_1 or the first triplet state T_1 [22].

The energy distribution in the excited molecules is shown in Figure 1.5.

There are two types of photochemical processes, intra and intermolecular. The former process may be of the radiative (fluorescence and phosphorescence) or non-radiative (intersystem crossing and internal conversion) type. The latter process involves electronic transfer between molecules (i.e. energy transfer and chemical reactions).

The efficiency of photochemical reactions and photophysical processes may be expressed by

$$\Phi_r = \frac{\text{number of molecules produced}}{\text{number of quanta absorbed}} = \frac{\text{rate}}{I_a} \qquad (1.8)$$

Each of the photochemical processes proceeds at different rates for different molecular systems and each has an associated rate constant. The rate constant for the intramolecular processes can be evaluated by the elimination of energy transfer and chemical reactions from the rate equation whereas for the intermolecular processes, the intramolecular processes also have to be taken into account. A kinetic scheme for the photophysical and photochemical processes is given in Table 1.1.[22]

TABLE 1.1: Kinetic Scheme for the photophysical and photochemical processes.

Process	Representation	Rate
Excitation	$S_0(M) + h\nu \rightarrow S_1(M^*)$	I
Internal conversion	$S_1 \rightarrow S_0$	$k_{ic}(S_1)$
Fluorescence	$S_1 \rightarrow S_0 + h\nu_f$	$k_f(S_1)$
Intersystem crossing	$S_1 \rightarrow T_1$	$k_{isc}(S_1)$
Phosphorescence	$T_1 \rightarrow S_0 + h\nu_p$	$k_p(T_1)$
Intersystem crossing	$T_1 \rightarrow S_0$	$k_{isc}(T_1)$
Chemical Reaction	$T_1(M^*) + R \rightarrow$ radicals or stable products	$k_r(T_1)(R)$
Energy Transfer	$T_1(M^*) + S_0(A) \rightarrow S_0(M) + T_1(A)$	$k_e(T_1)(A)$

where

M* excited molecule

R is a reactant

I the rate of absorption of incident radiation

A is the energy acceptor species

k_r is the rate constant for chemical reaction step.

k_e is the rate constant for triplet-triplet energy transfer.

The range of values of the rate constants for these various processes for a typical organic molecule are [20]

$$k(S_2 \rightarrow S_1) = 10^{11} - 10^{14}\ s^{-1}$$
$$k(S_1 \rightarrow S_0) = 10^{4} - 10^{8}\ s^{-1}$$
$$k(S_1 \rightarrow T_1) = 10^{7} - 10^{8}\ s^{-1}$$
$$k(T_1 \rightarrow S_0) = 10^{-1} - 10^{4}\ s^{-1}$$

The main type of photochemical reactions may be divided into : 1. Photoreduction, 2. Photo-oxidation and 3. Photo-addition. [22]

Light induced reduction of carbonyl compounds in the presence of hydrogen donors is a very important photochemical reaction. In the majority of cases the photoreduction occurs [22] <u>via</u> the T_1 state of the photo-excited carbonyl compound. Molecules in this state react

by abstracting hydrogen from a substrate species (RH) to give a hydroxymethyl radical and a radical R·

$$R'_2C = O(T_1) + RH \rightarrow R'_2\dot{C}OH + R^{\cdot} \qquad (1.9)$$

The final reaction products are formed by self-combination and cross-combination reactions of the radicals produced in the hydrogen abstraction step. The efficiency of the hydrogen abstraction depends on the nature of the T_1 state and the structure of the carbonyl compound, the dissociation energy of the R-H band and the solvent type. An example of this is photoreduction of benzophenone by benzhydrol to give benzpinacol.

Irradiation of an organic compound in the presence of a sensitizer and oxygen can lead to the formation of oxygenated products. The examples of photo-oxidation are

1. Photo-oxidation of secondary alcohols to hydroxy-hydroperoxides by benzophenone sensitizer, and
2. Olefenes, dienes and polycyclic aromatic hydrocarbons which can be oxidized using dye sensitizers (e.g Rose Bengal, Fluorescein, etc.)

Photo-addtion involves the combination of the electronically excited molecule with an unlike ground state molecule to give 1:1 photoadduct. This commonly happens when mixtures of alkenes are irradiated.

Apart from all these photochemical reactions described above, some inorganic and organic materials exhibit a photo-induced reversible colour change. This

phenomena is known as photochromism and can be defined [23] as a reversible change of a single chemical species between two states having distinguishably different absorption spectra, such changes being induced in at least one direction by the action of electromagnetic radiation. This inducing radiation, as well as the changes in absorption spectra are usually in the ultraviolet, visible or infrared region. The change in one direction is thermally induced (dark) and usually occurs spontaneously. This branch of photochemistry is gaining more "prominence" in recent years. A more detailed discussion of this will be presented in Chapter Three.

1.2.6 Calorimetric Techniques

For the study of the absorption of electromagnetic radiation, calorimetric techniques [24] provide a useful alternative to the other more conventional methods of transmission and reflectance spectroscopy.

Calorimetric techniques measure the heating effect produced within the sample resulting from radiationless decay or chemical reactions of excited states following the absorption of electromagnetic radiation. Thus the methods can be used for the study of energy yields of non-radiative processes, photochemical and photophysical processes, enthalpies of photochemical reactions and the lifetime of excited states.

A typical calorimetric system consists of a source and filter train to produce monochromatic radiation, a sample cuvette equipped with a temperature sensor and an

insulating chamber to prevent spurious environmental temperature changes.

Conventional calorimeters, employing thermocouples, thermopiles and thermistors have already found particularly useful applications in the determination of luminescence quantum efficiencies [25-27]. The temperature rise of an irradiated luminescent sample is compared with that of a non-luminescent sample of similar optical density. The ratio of heating of the two samples gives the fraction of the absorbed energy which is lost by radiationless processes in the luminescent sample i.e. the energy yield from which the luminescence efficiency can be calculated.

Although intrinsically accurate, conventional calorimetric experiments have remained unpopular because they are lengthy and tedious to perform due to the difficulties of effective thermal insulation of the sample chamber. However there has been a recent upsurge in the development of calorimeters [24] which utilise the modern instrumental facility of source intensity modulation and synchronous signal detection in order to eliminate spurious background signals. With the availability of the laser sources and extremely sensitive heat flow transducers, these modern instruments are reported to be sensitive, rapid and accurate.

The flash calorimeter [24] which has been designed specifically for liquid systems, incorporates the capacitor microphone in a system capable of detecting temperature rises of 10^{-6}°C. It has been used to determine the quantum efficiency of triplet formation of 10^{-4}M anthracene

in ethanol [28].

The piezoelectric calorimeter [24] is particularly useful for the study of radiationless processes in bulk solids and uses a piezoelectric crystal to measure pressure changes in the samples produced by heating at constant volume. Its sensitivity is similar to that of the flash calorimeter and it has been applied to determine the triplet yield 10^{-4}M anthracene in polymethylmethacrylate [24].

Because of the mechanism of the optoacoustic effect, OAS can be considered as a unique calorimetric technique. The essential difference between OAS and other modern calorimeters is that the microphone is remote from the sample [29] and monitors the sample heating indirectly by responding to the pressure wave in the surrounding gas caused by heat flow from the sample [30]. OAS can easily detect microwatts of absorbed radiation and can be applied to samples of any condensed form. Preliminary results for luminescence efficiency determinations [31,32] illustrate the promise that this technique holds for the future.

1.3 OPTOACOUSTIC SPECTROSCOPY

1.3.1 Introduction

In OAS the sample is usually sealed within a closed cell containing a gas, usually air at atmospheric pressure and is fitted with a window transparent to incident radiation and a sensitive microphone whose diaphragm forms part of the wall of the cell. When radiation (basically 250 nm to 2500 nm) is allowed to fall on the sample, the energy may be absorbed. Provided the material does not

degrade photochemically or luminesce the absorbed energy is converted into kinetic energy. This takes place very rapidly, as the energy absorbed by electronic or vibrational excitation of the molecules of the sample may be degraded through the cascade process to the lower electronic and vibrational energy levels within nanoseconds of absorption. If the incident radiation is interrupted periodically, by the use of a rotating chopper, the absorption of energy is interrupted at the frequency of modulation and consequently the heat produced in the sample after energy conversion also appears at this frequency. The periodic heating produces a periodic increase in the pressure of the atmosphere surrounding the sample which follows the modulation frequency of the incident radiation. The optoacoustic effect is observed only when radiation is absorbed by the sample. If the wavelength of the incident radiation is varied, the amplitude of the OAS signal observed at a given wavelength will provide a measure of the ability of the material to absorb radiation at that wavelength, consequently an absorption spectrum will be obtained. The OAS spectrum therefore closely resembles the electronic and vibrational absorption spectrum and is complementary to the reflectance spectrum.

It was Alexander Graham Bell [33] who first observed the optoacoustic effect in 1880. While giving a report to the American Association for the Advancement of Science on his work on the photophone, he very briefly reported that thin discs of certain solid substances when subjected to irradiation from a rapidly interrupted beam of sunlight

emitted an audible sound.

Wilhem Röntgen [34] later demonstrated the optoacoustic effect on gases such as ammonia. According to Röntgen the gas sample following absorption of light expands due to heat production within the sample. The subsequent cooling and contraction produces the acoustic signal.

John Tyndall [35], in the company of Bell, conducted several experiments to show that strongly absorbing gases and vapours produce sounds more intense than from solids. The lack of a sensitive pressure transducer prevented Tyndall from exploiting the technique for quantitative analysis.

Bell [36] continued the work with the investigation of a large number of solids, liquids and gaseous substances. Studying the effect on illuminated solids in the form of thin discs, Bell supported the theory of Lord Rayleigh [37], who concluded that the primary source for the production of sound was the mechanical vibration of the disc resulting from uneven heating of the disc when struck by the beam of light. In the study of liquids and gases, weak signals were usually obtained for liquids and strong signals for gases.

Mercadier [38] and Preece [39] also reported the studies on optoacoustic effect.

After early experiments in 1880 experimentation with the optoacoustic effect stopped for 50 years.

1.3.2 Gas Analysis

Optoacoustic studies were revived again in 1938 by Veingerov [40] who attempted to analyse for gaseous species

in gas mixtures. With the aid of a moving coil microphone as a transducer and a heated filament radiation source he could detect 0.2% volume of CO_2 in a non-absorbing gas such as nitrogen.

Pfund [41] and Luft [42] reported a number of optoacoustic analysers for use in gas analysis using infrared sources of illumination. This type of equipment permitted the determination of CO_2 in air at the ppm level. Pfund used a thermopile detector to monitor directly the heating often produced within the sample whereas Luft employed a condenser microphone as transducer. These simple gas analysis instruments utilizing the optoacoustic effect were of the non-dispersive type and instruments capable of recording the absorption spectra of gas samples over a defined wavelength range using monochromatic radiation were not developed until later studies by Veingerov [43].

Gorelik [44] proposed the use of the optoacoustic-effect to investigate the rate of energy transfer between vibrational and translational degrees of freedom of gas molecules and several workers [45,46] have since presented theoretical treatments of the optoacoustic effect in gases.

Before the recent developments in coherent and intense radiation sources thermal sources were the only available sources of infrared and limited the sensitivity of optoacoustic detectors for gas analysis. The availability of laser sources of infrared radiation has greatly increased the range of analytical problems which can be solved by infrared spectroscopy. With a laser infrared source, the optoacoustic effect has proved an effective

method for the measurements of very low gas concentrations. With their high power and narrow spectral bandwidth the sensitivity and selectivity of optoacoustic gas analysis have been extensively increased. Kerr and Atwood [47] first reported the use of laser as an exciting source for optoacoustic spectroscopy; using a pulsed ruby laser to determine the absorptivity of water vapour in air. Kreuzer [48], with a 15 mW Hc-Nc laser operating at 3.39μm, could measure the absorption of a concentration of 10^{-8} methane in nitrogen. With a Ram spin-flip laser Kreuzer and Patel[49] could detect nitrogen oxide pollution in air to a concentration of 0.01 ppm. Later Kreuzer et al [50] employed molecular gas lasers. These gas lasers are not continuously tunable and can be made to emit radiation at a number of discrete wavelengths corresponding to the transitions between various inverted energy levels in the laser gas. They could detect ethylene concentrations in air as small as 5 parts per billion. There are numerous others [51,52] who worked in the area of laser source opto-acoustic spectrometry.

1.3.3 Solid/Liquid Studies

In 1935 Hayes [53] described a detector employing the optoacoustic effect. This consisted of a black absorber called "fluff" (Carbonised Pappus of a flower), confined to a hermetically sealed chamber, one side of which was a thin metal diaphragm forming an element of a condenser microphone. When modulated infrared radiation was allowed to fall upon the absorber, the resultant pressure waves were monitored by the microphone

and measured with the aid of an ammeter.

Golay [54,55] investigated the Hayes detector and tried to improve the sensitivity of the device. Golay used a black antimony film deposited on an organic substrate as the absorbing medium and developed the now famous optical pressure transducer to monitor the acoustic signal produced within the cell. Weber [56] and Luchin [57] used a very thin layer of black pigment. Terenin and Yaroslavkic [58] used carbonised duck down. In 1949 Golay [59] using xenon as filler gas, redesigned the detector in the present form as a detector for infrared radiation.

In 1964 Houghton and Acton [60] observed audible signals from films of acetylene soot, camphor soot and black body cavities using a xenon flash tube source and proposed that the thermal absorptivity of absorbing samples could be evaluated by this technique.

In 1973 Parker [61] while carrying out studies concerning collisional deactivation in gases (oxygen, nitrogen and neon) noted strong optoacoustic signals at wavelengths where no absorption by the gas sample was expected. Parker attributed the signal to the absorption of radiation with the cell window.

Kerr [62] attempted to use the optoacoustic technique for measuring the absorption of thin solid films at laser wavelengths. The samples examined were optical window materials coated with layers, one quarter wave thick at 10.6μm, of calcium fluoride. Other samples had a layer of zinc sulphide over a binder layer of thorium fluoride. Theoretical calculations of typical pressure signals were also included in his paper.

Harshbarger and Robins [63] interest in the OAS technique arose from the work of Kreuzer et al [48-50] and these workers have described an experimental assembly for OAS in the UV/visible region and reported its application to the examination of powdered potassium dichromate, flower petals, dried blood smears, ultramarine blue, etc.

Rosencwaig et al [64-66] used the OAS technique for exploring the absorption spectra of both inorganic samples and biological materials.

It was Bell [33,36] who first observed the audible weak signals from coloured liquids. Recently the interest of optoacoustic technique in liquids have grown [67,32] and Lahmann et al [68] by introducing piezoelectric transducers in liquids have reported a detection limit of an absorption coefficient of 2.2×10^{-5} cm^{-1} arising from β-carotene dissolved in chloroform by using a CW ion-laser producing two lines at 488nm and 514.5nm, each of 0.7W power. Because of large amounts of low frequency noise their technique was not successful in obtaining spectra of weakly absorbing pure liquids.

More recently Patel et al [69,70] used a submersed piezoelectric transducer together with a pulsed tunable dye laser to study the weak 607 nm absorption band of benzene dissolved in various concentrations of CCl_4. They could measure an absorption coefficient as small as 10^{-6} cm^{-1} with an absorbed energy of 10^{-9}J. They applied this technique to measure the weak sixth harmonics of C-H stress in liquid benzene.

1.3.4 Theory of Optoacoustic Spectroscopy for Solids

Introduction

The optoacoustic effect is a result of an energy conversion process. Irradiation of a sample by chopped radiation results in localised heating within the absorbing material due to non-radiative de-excitation processes occuring from excited states. Some of this heating is transferred by thermal diffusion from the solid to a thin boundary layer of gas adjacent to the surface of the solid. Adiabatic expansion of the gas then gives rise to a pressure wave in the gas which is detected by a microphone. The important characteristics of the sample which determines the magnitude and nature of the optoacoustic signal [71] are its optical absorption coefficient, the efficiency of internal radiationless de-excitation processes and thermal transfer coefficients, in particular the thermal diffusivity:

Optoacoustic signal magnitude = Radiant power absorbed × Efficiency of radiationless conversion × Efficiency of heat transfer to sample/gas interface

The optoacoustic signal is a function of the radiant power absorbed by the sample and an inverse proportionality is generally observed between the signal magnitude and the modulation frequency. For solid samples, the optoacoustic signal power may be expected to vary with particle size for two reasons [29]-

1. when the particle size (surface area) varies, the power absorbed will vary owing to changes in the reflectivity

of the sample.

2. As the particle size decreases the surface area in contact with the gas phase increases. This may result in a more efficient transfer of power between the solid and the gas phases so that a reduction in the particle size tends to increase the magnitude of the observed signal.

The power transfer at the solid-gas interface may also be influenced by thermal conductivity of the sample and the filler gas; this would then be expected to affect the manner in which the observed optoacoustic signal varies with sample characteristics. The amplitude of the signal would also be expected to be inversely proportional to the heat capacity of the filler gas.

Although thermal diffusivity [72] is a derived quantity it is of direct importance to heat flow studies as it determines the transient heat propagation through a sample. Thermal diffusivity is the ratio of the thermal conductivity to the product of specific heat and the density of the material. The absorption of the radiant energy and the subsequent de-excitation processes in the sample may occur in a few nanoseconds, whereas the heat transfer mechanism through the sample to the surface may take several milliseconds i.e. it is of the same order of magnitude as the period of modulation of the incident radiation. Hence phase-sensitive detection of the optoacoustic signal may provide considerable information concerning the nature of the sample.

Present Theory

The optoacoustic theory for gases has been well developed [46,48,73,74] for a number of years but the theory relating to the study of solids has been of relatively recent origin. Parker [61], while studying the optoacoustic effect in gases, noticed that a small measurable signal was being produced in the gas cell even when the gas was not absorbing the incoming light. He determined that this signal resulted from the absorption of light within a small layer of the quartz window of his cell and he analysed his results in terms of periodic heat flow from the window to the enclosed gas. Kerr [62] tried the technique of OAS for measuring the absorption of thin films at laser wavelengths. Whilst the theoretical model he produced was adequate for his system, this has to be regarded as a special case.

A theoretical model for the prediction of the magnitude of optoacoustic signals has been explained by Adams et al [29].

Other workers who have contributed to the theory of optoacoustic effect have been Aamodt et al [75,76] and Bennet and Forman [77-80].

The most comprehensive theory has been developed by Rosencwaig and Gersho [30] to account for all the effects observed in the optoacoustic spectroscopy of solids.

Any light absorbed by the solid under investigation is converted partially into heat by non-radiative de-excitation processes within the solid. A diagram illustrating a model of the sample contained within a gas-tight cell of cylindrical symmetry is shown in Figure 1.7.

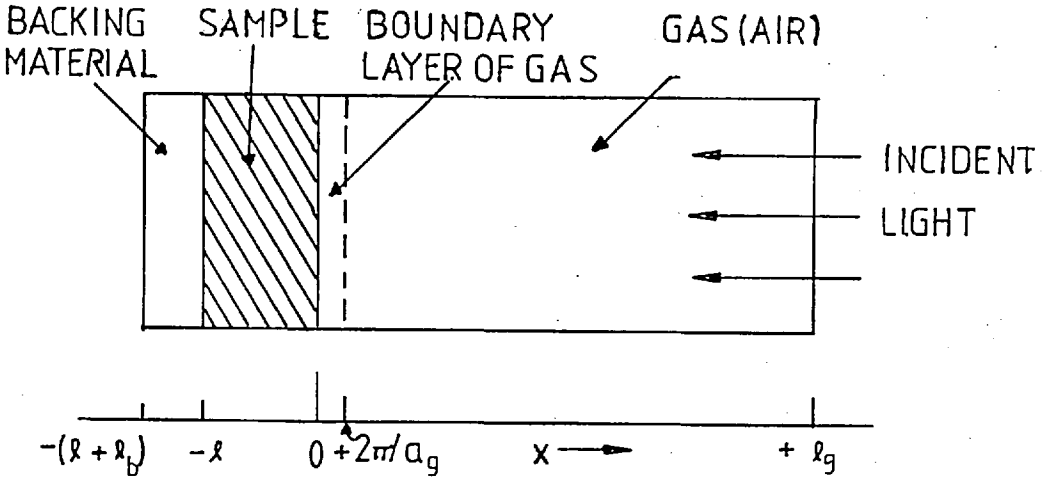

30

Fig. 1.7. Cross-sectional view of a simple cylindrical optoacoustic cell.

It is assumed that the length of the cell is small compared with the wavelength of the acoustic signal and the average pressure produced in the cell is detected by a microphone. The sample is considered to have a thickness ℓ and is mounted so that its front surface is exposed to the gas within the cell and its back surface is in contact with a poor thermal conductor of thickness ℓ_b. It is also assumed that the gas and backing material are not light absorbing. The following parameters are defined.

k_i, the thermal conductivity of material i ($cal\ cm^{-1}s^{-1}K^{-1}$)

P_i, the density of material i ($g\ cm^{-3}$)

C_i, the specific heat of material i ($cal\ g^{-1}\ K^{-1}$)

$\alpha_i = \frac{k_i}{C_i P_i}$, the thermal diffusivity of material i ($cm^2 s^{-1}$)

$a_i = \sqrt{(\omega/2\alpha_i)}$, the thermal diffusion coefficient of material i (cm^{-1})

$\mu_i = 1/a_i$, the thermal diffusion length of material i (cm)

ω, the chopping frequency of the incident light beam (rad s^{-1}).

If the incident radiation is assumed to be modulated sinusoidally at a wavelength λ, the intensity is given by

$$I = \tfrac{1}{2}I_o(1+\cos \omega t), \qquad (1.10)$$

where I_o is the incident monochromatic light flux. If β is used to denote the absorption coefficient of the solid then the energy density produced by the absorption of light at a point x in the solid is given by differentiating Beer's law with respect to x and substituting in Equation 1.10. Thus

$$\tfrac{1}{2}\beta I_o \exp(\beta x)\ (1+ \cos \omega t) \qquad (1.11)$$

when x takes negative values according to the definition in Figure 1.7.

The optoacoustic signal arises from the periodic heat flow from the solid to the surrounding gas in the sample cell. Rosencwaig and Gersho's theory results in a complex expression for the envelope of sinusoidal pressure variation -

$$P = \frac{A.B.\beta}{k_s.a_g(\beta^2-\sigma_s^2)} \qquad (1.12)$$

where P is the pressure variation in the cell filler gas for sinusoidally modulated incident radiation, A is a constant factor, which is proportional to the incident radiant energy and the ambient pressure within the cell,

β is the optical absorption coefficient (cm^{-1}) of the sample and k_s is its thermal conductivity.

$$\sigma_s = (1+j)a_s \tag{1.13}$$

a_s and a_g are the thermal damping functions of an alternating temperature wave passing through the sample and gas respectively and are given by

$$a_i = (\omega/2\alpha_i)^{\frac{1}{2}} \tag{1.14}$$

where ω is the modulation frequency and α_i is the thermal diffusivity of the material.

B is a complex function which may be expressed as

$$B = \frac{(r-1)(b+1)\exp(\sigma_s x) - (r+1)(b-1)\exp(-\sigma_s x)+2(b-r)e^{-\beta x}}{(g+1)(b+1)\exp(\sigma_s x)-(g-1)(b-1)\exp(-\sigma_s x)} \tag{1.15}$$

Where x is the thickness of the sample and the other functions are given by

$$r = \frac{(1-j)\beta}{2a_s} \tag{1.16}$$

$$b = \frac{k_b . a_b}{k_s . a_s} \tag{1.17}$$

$$g = \frac{k_g . a_g}{k_s . a_s} \tag{1.18}$$

The subscript"b"refers to the backing material of the sample. The product $k_i\ a_i$ may be considered as a thermal flux coefficient for the material.

Rosencwaig and Gersho have described its application to a number of special cases [30,81].

For solids which are reasonably transparent to light ($\beta\ell<1$), the pressure $\delta p(t)$ is proportional to $\beta\ell$ unless the thermal diffusion length of the solid, $\mu s = 1/a_s$, is less than ℓ. In that the pressure is proportional to $\beta\mu_s$.

For optically opaque solids ($\beta\ell >> 1$), the pressure $\delta p(t)$ is independent of β when the thermal diffusion length μ_s is greater than the light absorption length $1/\beta$. In this case the sample, as well as being optically opaque, is also "optoacoustically opaque", i.e. the acoustic pressure is independent of the optical absorption coefficient β. However, when μ_s is less than $1/\beta$ i.e. when $\beta\mu_s << 1$, the pressure amplitude is proportional to $\beta\mu_s$ irrespective of the magnitude of the optical absorptivity $\beta\ell$. Thus, even though the sample is optically opaque ($\beta\ell >> 1$), it is not optoacoustically opaque, i.e. the acoustic pressure is now dependent on the optical absorption coefficient β.

The effect of reflection losses by the incident light at the sample surfaces was not considered in the above theoretical treatment. For small optical absorption coefficients this loss has been considered very important [82,83]. Rosencwaig and Gersho's theoretical treatment has been extended for the measurement of spatially varying absorption in solids [84] and also for the determination of absolute optical absorption coefficients for strongly absorbing solids and liquids [85]. McClelland and Kniseley have

examined the signal saturation effects in OAS [86] and later in another paper [87] reported the sample backing substrate on the observed signal magnitude.

The remainder of this thesis is concerned with the descriptive apparatus for optoacoustic spectroscopy in the ultraviolet, visible and near-infrared regions of the spectrum and its application to a variety of sample types. The theoretical treatments discussed above for the magnitude and phase of the recorded optoacoustic signal are examined in an attempt to examine the technique as a quantitative means of analysis and studying radiant absorption in solid samples.

CHAPTER TWO

INSTRUMENTATION

2.1 Introduction

In optoacoustic spectroscopy the modulated radiation absorbed by the sample is converted into heat causing a periodic pressure wave in the optoacoustic cell which is monitored by a suitable transducer.

The basic requirements of an optoacoustic spectrometer are (1) a radiation source, (2) a modulation system, (3) a monochromator, (4) cell for the sample containment, (5) detector, (6) electronic system for signal detection, amplification and readout. A schematic diagram of a typical system is shown in figure 2.1.

2.1.1 Radiation sources

The original optoacoustic studies by Bell [36] employed solar emission as a wide-band source radiation. The spectral output from the sun matches that of a black body at 5900K, providing a useful continuum emission from ca 300 nm to beyond 1 μm [88].

The radiant sources commonly used for spectroscopy may be divided into two types, the broad-band or continuum and the narrow band or line emission sources. As optoacoustic measurements are monitored at a wide range of wavelengths, high intensity continuum sources (many of their properties can be described in terms of black body behaviour) are appropriate for an optoacoustic spectrometer and are the most commonly employed sources for solid and liquid sample studies. A survey of these incoherent sources of continuum radiation extending from the ultraviolet to the infrared region is given by Cann [89]. The major

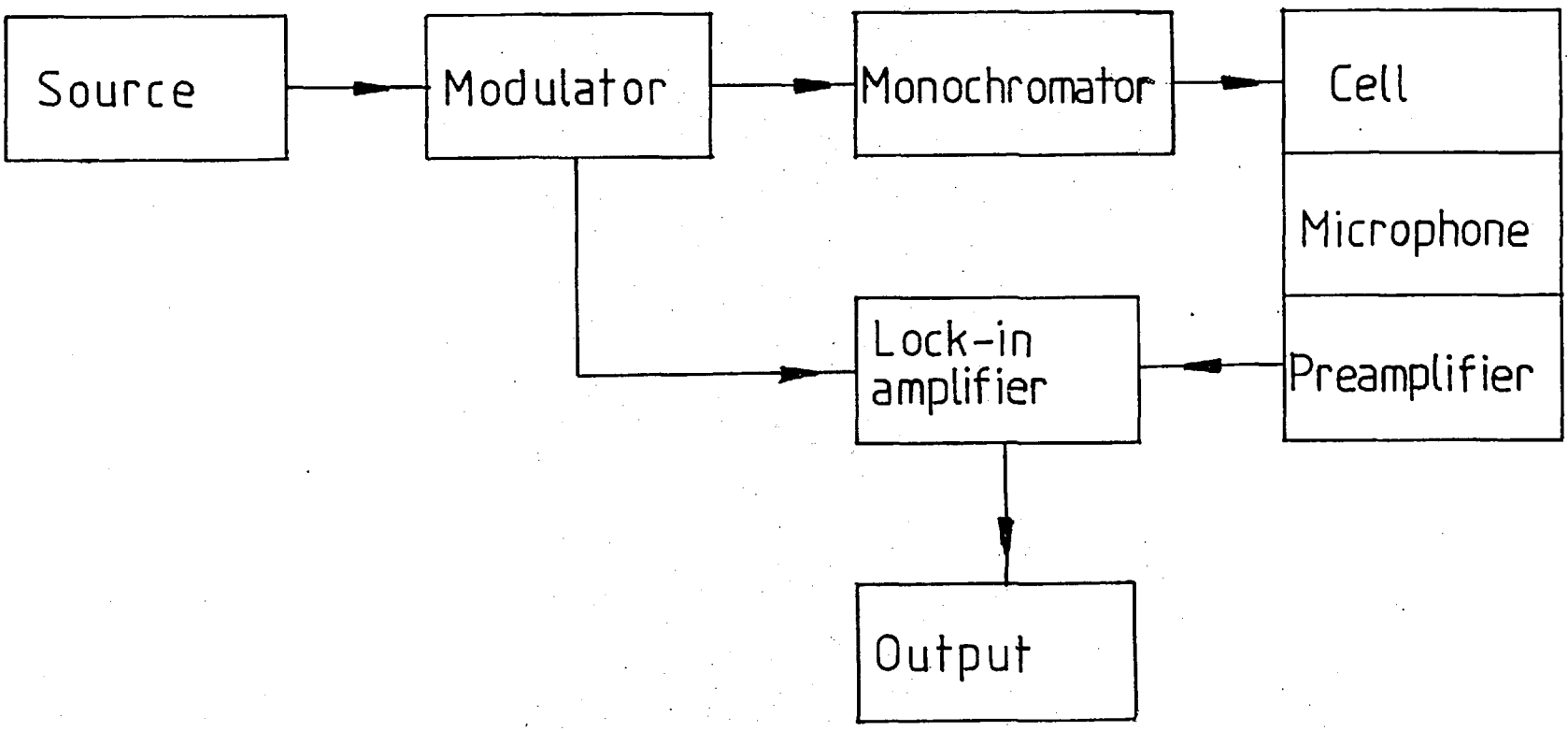

Fig. 2.1. The essential components of an optoacoustic spectrometer.

types of incoherent source are incadescent emitters (true continua) and arc sources.

High pressure arc sources are available with a usable broad-band emission spectrum extending from the ultraviolet to the infrared. The emission is produced by passing a high current discharge through a vapour usually contained within a glass or quartz envelope. The pressure inside the envelope may be from a millitorr to several hundreds of atmospheres. Many workers [90,91] have investigated the use of xenon arc lamps operating typically at pressures of 50-70 atmospheres, and these have been found to be efficient emitters of ultraviolet and visible radiation.

High pressure mercury arcs have a high emission intensity e.g. a 1kW mercury arc may generate more than 170W of radiative power throughout the UV and 240W in the visible region [88].

The tungsten filament lamp is a particularly simple and convenient source of continuum radiation and emits the major portion of its energy in the near infra-red region, [6,9] only ca 15% of the radiant energy is emitted within the visible region depending upon the power applied. The tungsten filament is contained in a glass or, preferably, quartz envelope and operates typically at 3000K. To improve the useful life of the source and to enhance the intensity a halogen gas may be included in the bulb which prevents the deposition of vaporized tungsten on the inner surface of the envelope. Also a dynamic equilibrium is set up between the tungsten metal filament and the tungsten halide in the vapour phase

resulting in a more even filament ageing. This enables the tungsten-halogen lamp to be run at much higher temperatures than is possible with the conventional tungsten source.

Lasers [88,6,92,93] are coherent sources which are finding increasing applications in spectroscopy. Laser radiation is highly collimated and is of high intensity and very narrow spectral bandwidth. Tunable dye lasers are available for the visible and part of the near-infrared spectral regions, but although dye lasers may be operated in the wavelength range 340 nm - 1200 nm the tuning range of each dye is only of the order of 50 - 100 nm, making it necessary to make several dye changes during a wavelength scan. For this reason and because of their high cost dye lasers have not replaced continuum sources where a scan over a wide wavelength range is required. Furthermore, analytical molecular spectroscopy in the ultraviolet and visible regions is undertaken often with a monochromatic half-spectral bandpass of several nanometers and over such a relatively wide bandwidth, the emission intensity of conventional devices may be superior to that of a laser source.

2.1.2 Modulation system

For the production of the optoacoustic effect modulation of the incident radiation is necessary; if the incident radiation is not chopped an optoacoustic signal will not be observed. Modulation can be effected mechanically or electronically. Mechanical choppers, usually achieved with the aid of a rotating sector or a

vibrating plate provide a one hundred percent depth of modulation. Disadvantages with such systems include a limiting of the frequency which can be attained and the mechanical noise produced by the apparatus. With electronic modulation one hundred percent modulation is difficult to achieve and the stability and life time of the source is often reduced. However mechanical noise is eliminated and higher frequencies can usually be obtained.

The use of pulsed sources for the examination of solid samples has received comparitively little study. Such sources usually exhibit poor reproducibility with regards to pulse intensity, nevertheless, pulsed laser sources have been extensively employed for infrared gaseous OAS.

2.1.3 Monochromator

A monochromator is a device which disperses radiation into its component wavelengths. A typical monochromator consists of :

(1) an adjustable entrance slit,
(2) a collimation mirror or lens,
(3) a dispersing element,
(4) a mirror or lens to focus the dispersed radiation, and
(5) an exit slit of adjustable width.

Prism based monochromators are not commonly encountered in modern instruments as their wavelength range is limited and the non-linear angular dispersion of the prism is a

great disadvantage. Nevertheless, the prism based monochromator has the advantage of there being no secondary orders of dispersion and the light losses are lower than with a grating monochromator in the ultraviolet region. Diffraction gratings [94] are more commonly used and can be used either in the transmission or reflection mode but the dispersion of incident wavelengths depends on the geometry of the grating. A transmission grating is made by ruling parallel grooves on glass or silica with a diamond edge. The reflection grating is commonly used and this is made by ruling parallel grooves on metal surfaces or by evaporating a thin film of aluminium on to the surface of replica grating. The radiation is reflected from the unruled portions of the grating and interference between the reflected beams produces dispersion. Gratings have a good linear dispersion, resolving power and greater wavelength range than a prism. The angular dispersion of a grating can be calculated as follows. Assuming a constant angle of incidence, then the angle of diffraction as a function of wavelength is given by:

$$\frac{d\theta}{d\lambda} = \frac{n}{d \cos\theta} \quad ,$$

where θ is the angle of diffraction

λ is the wavelength

n is the order of interference

d is the distance between adjacent grooves.

The resolving power of a grating is a product of the number of rulings and the order of diffraction.

Interference due to overlapping orders will occur with grating type monochromators at wavelengths which are at $\lambda/2$, $\lambda/3$... of the first order radiation (Fig. 2.2). Therefore if a source emits over the wavelength range 250 - 1000 nm, overlaps from the second order diffraction of 250 nm will occur at 500 nm in the first order spectrum. Therefore it is necessary to include order sorting filters in the light path after the monochromator if there is any chance of interference by overlapping orders occurring in the region of the spectrum being investigated. The use of order sorting filters is particularly necessary in the near-infrared where there is substantial overlap from high orders of visible radiation. Additionally the wavelength range scanned in the near-infrared is greater than the visible region and a different order sorting filter must be inserted everytime the wavelength is doubled.

A grating may be blazed in order to suppress underived orders of diffraction. This is achieved by the adjustment of the angles of the sides of the grooves ruled on the grating.

The light gathering ability of an optical system is a function of the effective optical apertures and reciprocal of the focal length.

2.1.4 The Optoacoustic Cell

In optoacoustic spectrometry a microphone transducer forms part of the sample cell in order to monitor indirectly the radiative energy absorbed by the sample and the design of the cell is an important feature for any optoacoustic system. Several types of OAS cell have been reported in

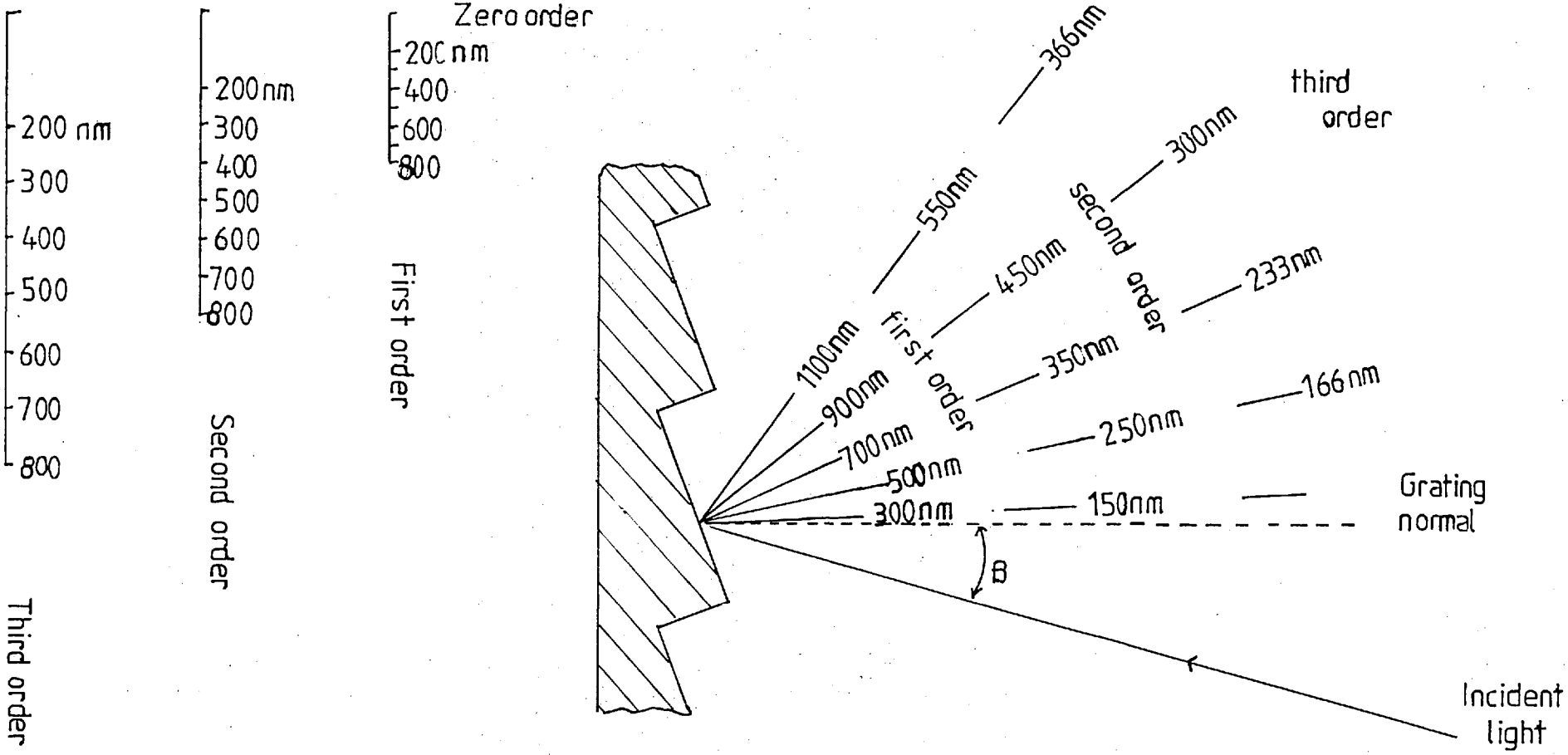

Fig. 2.2. Overlapping orders of spectra from a reflection grating.(9)

the literature but the main criteria governing the actual design of the cell are :[95]

1. Acoustic isolation from external noise - the cell is normally sealed and the walls should be smooth and of sufficient thickness to form an efficient acoustic barrier.

2. Minimization of the background signal arising from the interaction of the light beam with the walls, windows and the microphone in the cell. The windows should be optically transparent and the material of the cell should not have such high thermal conductivity that the thermal energy produced in the gas is quickly absorbed. Aluminium or stainless steel optoacoustic cells are good since the walls of these cells may be polished and will absorb very little of the incident radiation.

3. The internal volume of the cell should be as small as possible for maximization of the acoustic signal within the cell. As the signal produced in the optoacoustic cell from solid samples varies inversely with the gas volume in the cell, minimization of gas volume is very important. Too small a volume should be avoided, however, otherwise the acoustic signal produced at the sample suffers appreciable dissipation to the cell walls through thermo-viscous damping effects before reaching the microphone. To prevent this all the areas

through which the acoustic wave passes should be sufficiently large, so as to allow the flow of acoustic pressure wave with minimal dissipation of the sound energy to the surrounding walls.

In particular it should be ensured that the acoustic or thermal energy is not lost to the window directly in front of the sample. The distance between the sample surface and the cell window should be greater than the thermal diffusion length of the gas. For air at room temperature and pressure the thermal diffusion length is ~ 0.02 cm at a modulation frequency of 100 Hz [95].

4. The microphone in the cell should not be exposed to direct source illumination. If the microphone sees the source radiation, either directly or by reflections within the cell, the diaphragm may absorb the energy giving rise to spurious signals.

2.1.5 Detector System

A sensitive microphone transducer is employed in order to monitor the amplitude of the periodic pressure changes produced in the cell. For optoacoustic spectrometers, a condenser microphone is frequently used because of its flat frequency response, high sensitivity and high stability over a wide range of frequencies and low internal noise. Such a microphone consists of a thin metal diaphragm

and a rigid conducting back plate forming the plates of a capacitor [96,97]. If a charge is applied to the capacitor by an external DC supply, capacitance modulation caused by sound pressure variation induced changes in plate separation will produce a current flow between the plates. The signal output from the microphone depends on the microphone capacitance, the magnitude of the pressure induced changes in capacitance and the magnitude of the applied voltage ($C = \varepsilon_0\varepsilon_r A/d$, where C is capacitance, ε_0 is permittivity of free space, ε_r relative permittivity, A is surface area of the capacitor and d is the distance between the plates). As the magnitude of the signal is directly proportional to the inverse of the total circuit capacitance, it is important that the microphone capacitance, amplifier input capacitance and stray circuit capacitance are kept to a minimum. An equivalent circuit diagram of a condenser microphone and preamplifier is shown in fig. 2.3 [97].

The output voltage can be given by the expression

$$v_o = \frac{\Delta C(t)}{C} \cdot E_o \cdot \frac{j\omega RC}{1+j\omega RC}$$

where E_o - the polarisation voltage

$\Delta C(t)$ - variation of capacitance due to sound pressure

$C = C_t+C_s+C_i$ - C_t is the microphone capacitance
C_s is the stray capacitance
C_i is the input capacitance of preamplifier.

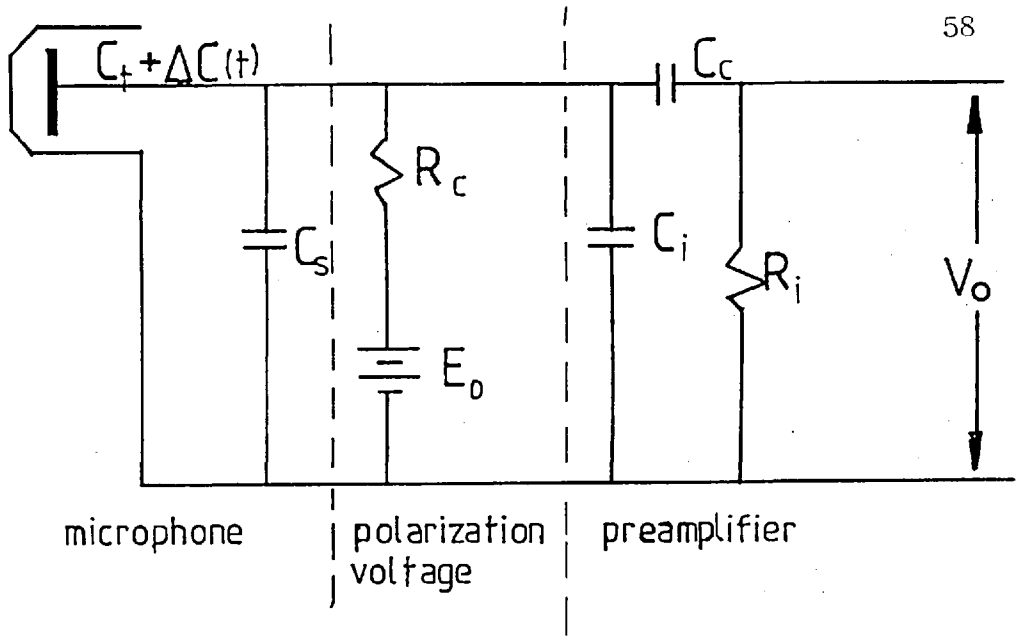

Fig.2.3. Equivalent circuit of a Brüel and Kjaer microphone and preamplifier (97).

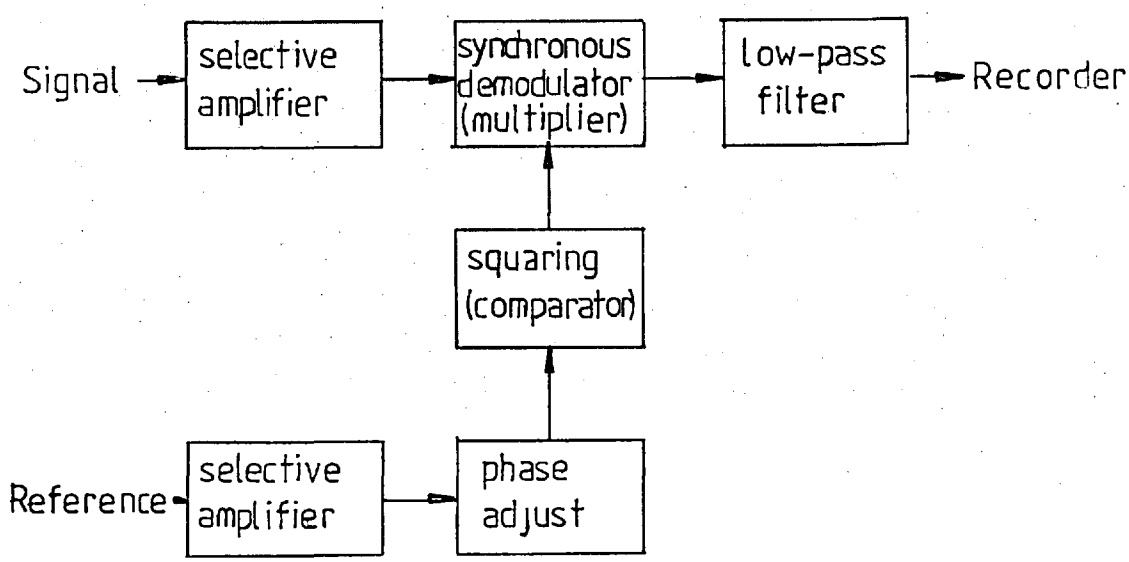

Fig.2.4. Block diagram of a lock-in amplifier (98).

C_c = is the coupling capacitance.

$R = \frac{R_i R_c}{R_i + R_c}$ R_c - charging resistance

R_i - preamplifier input resistance.

In the high frequency limit ($\omega RC >> 1$) the useful sensitivity is reduced by stray circuit capacitance and the input capacitance of the preamplifier. Therefore the preamplifier should be situated adjacent to the microphone.

2.1.6 Signal amplification and Readout

The optoacoustic signal from the microphone is taken to a sensitive lock-in-amplifier: an AC amplifier with a synchronous detection system. A lock-in amplfier measurement system consists of four main operations[98]: modulation, selective amplification, synchronous demodulation and low pass filtering. The latter three operations are carried out by the lock-in amplifier itself.

A block diagram of the functions of a lock-in amplifier is shown in Figure 2.4 [98]. The lock-in amplifier normally has a modulated sample signal input channel and an input for the modulated reference signal. Modulation of the sample signal is the first operation step in the lock-in amplfier measurement technique. This transforms the signal from DC to AC to minimize drift, 1/f and other noises, e.g. 50Hz ripple from AC mains. The technique used to amplitude modulate the sample signal is employed also to provide a reference signal of similar frequency for frequency-tracking and phase-locking

by the lock-in amplifier system.

The modulated carrier wave is first selectively amplified. This amplification is carried out by a variable frequency tuned amplfier on the signal wave as well as on the reference signal.

The amplified carrier wave is synchronously demodulated by multiplying the modulated carrier wave by a bipolar reference square wave signal that is equal in frequency and phase locked to the carrier wave. Synchronous demodulation discriminates, against random noise components and only the phase locked carrier wave is demodulated by this multiplication operation. Finally the output from the synchronous demodulator is low pass filtered to regenerate the original signal. This phase sensitive detection (PSD) system gives information concerning the amplitude of the signal and its phase relationships to the reference signal.

2.2 Single beam instrumentation

The instrumental assembly of a single beam optoacoustic spectrometer is shown in Figure 2.5 [29,99]. A 1000 watt xenon arc high pressure continuum source (Oriel Corp., Stamford, Conn., U.S.A., Model 6269) was employed since this provided a high radiant flux continuum radiation having a resonably constant intensity with wavelength. The maximum intensity of this 1 kW source in the UV-VIS region was 1.16mW [100]. This instrument was operated in an air cooled housing fitted with a UV grade fused silica double element condensing lens assembly and a special rear reflector. This optical arrangement provided for f/1.0 collection efficiency of radiation from

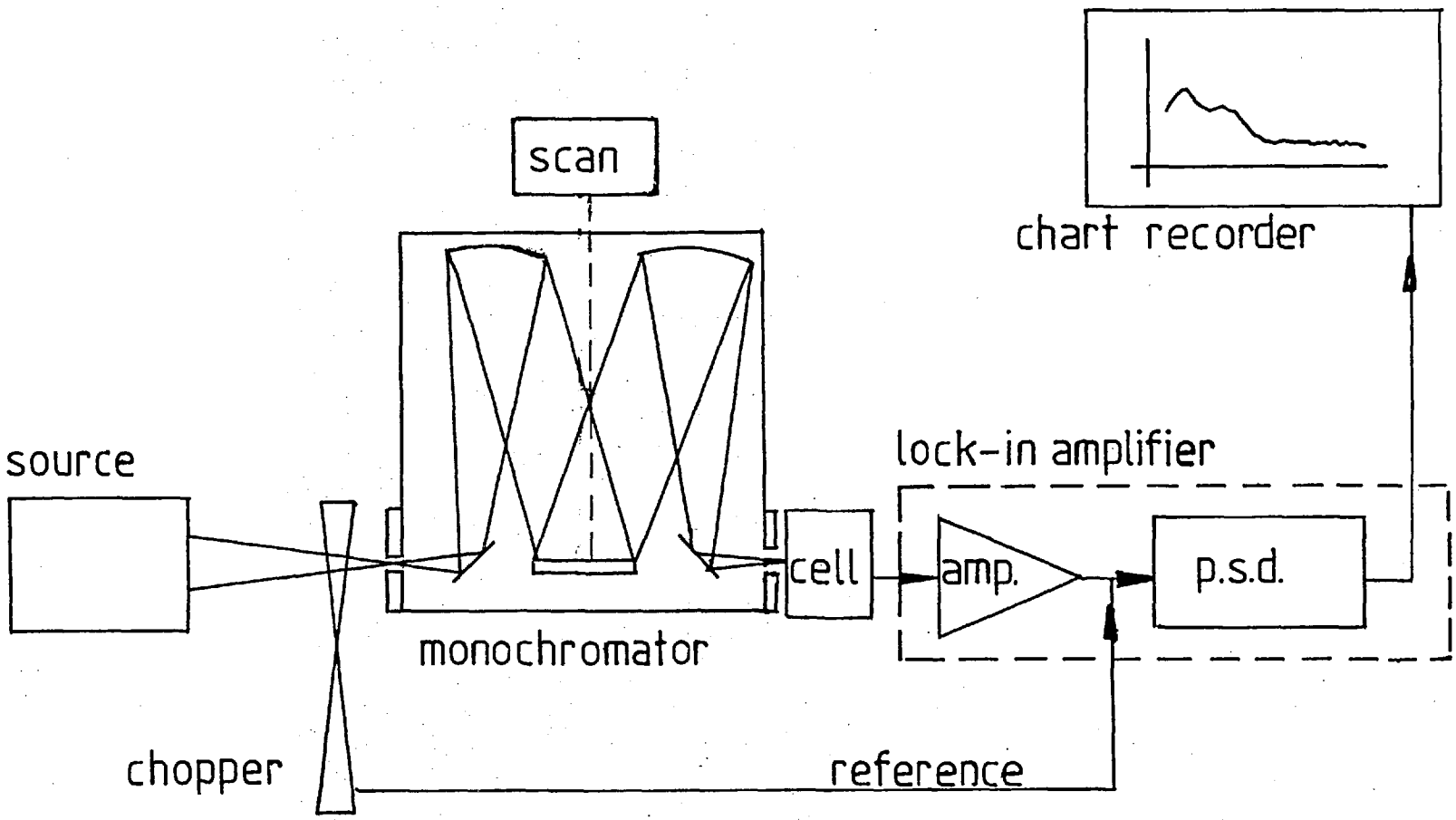

Fig. 2.5. Schematic diagram of the single beam optoacoustic spectrometer.(29,99)

the arc lamp.

The radiation from the source was focused through the blades of a variable speed rotating chopper (Brookdeal Electronics, Ltd., Bracknell, Berks, Model 9749) and on to the entrance slit of the monochromator. By choosing a suitable sector chopping blade frequencies in the range 1Hz to 100Hz and 1Hz to 1000Hz could be selected. The reference signal was derived from a LED-photoiodide pair mounted on opposite sides of the chopper blade followed by suitable signal conditioning.

The f/4 200 mm monochromator (Metrospec., Diffraction Grating and Optics Ltd., Chobham, Surrey) was fitted with a 50 x 50 mm, 1200 lines mm^{-1} plane grating blazed at 300 nm (for use in the UV-visible region), interchangeable slits and a wavelength scanning motor was mounted on to the optical rail of the system. The reciprocal linear dispersion obtained at the exit slit of the monochromator was 4 nm mm^{-1}. Five fixed slits ruled on a single ultraviolet transmitting quartz plate are provided and allow half-spectral bandpass values of 1,2,5,10 and 20 nm to be achieved. Then radiation from the exit slit of the monochromator was focused with the aid of a front-surfaced concave mirror (50 mm in diameter, 200 mm focal length) into the optoacoustic cell.

Either of the two types of sample cells can be employed as shown in Figure 2.6 and 2.7 [101]. The sample cell (Figure 2.6) was made from stainless steel to produce a sealed internal volume of about 5 cm^3. Illumination of the sample within the cell was achieved *via* a silica window of 25 mm diameter and 2 mm thickness. The sample holder was also constructed from stainless steel and was fitted with a silica disc

of 20 mm diameter and 1 mm thickness to support the sample. This sample holder could be screwed into the cell, against a rubber O-ring, to form a pressure tight system. Through the side of the stainless steel cell body a ½" diameter condenser microphone transducer (type 4166, Brüel and Kjaer Ltd, Hounslow, Middx.) was positioned with the diaphragm close to the sample tray. Thus, the microphone diaphragm forms part of the cell wall and was sealed tightly into the cell. In order to prevent any damage to the microphone a pressure release valve was provided in the cell opposite to the microphone diaphragm. This pressure release valve allows the sample insertion without any internal pressure build-up in the cell. The polarization voltage to the microphone was provided by a 200V dry-cell power supply, the associated preamplifier being powered from a 28V separate supply. The microphone sensitivity was reported as being 5mV μbar^{-1}.

The sample cell in Figure 2.7 [101] was constructed from aluminium with a 20 mm diameter silica entrance window. Samples were placed in highly polished aluminium cups of 16 mm internal diameter, 3-5mm deep, and sealed within the cell by means of four locking nuts. The type of microphone, preamplifier connections, etc. are exactly the same as for the cell in Figure 2.6.

The optoacoustic signal from the microphone was taken directly to a sensitive lock-in amplifier (Princeton Applied Research Corp., Princeton, New Jersey, U.S.A., - Model 186) which utilized the reference signal generated at the variable speed chopper to extract the signal wave form and present this

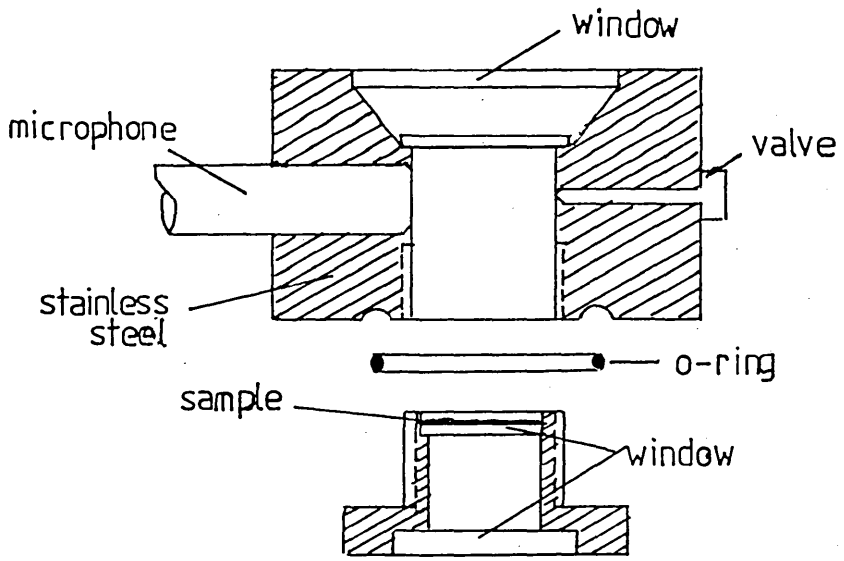

Fig. 2.6.(99)

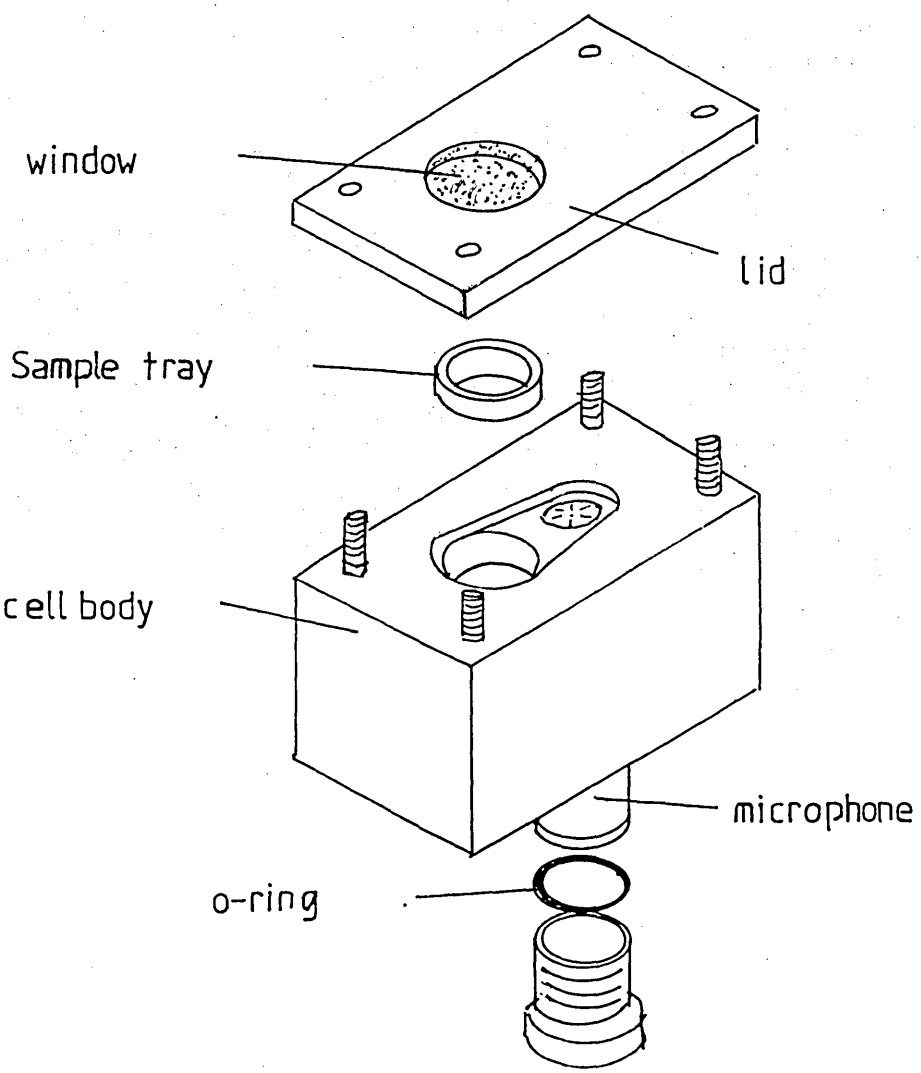

Fig. 2.7.(101)

as DC potential to a potentiometric chart recorder (Servoscribe, Model 511).

Alternatively, for producing corrected spectra, the output from the lock-in amplifier was taken to a scan recorder (Model4101 Princeton Applied Research Corporation). This scan recorder was employed in the two channel mode to store a reference spectrum of carbon black and a sample spectra. The spectral correction was then performed by an internal ratiometer unit and the corrected spectra displayed on the potentiometric chart recorder.

The single beam instrument could be used for near-infrared studies by changing the grating and source. The grating employed in such work was a plane diffraction grating of (50 x 50 mm, 300 lines mm^{-1}) blazed at 2μm with fixed, 2.5 mm wide entrance and exit slits. This arrangement provided a half-spectral bandwidth of 30 nm at the exit slit of the monochromator. To prevent overlapping of spectral orders of diffraction cut-on filters were used. The spectral range of the two filters are 0.8-1.5μm and 1.5 to 2.7μm. The source employed was a 250W quartz-halogen tungsten filament lamp which had a maximum emission intensity of 0.603 mW in the near-infrared region [100], (Type A1/223 Phillips Electricals Ltd., Croydon) and having a recommended operating voltage of 24V/DC. At this voltage the source has a reported average useful lifetime of 50 hours. By operating the lamp at a slightly lower voltage the lamp can provide similar radiant power and hence an extended lifetime may be obtained as can be seen from the manufacturers data, Figure 2.8. Although the xenon source has twice the emission intensity of the tungsten source [100] in

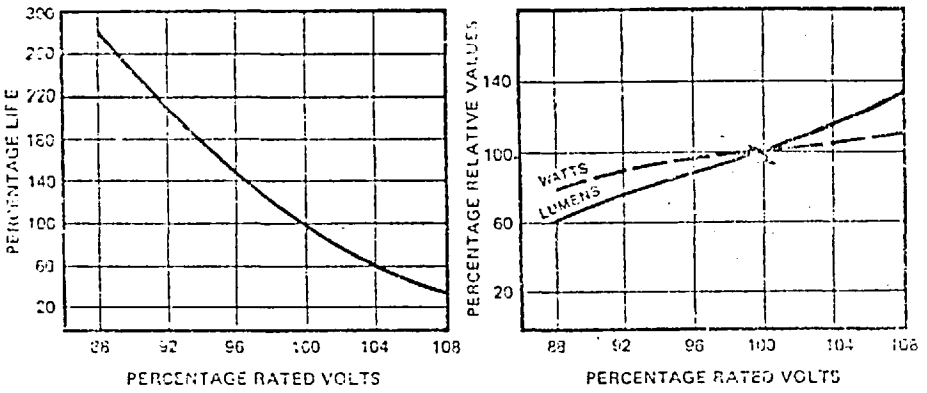

Figure 2.8: Effect of voltage variation on lamp life of the 250W tungsten source.

the near-infrared region, the spectrum from the xenon arc lamp has the disadvantage of having some broadened xenon lines superimposed upon the continuum. This can result in some difficulties occurring in the power spectrum correction procedure

2.3 Double beam instrumentation

Figure 2.9 shows the instrumental assembly of a double beam optoacoustic spectrometer [102]. The source employed was a 300W, short-arc high pressure xenon lamp with integral aluminium parabolic refelctor and 25mm diameter sapphire windows (Type VIX 300UV, Varian Associates). This source was comparatively smaller than the 1kW xenon arc, had a good collection efficiency at the monochromator entrance slit and also had a ultraviolet-visible maximum intensity of 1.11mW [100]. The lamp was mounted within a fan-cooled housing (Type R300-1, Varian Associates) and powered at 15V and 20A by a Varian Associates PS-300-1 power supply unit. The radiation was focused by means of a silica lens (25mm diameter with 70mm focal length) on to a plane of rotation of a variable-speed rotating sector (Model 9479, Brookdeal Electronics Ltd) placed adjacent to the entrance slit of the f/4 grating monochromator (Metrospec.DGO Ltd - Surrey). For use in the UV-visible region the mono-

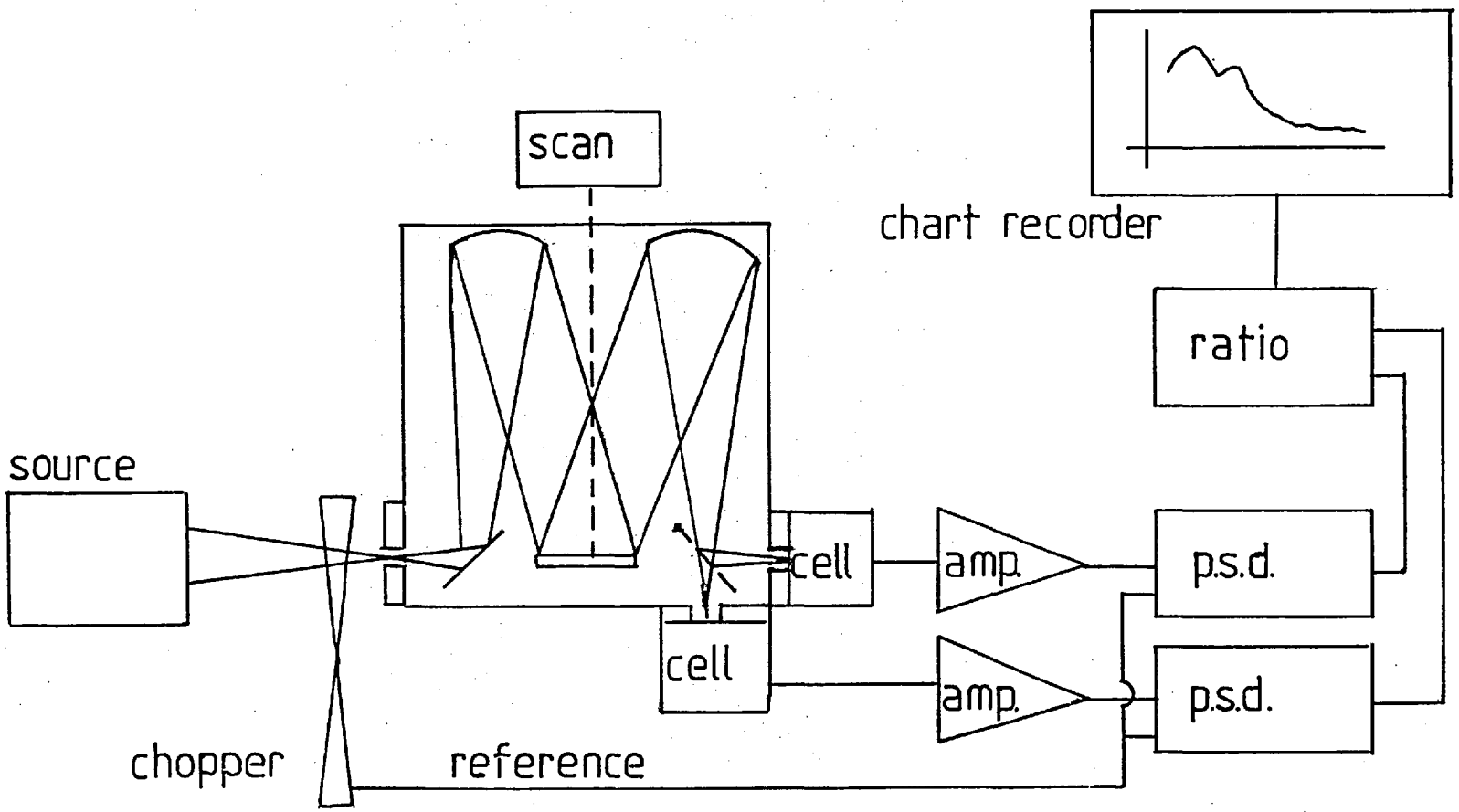

Fig. 2.9. Schematic diagram of the double beam optoacoustic spectrometer.(102)

chromator was fitted with a plane diffraction grating (50x50 mm, 1200 lines mm^{-1} blazed at 300nm). (For near-infrared studies the monochromator was fitted with a plane diffraction grating (50x50 mm, blazed at 2μm). Chance OX5 filters were used at each exit slit of the monochromator to reduce interference from overlapping spectral orders of diffraction). The monochromator was also fitted with two exit slit assemblies in each of which fixed slits ruled on silica plates could be positioned to provide spectral half-bandwidths of 1,2,5,10 and 20 nm in the UV-visible region. In order to prevent the transmission of radiation at wavelengths less than 490 nm from overlapping spectral orders of diffraction, yellow coloured glass filters (Type 26-4317, Ealing Beck) were used at each exit slit when measuring optoacoustic spectra in the visible region at wavelengths greater than this. Within the monochromator housing the dispersed radiation was split by a plane mirror positioned so as to direct radiation of equal intensity at each exit slit. Radiation emerging from the exit slits was focused by using front-surfaced concave mirrors (50 mm in diameter, 200mm focal length) and directed into the optoacoustic cells as shown in Figure 2.10. The microphone transducers employed were of the same type described for the single beam instrument.

Two aluminium cells of the same design (Figure 2.10) were placed at the exit slit of the monochromator. The cells were sealed by means of double silica windows and samples were positioned on a silica plate of 20 mm diameter mounted in an aluminium tube, which was placed in the cell and sealed by means of three locking-nuts.

Wavelength scanning of the continuum radiation was achieved by means of a stepping motor connected directly to cam-drive mechanism of the grating mount within the mono-

OPTOACOUSTIC CELL.

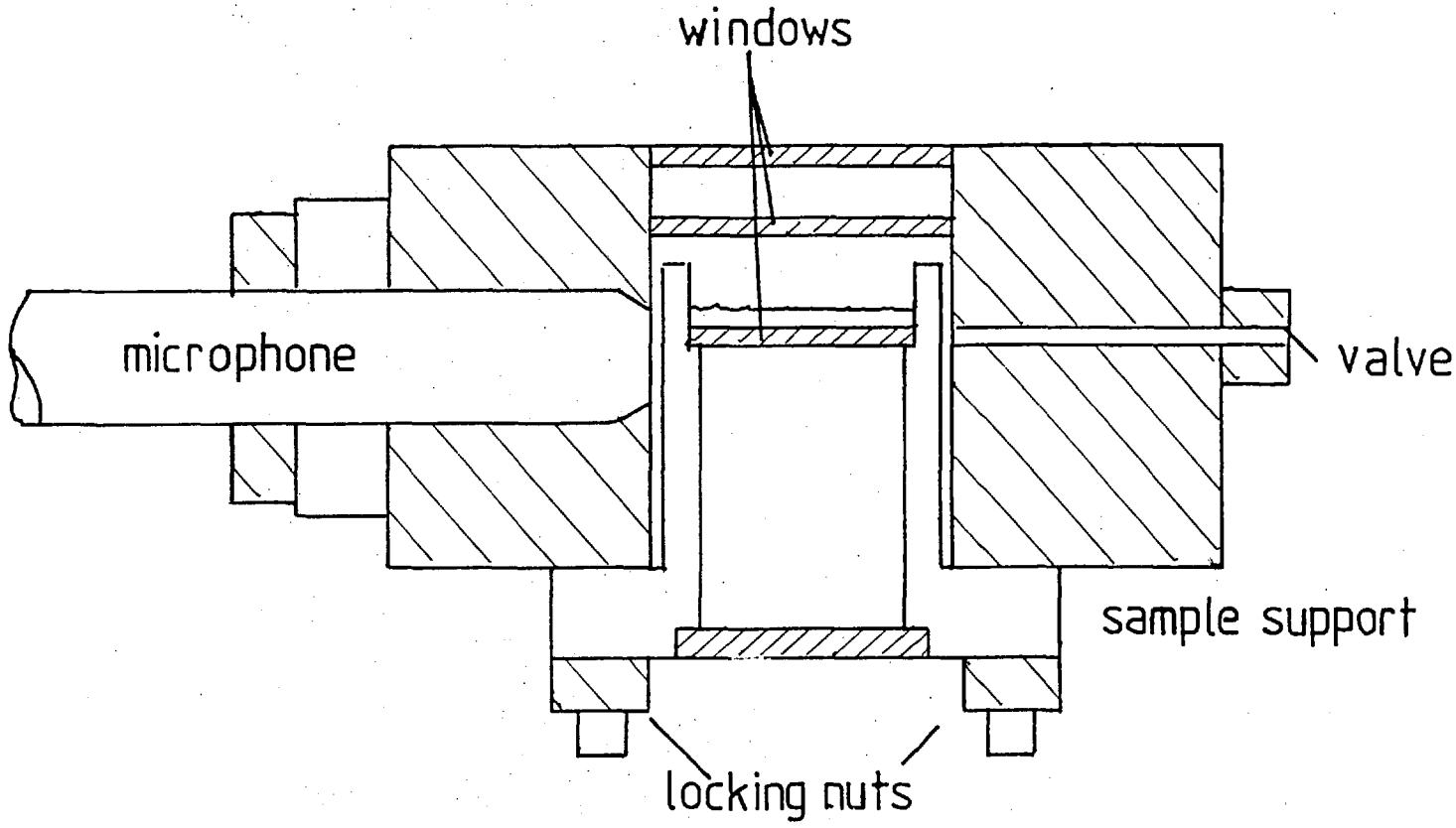

Fig. 2.10.(102)

chromator. Pre-selected scanning rates of 200, 100, 50, 15 nm min^{-1} were available by push button controls; with the forward and reverse scanning direction selection and modulation frequency controls were all mounted on to a front panel of the spectrometer assembly. The optoacoustic signals from the microphone were led directly *via* screened cables to two lock-in amplifier systems (Reference Channel, Model 124A amplifier, Princeton Applied Research Corp., sample channel, model 9502 Brookdeal Electronics Ltd). The reference signal for each amplifier was that generated by the LED-photoiodide assembly associated with the variable speed rotating sector. The lock-in amplifiers extracted the signal waveform and presented these as DC potentials to a ratiometer unit (Brookdeal Electronics Ltd, Model 5047); the signal from the reference cell was presented directly to the denominator input whilst the sample signal was taken to the numerator input. The ratiometer output was shown as a DC potential and taken *via* a resistant-capacitor time constant circuit (2s), to a potentiometric chart recorder (Servoscribe Model RE511). Corrected optoacoustic spectra were obtained by recording the output of the ratiometer against the wavelength of the incident radiation during wavelength scanning at the monochromator.

The model 9502 (Brookdeal Electronics Ltd) lock-in amplifier was capable of either making two-phase p.s.d. measurements or use as an automatic vector voltmeter. In the vector voltmeter mode, direct measurements could be made of signal amplitude without the need to optimise the phase of this signal relative to that of the reference signal which had previously been the case for the Model 186 lock-in amplifier. In addition, a direct readout of the phase of the optoacoustic signal relative to the reference

signal was provided by this system.

2.4 Power spectrum correction

The OAS spectrum of carbon black was assumed to be identical to the power spectrum of the source. Hence carbon black was used as a reference abosorption material and employed for the correction of observed spectra of other samples for the variation of source power with wavelength. Because of its smaller particle size and enhanced surface area compared with powdered carbon black, a smoked glass plate (microscope cover slip) was used as the reference absorber.

An optoacoustic cell containing a black absorber serves as a radiometric detector of incident energy and, hence, other similar types of detector may be employed as a reference for the spectral correction of optoacoustic spectra. The pyroelectric detector is such a device and is being used increasingly in modern infra-red spectrometers as a thermal detector of radiation. The pyroelectric effect is based on a crystal structure possessing a permanent dipole moment. The absorption of modulated radiation produces temperature fluctuations within the crystal causing a change in the dipole moment. An electric signal, the magnitude of which is dependent upon the energy of the incident radiation, is detected by a pair of electrodes bonded to the crystal. By coating the pyroelectric crystal with a fine metal black surface, the detector may be employed in the ultraviolet and visible spectral regions. A commercially available (Eltec. 404 cm Rofin Ltd, Egham, Surrey) lithium tantalate pyroelectric detector was examined for use as a reference detector

for spectra correction and this was mounted in a sealed steel cell, to minimise thermal noise, at an exit slit of the monochromator of the double beam optoacoustic spectrometer.

With the double beam instrument, transmission spectra could also be obtained from suitable samples by placing the sample between the entrance to the sample optoacoustic cell and the exit slit of the monochromator. Both the sample and reference cells were loaded with identical carbon black samples for these measurements.

CHAPTER THREE

SOME QUALITATIVE STUDIES BY OPTOACOUSTIC SPECTROSCOPY (OAS)

3.1 Introduction

This chapter discusses experiments which illustrate the complementary nature of optoacoustic, reflectance, and transmission spectroscopy and demonstrates the relative freedom from interferences caused by scattered light effects exhibited by optoacoustic spectroscopy.

The optoacoustic effect is observed only when modulated electromagnetic radiation is absorbed by the sample under investigation. In optoacoustic spectroscopy the signals observed at a given wavelength will provide a measure of the ability of the samples to absorb incident radiation at that wavelength. Therefore, as might be expected, if the wavelength of the incident radiation is varied an optoacoustic spectrum is obtained which closely resembles a conventional absorption spectrum as determined by measurements of the transmitted radiation and is complementary to the diffuse reflectance spectrum.

The optoacoustic spectrum can provide optical information about the bulk of the material when the surface of a solid is not highly reflective. This is useful in the study of semiconductors, insulators and even metallic systems that may be difficult to study by conventional absorption or reflection techniques.

For air and water sensitive materials optoacoustic spectroscopy offers a simple technique, compared with the conventional optical spectroscopic methods, as an absorption spectra can be obtained in an inert atmosphere within a closed cell under controlled conditions.

The OAS signal is obtained from a relatively shallow surface layer of the sample, the depth of which is determined not only by its optical absorption coefficients but also by the thermal characteristics of the sample and the manner in which these control the heat transfer of the alternating temperature wave produced within the sample. As discussed previously in Chapter One the rate and efficiency of this temperature transfer varies with the frequency of modulation of the incident radiation. By varying the modulation frequency it is possible to select the sample depth examined and thereby, in principle, absorption spectra of completely opaque samples may be obtained.

Unlike most optical spectroscopic technique opto-acoustic spectroscopy is not limited by the wavelength range of a photoelectric detector. The sample itself constitutes the radiation detector and a microphone rather than a photoelectric device is employed as the signal detector. Therefore, studies over a wide range of wavelengths are possible without changing the detector, provided the radiation of sufficient intensity is available at the wavelength of interest.

Optoacoustic spectroscopy is relatively insensitive to errors caused by light scattering from the sample; unlike conventional absorption spectroscopy only the photons absorbed by the sample produce an OAS signal. Thus opto-acoustic spectra may be obtained directly from powders and biological fluids containing high molecular weight proteins or fat membranes without sample pretreatment.

A recent application of the optoacoustic effect as a calorimetric technique for the determination of the absorption characteristics of solid samples has been in the study of the absorption properties of optical components employed in laser technology. With the aid of pulsed laser sources several workers [77,80] have employed this technique for the determination of low absorption coefficients of optical windows.

To demonstrate the complementary nature of optoacoustic spectrometry to the more conventional techniques of absorption and reflectance spectroscopy a study has been undertaken of a variety of laser mirror samples, produced by the deposition of layers of dielectric materials onto a silica substrate. The results obtained show not only the versatility of the optoacoustic spectrometer employed but provide an interesting example of the 'depth control' achieved by this technique.

3.2 AN EXAMINATION OF THIN-FILM, DIELECTRIC COATINGS ON LASER MIRRORS

3.2.1 Introduction

With the increasing use of more powerful laser sources in both research and the manufacturing industries it is becoming of great importance to be able to monitor and determine the radiation absorption characteristics of the optical components employed with such intense sources. For the examination of materials with low absorption coefficients and highly reflecting surfaces conventional transmission methods are rarely employed due to the large errors induced by the highly scattering nature of

the samples.

In the studies described here samples of laser mirrors have been examined to determine the spectral characteristics within the ultraviolet and visible regions of the spectrum.

3.2.2 Experimental

The laser mirror samples were supplied as 50 mm square, 1 mm thick, flat plates (Laybold-Heraeus Gmbh, Hanau, West Germany) 16 mm diameter discs were cut from these for examination by OAS. Four samples were examined using a double beam optoacoustic spectrometer similar to that described in Chapter Two. A pyroelectric detector fitted with a sapphire window (Eltec. Type. 404 cm, Rofin Ltd., UK) and mounted inside a stainless steel housing was employed as the reference channel to correct the spectrum for the variation of the incident intensity with wavelength.

Two samples of laser mirror were of multilayer composition (of alternate layers of titanium dioxide and silicon oxide) on a glass substrate. The third sample comprised a single coating of titanium dioxide and the fourth sample examined was an uncoated glass plate of similar composition to the substrate employed to produce the coated samples.

Optoacoustic spectra of the samples were obtained by placing the sample discs on the silica tray and sealing these within the optoacoustic cell. Transmission spectra were obtained by positioning the samples above the opto-acoustic cell, which contained a carbon-black sample prepared

by smoking a glass plate. Suitable masking of the entrance windows to the cell ensured that only radiation transmitted by the sample entered the cell and produced an OAS signal. Zero and 100% transmission levels were set by blanking-off the sample beam and having no samples present, respectively. The sample reflectance spectra were obtained in a similar manner, employing the optoacoustic cell as a black-body radiometric detector. The samples were mounted onto black, non-reflecting cloth and positioned over the folding mirror employed to direct the radiation from the exit-slit of the monochromator into the optoacoustic cell. In this manner, only radiation reflected by the sample entered the optoacoustic cell containing a carbon-black sample.

The spectra of the four samples were obtained with a spectral half-bandwidth of 10 nm within the wavelength range 300 nm to 650 nm. A scan rate of 50 nm min^{-1} was employed with an instrumental time-constant of 3 seconds. Wavelength calibration was achieved by reference to an optoacoustic spectrum of powdered holmium oxide obtained under identical experimental conditions.

3.2.3 Results

The optoacoustic (——), transmission (---), and reflectance (•••) spectra of the four samples are shown in Figures 3.1 - 3.4 and may be considered for comparison purposes in three wavelength regions, the ultraviolet (300 nm - 400 nm), the blue (400 nm - 550 nm) and the red (550 nm - 650 nm) spectral regions.

Figure 3.1 shows the spectra obtained from the uncoated glass substrate. The reflectance spectrum exhibits

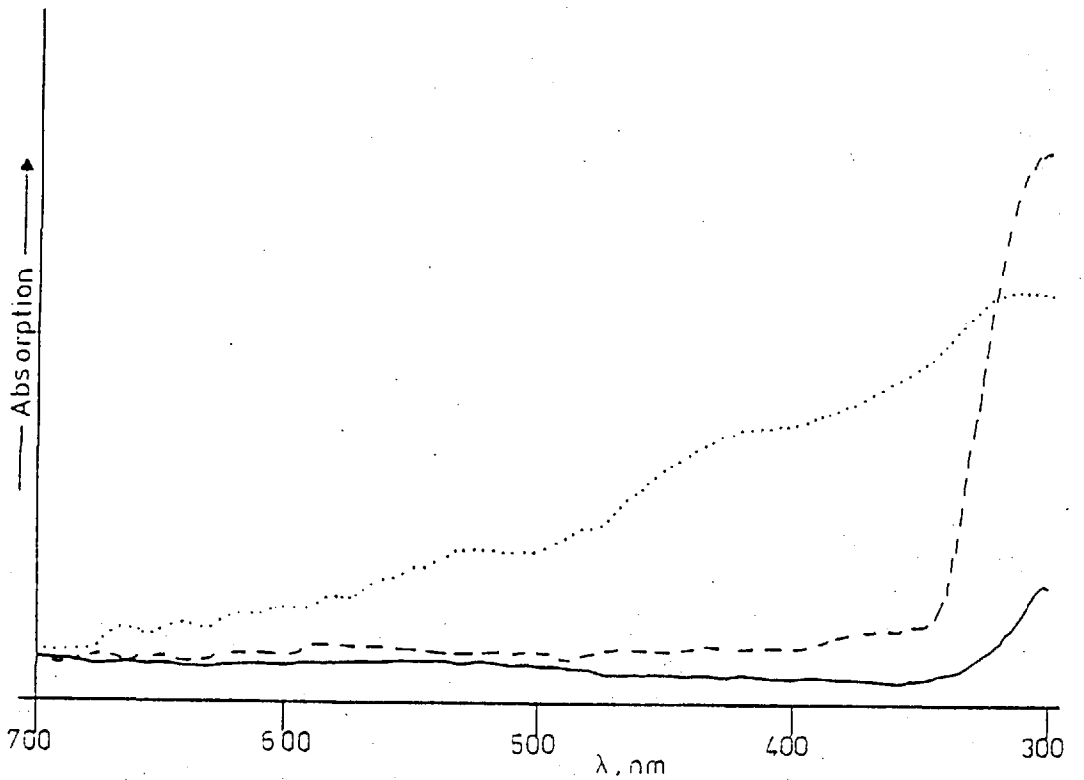

Figure 3.1: The optoacoustic (——), transmission (---) and reflectance (···) spectra of the uncoated glass substrate plate.

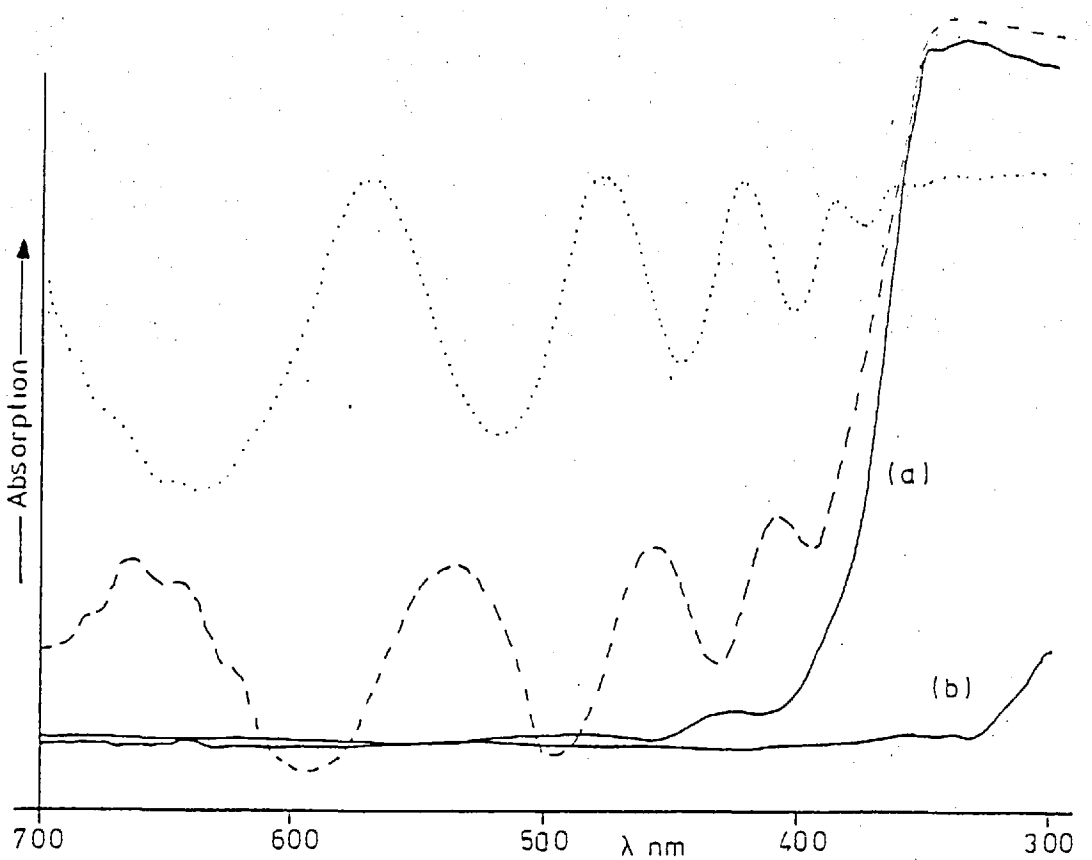

Figure 3.2: The optoacoustic (——), transmission (---) and reflectance (···) spectra of the plate of glass substrate with a single coating of titanium oxide.

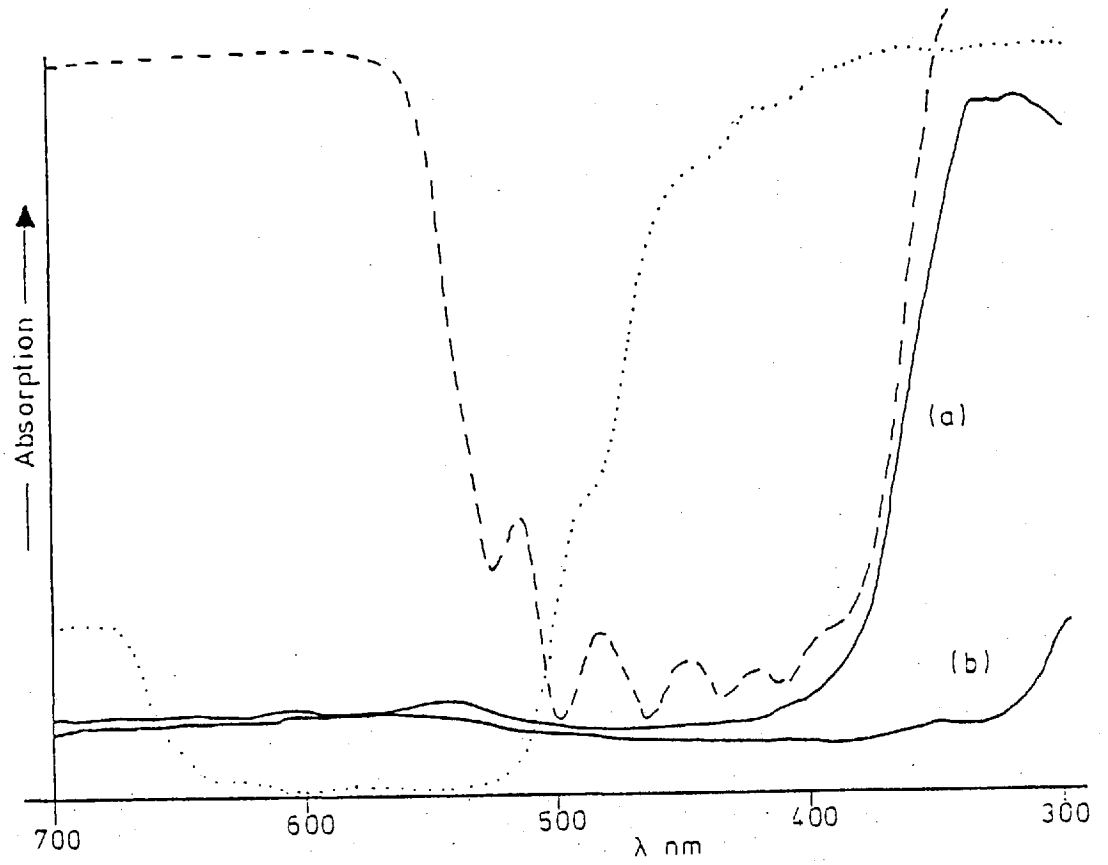

Figure 3.3: The optoacoustic (——), transmission (---) and reflectance (···) spectra of glass substrate with alternate multilayer coatings of silicon and titanium oxides.

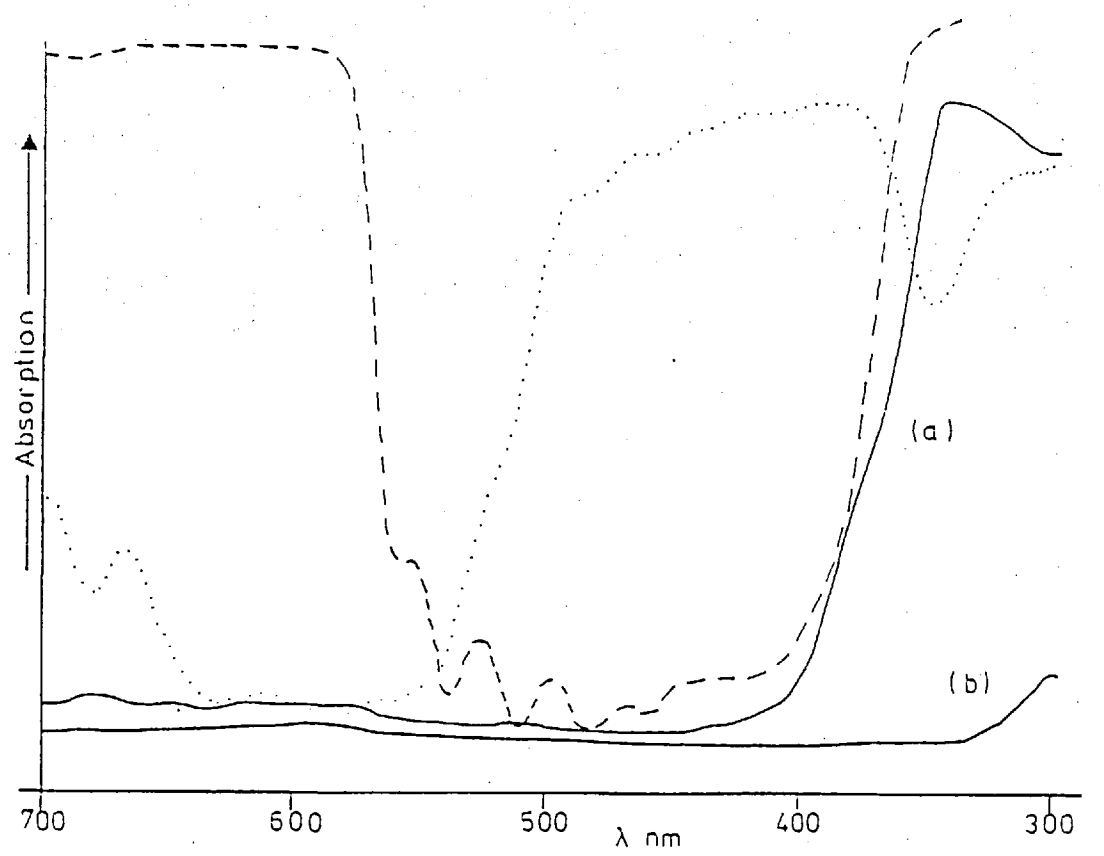

Figure 3.4: The optoacoustic (——), transmission (---) and reflectance (···) spectra of the glass substrate with alternate and multilayer coatings of silicon and titanium oxides.

a high specular component and little spectral detail is available. Both the optoacoustic spectrum and the transmission spectrum show similar ultraviolet absorption by the glass. The optoacoustic spectra obtained from the glass blank were found to be identical irrespective of which surface was examined.

The spectra from the titanium dioxide coated glass is shown in figure 3.2. An ultraviolet absorption band is shown in both the transmission spectrum and the reflectance spectrum. At longer wavelengths the spectrum is complicated by the apparent absorption maxima produced by the appearance of an interference pattern giving rise to apparent absorption maxima. The optoacoustic spectra are more simple. If the top, coated, surface of the glass is examined (spectrum a) then a clear absorption band characteristic of titanium dioxide is observed in the ultraviolet region with a cut-off at ca 380 nm. When the uncoated glass surface is examined (spectrum b) the glass substrate absorption spectrum is obtained.

Figure 3.3 shows the spectra obtained from a dielectric-coated laser mirror. The reflectance spectrum shows the sample to be highly reflecting in the red region but to have apparently high absorption characteristics in the blue and ultraviolet spectral regions. The interference pattern is from the alternate coatings of the dielectric layers. The transmission spectrum exhibits apparent absorption bands in the red and ultraviolet regions. The interference pattern caused by the multilayer coating is evident. The optoacoustic spectrum of the coated glass surface illustrates that strong absorption occurs only in the ultra-

violet region and is characteristic of titanium dioxide. There is relatively little absorption at wavelengths greater than 400 nm. Once again the optoacoustic spectrum obtained when the rear uncoated surface is illuminated directly (b) shows the weak ultraviolet absorption by the glass substrate.

Figure 3.4, the spectra of a second laser mirror, shows the complementary nature of the reflectance, transmission and optoacoustic spectra and is similar to figure 3.3. As before, simply by reversing the sample to illuminate the rear uncoated surface directly, the optoacoustic spectrum of the coating or substrate may be obtained. As the optoacoustic effect produces a signal only following the absorption of radiant energy the apparent absorption due to the interference effects of the multilayer coatings is not observed in the optoacoustic spectra.

Although the transmission and reflectance spectra differ for samples 3.3 and 3.4 it is apparent from the optoacoustic spectra that this difference is not due to the nature of the absorbing titanium dioxide but a function of the thickness and separation of dielectric layers deposited on the glass substrate.

3.2.4 Discussion

It is evident from the spectra presented here that optoacoustic spectrometry is a complementary technique to the conventional spectroscopic technique utilizing transmission and reflectance spectra. As only the radiant energy absorbed by the sample produce an optoacoustic signal the technique may be employed as a rapid calorimetric

method of analysis.

Unlike the more conventional calorimetric methods involving the use of temperature transducers to monitor directly the variations in temperature of a sample following the absorption of radiant energy, optoacoustic spectrometry employs a microphone to follow the pressure changes in an enclosed cell caused by the changes in temperature of the sample. The indirect monitoring of sample temperature provides a number of practical advantages. Direct contact between the transducer and sample is not necessary thus enabling a variety of sample types to be examined with little difficulty. Because the microphone transducer only responds to the periodic variations in the gas pressure within the cell, freedom from ambient temperature drift is ensured and lock-in amplifier systems are easily applied for analytical signal extraction and treatment. The use of an indirect method for temperature monitoring also provides OAS with the capability for the examination of surfaces as shown here. The sample depth examined is a function of the optical absorption coefficient of the material under study and its thermal characteristics. The spectra of laser mirrors discussed above demonstrates how by reversing the sample, the spectrum of either the dielectric coating or the substrate may be obtained.

3.3. Photochromic Effects Examined by OAS

As an example of the freedom from interferences caused by scattered radiation exhibited by optoacoustic spectroscopy a study has been conducted with a number of photochromic materials.

The production of a reversible light-induced colour change in a material is referred to as photochromism or phototropism [103], the latter term being rarely used by modern writers, and may be considered a particular branch of photochemistry. In the absence of an exciting radiation the photochromic system has a single stable electronic configuration with a characteristic absorption spectrum. When the system is irradiated by radiation of suitable energy the absorption spectrum of the system changes; upon removal of the excitation source the system reverts to its original state.

$$X(\lambda_1) \overset{h\nu}{\rightleftharpoons} Y(\lambda_2) \qquad (3.1)$$

The definition of photochromism [23,104] in terms of a single chemical species excludes reversible chemical processes operating through a cyclic series of reaction as

$$\begin{aligned} M &\longrightarrow N \\ N+O &\longrightarrow M+P \end{aligned} \qquad (3.2)$$

An example of such a reaction is the photoreduction (bleaching) of methylene blue with iron(II) ions and subsequent oxidation (recolouration) by air.

Early observations of photochromism were made by Meer [105] and later by Phipson [106]. Meer showed that the potassium salt of dinitromethane changed colour when exposed to exciting light. Phipson reported an unusual experiment concerning a painted gate post. During

daylight the gate post appeared black but after nightfall was white. This photochromic effect was due to the presence of the pigment 'Lethopone' in the paint used to treat the gate post.

The quantum yield, Φ, of a photochromic reaction is a measure of the fraction of the ground state molecules capable of absorbing radiant energy and being promoted to the excited state. Φ is always less than unity and the quantum loss may be attributed to deactivation process for the activated molecules.

Photochromic processes can be classified on the basis of their reaction mechanisms. The main types are heterolytic cleavage [107], homolytic cleavage [108], cis-trans isomerism [109], tautomerism [110] and development of colour centres in inorganic solids [111].

3.3.1 Salicylidene-2-chloroaniline

It was reported by Cohen and Schmidt [112] that anils such as salicylidene-2-chloroaniline are photochromic. On irradiation by near UV light (ie.350 to 400 nm), the colour of the material deepens from yellow to orange-red with the formation of an absorption band in the visible region (λ nm). Colour reversal from orange-red to yellow is achieved by the absorption of radiation at λ nm or, more slowly, in the dark. The structure of salicylidene-2-chloroaniline is

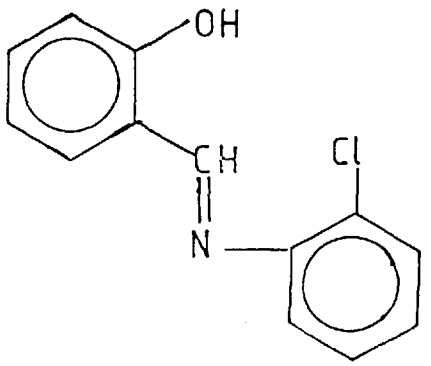

(3.3)

Salicylidene - 2 - chloroaniline

For the studies described here the salicylidene-2-chloroaniline sample was prepared by condensation under reflux between salicylaldehyde and an O-chloroaniline (1:1 mole ratio) in ethanol (Analar Grade, BDH) for 8 hours. The compound was then precipitated by cooling overnight and recrystallised twice from ethanol. The compound thus obtained was dried in a vacuum. It had a melting point of 86°C and the identity was confirmed by using IR and NMR spectroscopy.

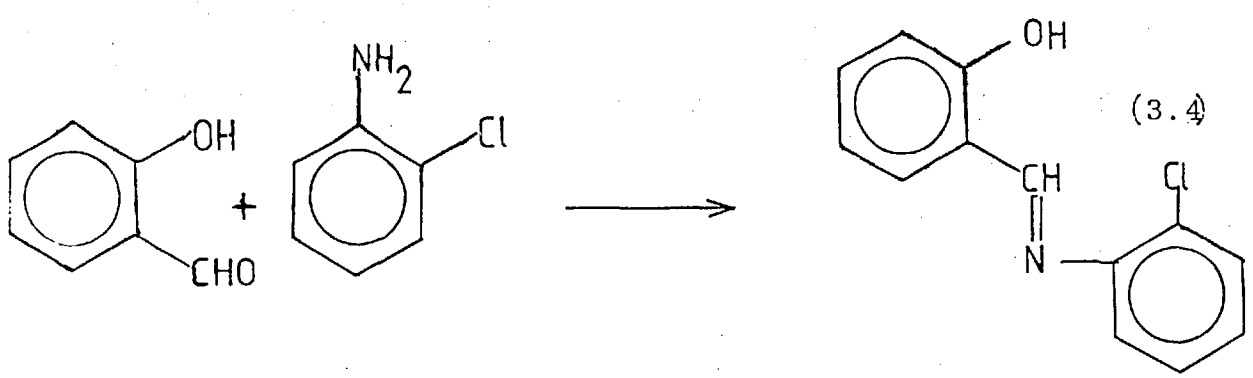

(3.4)

Salicylaldehyde 2 Chloroaniline Salicylidene-2-chloroaniline

The compound showed a strong >C=N- absorption peak (1615 cm^{-1}) in the IR spectrum (Fig. 3.5). The NMR spectrum showed singlets at δ8.4 and 13.2 ppm each integrating for one proton, which corresponds to a vinyl hydrogen and a phenolic

Figure 3.5: Infrared spectrum of salicylidene-2-chloroaniline.

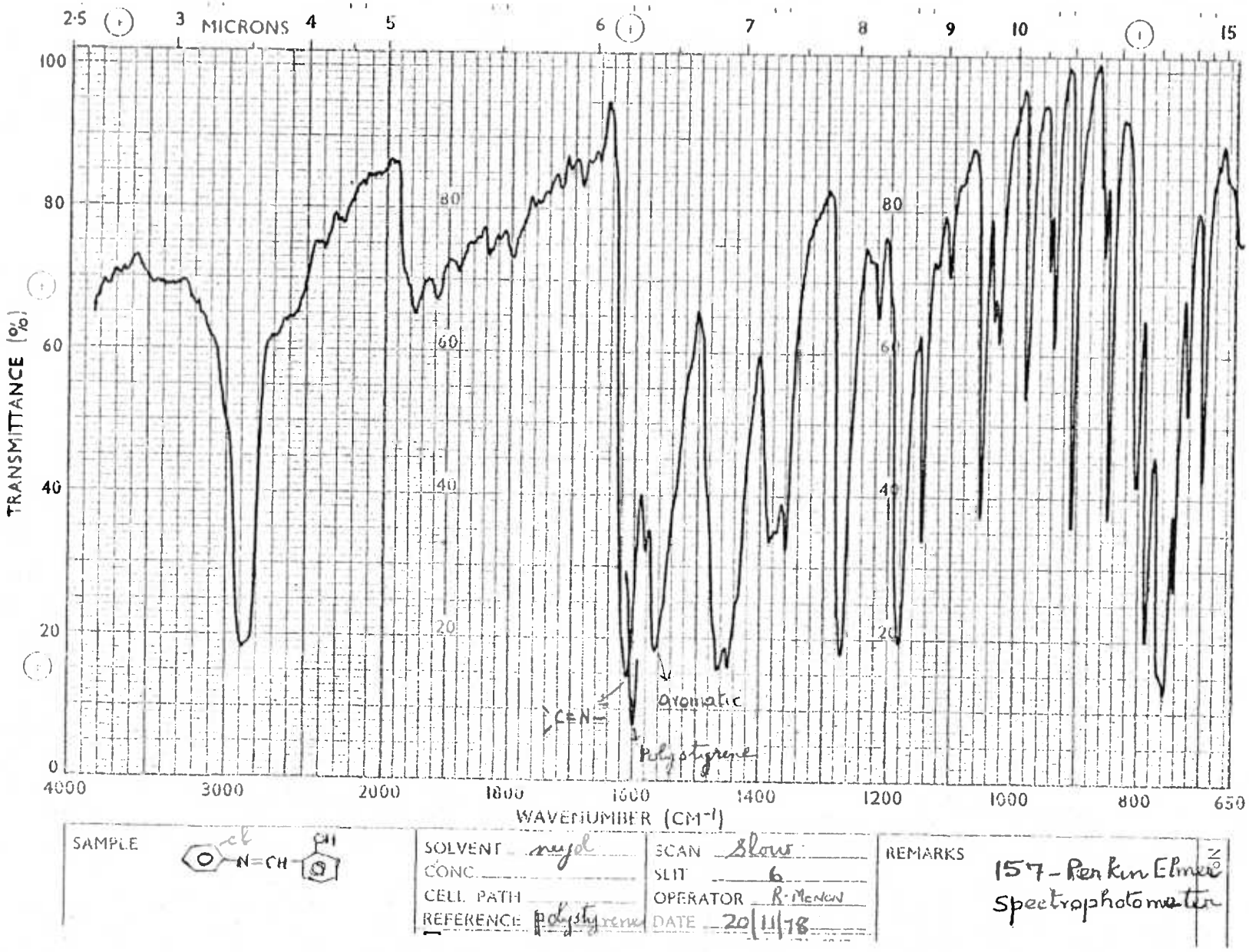

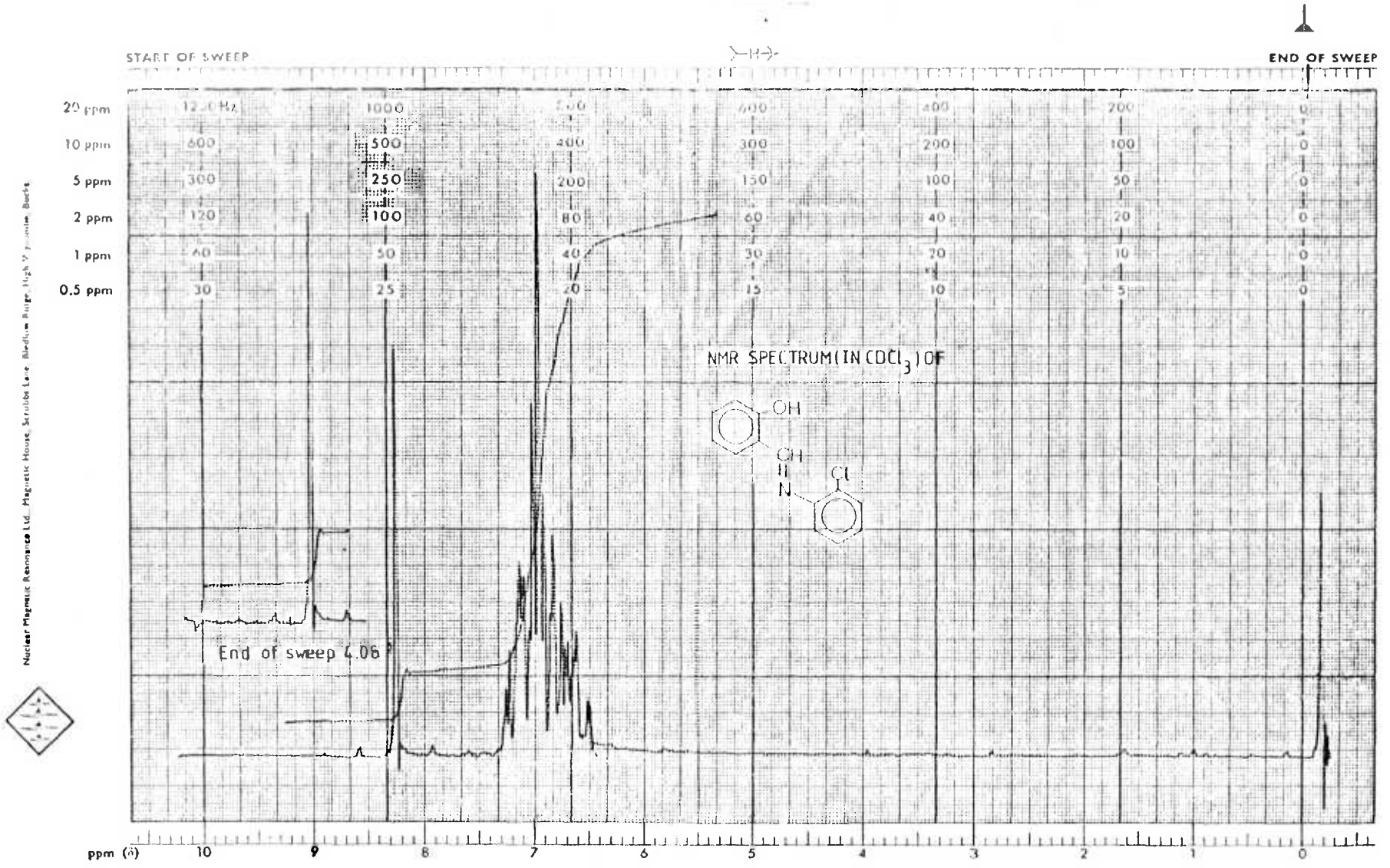

Figure 3.6: NMR spectrum of salicylidene-2-chloroaniline.

hydroxyl group, respectively, as shown in Figure 3.6.

For the examination of the photochromic nature of salicylidene-2-chloroaniline, a double beam instrument described in Chapter Two was employed in a single beam mode. The secondary illumination was effected by the use of a 250 watt UV lamp focussed by means of a silica lens (diameter 50mm and focal length 22.5mm) into the sample cell. An interference filter of narrow bandwidth (50 x 50 mm square with bandwidth of 25 nm at 375 nm (Baird Atomic, 31-31-2)) was inserted between the source and optoacoustic cell. Spectra were taken (Figure 3.7) both before the excitation by the mercury arc and whilst under illumination. The scan rate was 100 nm min^{-1} with a 20 nm monochromator bandpass and an instrumental time-constant of 1 second. The colour reversibility was obtained in thirty minutes in the dark. Wavelength calibration was carried out using a sample of powdered holmuim oxide and the spectra were corrected manually against a spectrum obtained using a sample of carbon black in the cell.

In the spectra of salicylidene-2-chloroaniline (Fig. 3.7) the absorption band in the visible region is due to the formation of an orange coloured product in the excited state as a result of the absorption of photons. This formation of colour in the excited state could be due to an intramolecular proton shift[112]. Photochromism in anils was first observed in the solid state and for this reason it was believed that the mechanism of photochromism in anils involved aggregation in crystal lattice interactions.[113] However Cohen _et al_ [112,114] by means of a low temperature

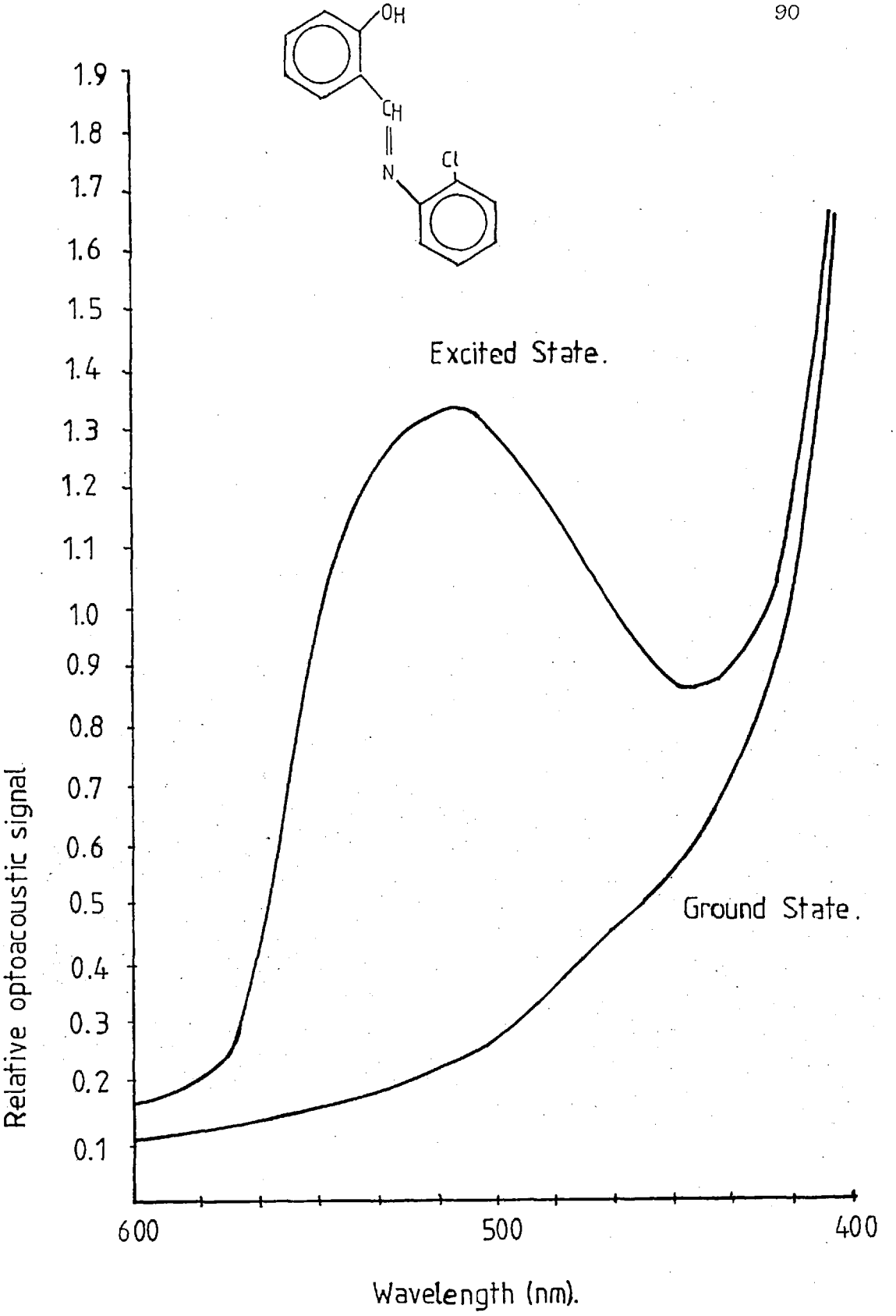

Figure 3.7. OAS Spectra of Salicylidene - 2 - chloroaniline in the in the ground and excited states. (Manually corrected.)

study of anils in solution demonstrated that an intramolecular phenomenon was involved in the mechanism. Cohen et al[112, 115] continued their extensive investigations and described two major types of anils, α and β. The α-type is photochromic and the β-type is thermochromic. In crystalline anils of salicylaldehyde photochromism and thermochromism are mutually exclusive properties. The α-type permits the photochromic formation of trans-keto structure whereas the β-type prevents this, but does allow the thermal formation of the cis-keto structure [110].

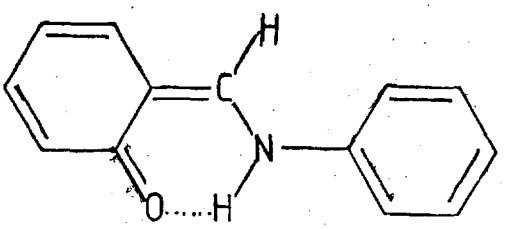

Cis-Quinoid or cis-keto

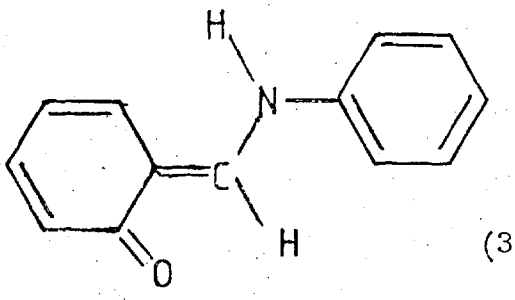

Trans-Quinoid or trans-keto (3.5)

In the α-type anils, the fading of the red colour follows first order kinetics with an activation energy in the range of 83.7 to 125.6 k $Jmol^{-1}$. Low temperature photochromic and spectroscopic studies on salicylidene anils have been undertaken by several workers [116,117] who have confirmed Cohen et al's[112,114] observation on the occurrence of the hydrogen transfer tautomerism to a keto-structure.

Therefore it appears likely that the photochromic reaction of 2-chlorosalicylidene aniline follows the reaction pathway

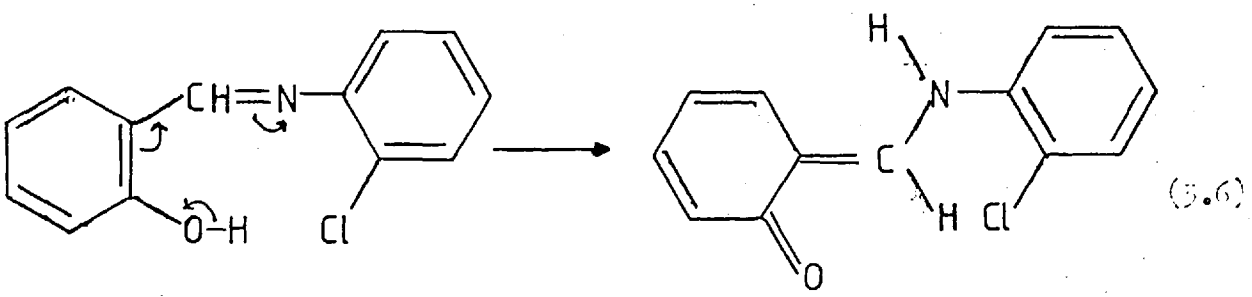

(3.6)

Yellow (ground state) Orange (excited state)

3.3.2 Silver Bromide

Silver bromide is widely used in photography today and it is well known that the prolonged exposure of silver bromide crystals to visible light causes darkening of the yellow colour of the crystals due to the formation of colloidal silver. Bromine is also released in the overall reaction:

$$2AgBr + h\nu = 2Ag + Br_2 \qquad (3.7)$$

It was shown by West and Saunders [118] that this decomposition can be prevented by introducing Copper(1) ions at concentrations greater than 0.0001 moles copper(1) per mole of silver bromide. This work of West and Saunders resulted from the earlier work of Urbach et al [119, 120]. Upon the absorption of a photon by silver bromide in the presence

of copper(I) ions, the excess energy is transferred to the copper(I) ions resulting the oxidation to copper(II) ions.

The reaction between Cu^+ in the lattice and the positive hole is reversible according to the equation [118],

$$(Cu^+1)_0 + (Br1)_{+1} \rightleftarrows (Cu1^{++})_{+1} + (Br1^-)_0 \qquad (3.8)$$

where the suffix 1 indicates that the species occupies a lattice site, the symbol $(Br1)_{+1}$ denotes the untrapped positive hole, and the suffix outside the brackets indicate the effective charge of the lattice site. The right-hand side of the equation represents a copper(II) ion occupying a lattice cation site, constituting the trapped hole, adjacent to a bromide ion in an anion site. Thus due to photolysis of silver bromide there is no detectable bromine evolution because the mobile untrapped holes attack the photolytic silver forming silver bromide.

Silver bromide containing copper(I) ions was prepared as follows. 20% aqueous silver nitrate (Analar Grade BDH) solution and hydrobromic acid (Analar Grade - BDH) were added together in a flask previously painted black on the outside. The precipitated silver bromide was then mixed with copper(II) sulphate solution (0.1% of the total weight) and the whole contents were allowed to stand for 1 hour. The precipitate was then filtered off and dried between filter papers. These procedures were performed in a dark room so as to avoid unnecessary bleaching of silver bromide. The silver bromide was then vacuum dried at room temperature. The optoacoustic spectrometer used was the same as for the salicylidene-2-chloroaniline already described. A 250 watt

mercury arc lamp was used as an excitation source. Spectra of the AgBr + Cu^+ were obtained both before the excitation by the mercury arc and while under this illumination as shown in Fig. 3.8. The reversibility of the colour was obtained after leaving it in the dark for a day.

The spectra of both the ground and excited states matches very well with the absorption spectrum reported by West and Saunders [118], especially the absorption of AgBr + Cu^+ in the excited state increases above 600 nm. The difference in the absorption at different wavelengths probably lies in the relation between the volume concentration of absorbed photons and copper(I) ions when the exciting wavelengths are in UV and visible regions respectively[118]. The photochemistry of silver bromide containing copper(I) illustrates a possible type of controlled storage of energy in crystalline solids. The interesting point with respect to energy storage is that trapping of positive holes by copper(I) ion is reversible. This behaviour of silver halides containing copper(I) had been made use of in the manufacture of photochromic glasses. Mechanisms of a typical photochromic silicate glass [121] with silver chloride impregnated with copper(I) ion can be described as follows.

The primary photolytics reaction can be represented as

$$Ag^+ + Cl^- \overset{h\nu}{\rightleftarrows} Ag^o + Cl^o \qquad (3.9)$$

An electron is released from the Cl^- and it is accepted by the Ag^+ ion. The silver atoms or very small aggregates of atoms form the colour centres. In the case of copper-sensitized photochromism the additional reaction can be

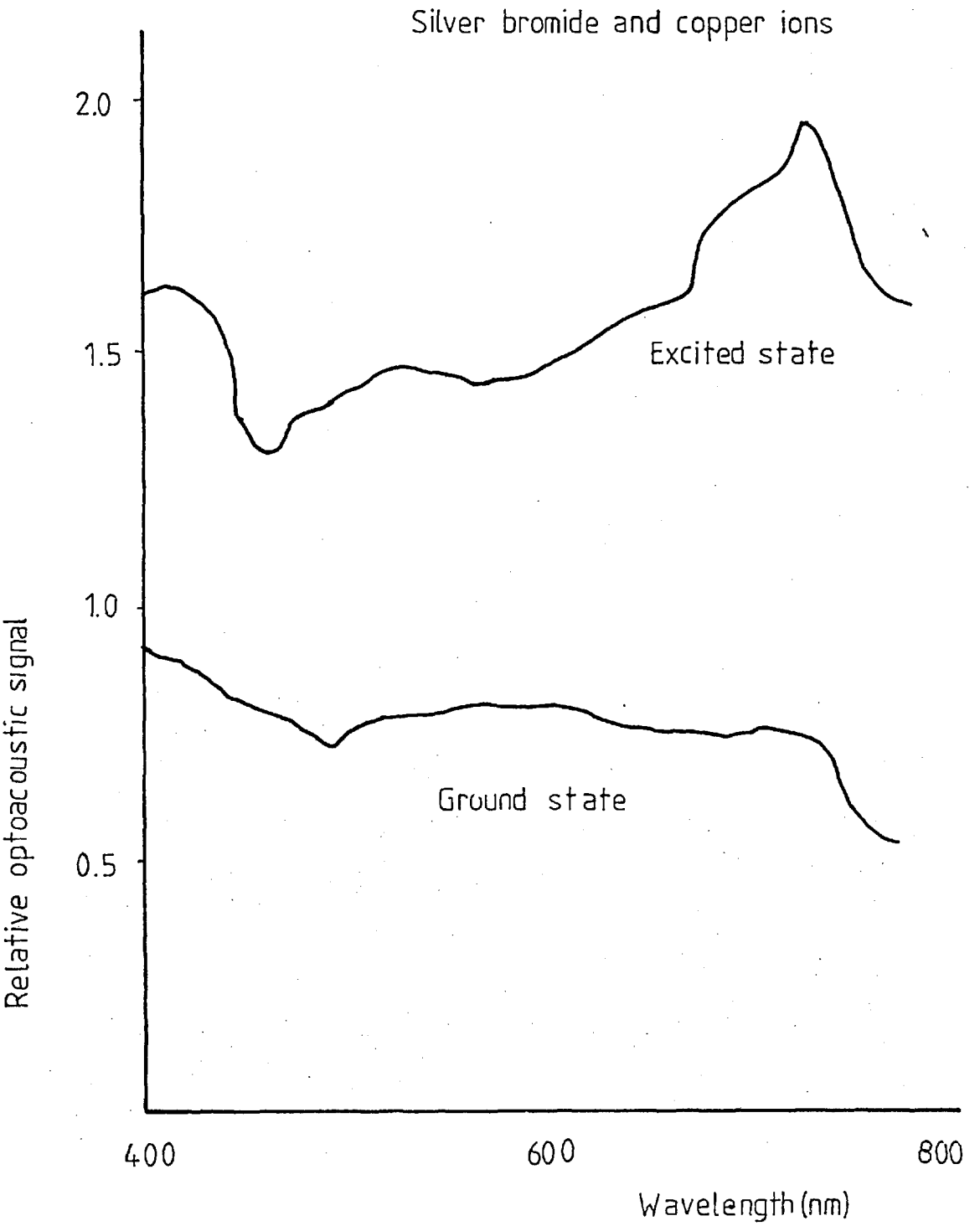

Figure.3.8. OAS Spectra of silver bromide and copper ions in the ground and excited states.(Manually corrected).

represented as

$$Ag^{+} + Cu^{+} \overset{h\nu}{\rightleftarrows} Ag^{o} + Cu^{++}. \qquad (3.10)$$

An electron is freed from the Cu^{+} ion and trapped by a Ag^{+} ion. Here the copper(II) ion as well as the silver contributes the absorption of visible light. These reaction products being metastable return to their original state if they are permitted to diffuse. Recently Malkin et al [122] have demonstrated the application of optoacoustic spectroscopy in relation to the photosynthetic process, especially in the determination of energy conversion efficiencies of the different stages of photosynthesis.

3.3.3 Reactolite Rapide

Photochromic glasses have gained commercial importance in recent years. These glasses are usually made by standard glass-melting and glass forming techniques and can be made in any desired shape. Being contained within a glass medium they have advantages over the other photochromic materials, e.g. the use of photochromic glasses for window materials and spectacle lenses. These glasses can be adapted in devices employing optical memory self-erasing display devices and architectural or automotive glazing.

The Reactolite Rapide sample examined was a photochromic glass supplied by the manufacturer (Chance-Pilkington, Asaph, Clwyd, North Wales). This is an alumino-phosphate based glass [123], exhibiting in its clear state a luminous transmittance of 90% at wavelengths above 400 nm and when exposed to bright sunlight darkens rapidly to 16% transmittance,

as shown in Figure 3.9.

Darkening of the photochromic glass was produced by its absorption of ultraviolet radiation and a 250 watt mercury arc lamp was employed as an excitation source in these studies. With the aid of UV transmitting optical filters, it was observed that the most rapid darkening of the sample was achieved by using all radio emission of wavelengths less than 400 nm.

The optoacoustic spectrometer used was the same as for the other photochromic substances already described. Prior to the examination, both the blank glass and photochromic glass were ground to produce a fine powder providing an enhancement of the optoacoustic signal due to increased sample surface area. The study of the photochromic material was undertaken by determining the visible absorption spectrum of the sample and blank, both before excitation by the mercury arc and while under this illumination. Figure 3.9 shows the excited and unexcited spectra of the Reactolite Rapide glass. The colour reversibility was obtained in 10 minutes in the dark. The spectra were manually corrected with measurements made using a sample of carbon black and wavelength calibration was carried out with the aid of a holmium oxide spectrum.

There is no difference in the absorption spectra in the blank glass before and after illumination whereas the photochromic glass shows constant absorption with wavelength in the visible region above 400 nm. This constant absorption following excitation (Figure 3.9) is similar to that observed in the transmission spectra (Figure 3.10). This demonstrates that optoacoustic spectra may be recorded with a minimum

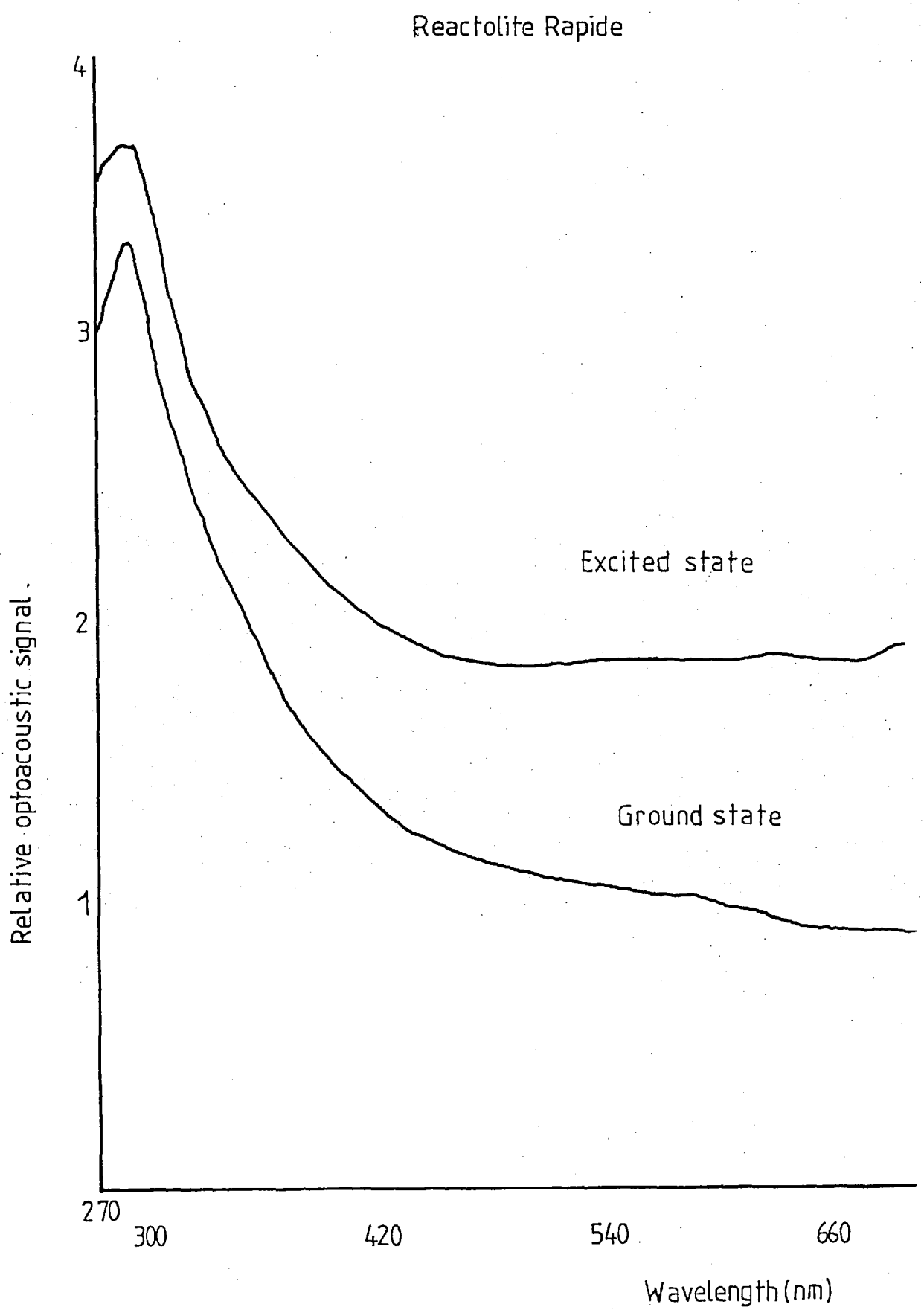

Figure.3.9. OAS Spectra of Reactolite Rapide in the ground and excited states.(Manually corrected).

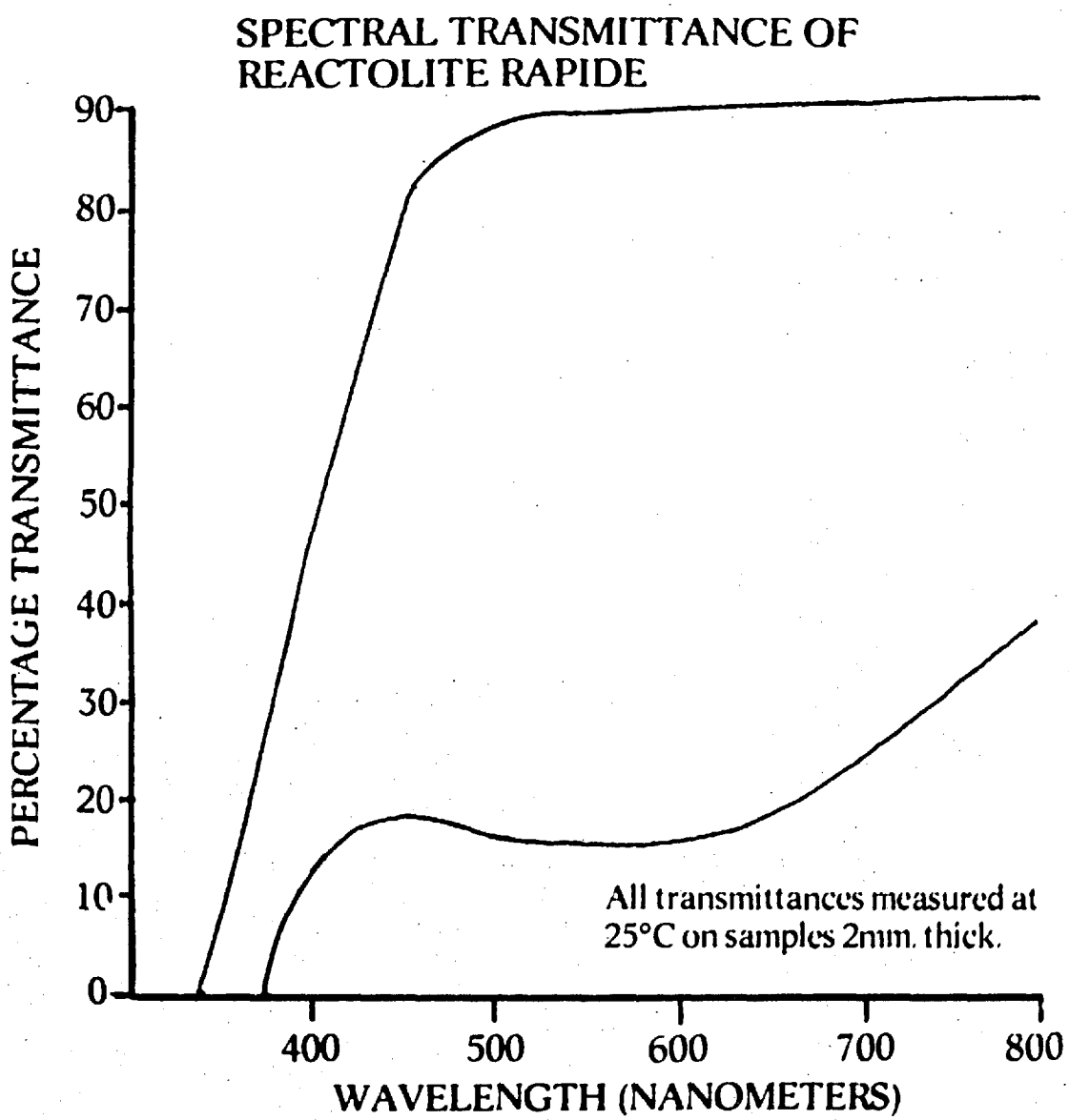

Figure 3.10: Transmission Spectra of Reactolite Rapide [123].

of intereferences from scattering effects while an intense unmodulated source is incident upon the sample.

3.4 Conclusion

It can be seen from the results described in this chapter that optoacoustic spectroscopy can be used as an complementary technqiue to conventional transmittance or reflectance spectroscopy. The studies of laser mirrors discussed above demonstrate how the optoacoustic spectrometer described in Chapter 2 may be employed to obtain absorption, transmission and reflectance spectra in addition to opto-acoustic spectra. In contrast with transmission and reflectance spectroscopic techniques, optoacoustic spectroscopy allows measurement of the absorption of dielectric coated materials without the complications of interference phenomena. In this respect optoacoustic spectroscopy competes favourably with more conventional calorimetric techniques in terms of the time required to obtain the spectrum and the capability for the study of materials with low optical absorption coefficients.

It has been demonstrated that optoacoustic spectroscopy may be employed for the examination of photochromic materials and thus spectra relatively free from errors due to scattering of light may be obtained. With other complementary techniques, like diffuse reflectance and transmission/absorption spectroscopy, scattering of light causes broadening of peaks and gives signals due to background noise. The requirement to illuminate a photochromic material with a relatively intense radiation source in order to obtain the excited species often results in difficulties when attempts are made to use

diffuse reflectance spectroscopy. The amount of scattered primary radiation tends to be relatively great and this may result in saturation of the photodetector system, or, in any case, a relatively poor signal to background ratio. With optoacoustic spectroscopy other radiation induced chemical and physical transformation could be studied in a similar manner. At present for photosensitive materials (e.g. copper blue)[124] it is difficult to obtain activation spectra by other techniques. In order to perform transmission or absorption studies on materials other than transparent solids, the substances have to be brought into solution form which may result in structural changes occurring. A possible disadvantage of OAS compared with diffuse reflectance spectroscopy occurs when substances are photodegradable due to the absorption of high energy intense primary illumination. In general, the intensity of the radiant source employed for diffuse reflectance studies is less than for a typical source used in an optoacoustic spectrometer.

In the case of optical absorption or reflectance spectroscopy the response of the photometric detector (photomultiplier or photocell) is proportional to the photon flux. In OAS the microphone response is proportional to both the photon flux and the individual photon energy. A photon at 250 nm can result in twice as much energy after absorption than a photon at 500 nm. Thus it is a power spectrum that is obtained.

CHAPTER FOUR

SOME STUDIES IN QUANTITATIVE OPTOACOUSTIC SPECTROSCOPY

4.1 Introduction

In Chapter one of this thesis a discussion has been presented of the modern theories of optoacoustic spectroscopy as applied to the examination of solid samples [30, 61, 125, 126]. All the treatments agree on the fundamental parameters governing the magnitude of the optoacoustic signal, i.e. the optical and thermal transfer coefficients of the sample under study and the modulation frequency employed.

Although there are several papers on the theory of the optoacoustic effect with solid samples, unfortunately, however to date there have been few published results to support the theoretical interpretations, in particular there is a dearth of results relating to the quantitative interpretation of the effects observed. Only absorbed radiation may contribute to the production of an optoacoustic signal and the important sample characteristics determining the magnitude and nature of the optoacoustic signal are the optical absorption coefficient of the material studied at that wavelength of the incident radiation, the efficiency of internal radiationless de-excitation and the thermal, heat-transfer coefficients (in particular the thermal diffusivity) for the material.

It is also observed that the amplitude of the optoacoustic signal is greatest for a sample presented as a fine powder of large surface area where more efficient heat transfer to the surrounding gaseous atmosphere is possible.

4.2 Effect of Sample Thickness

In this experiment a quantitative prediction for the dependence of the magnitude of the optoacoustic effect on the sample parameters can be shown to be valid for optically opaque samples of polyester films of differing thickness.

The amplitude of the optoacoustic signal obtained from the polymer samples examined was monitored with the aid of a double beam optoacoustic spectrometer operated in the single-beam, uncorrected mode. The constructional details and performance characteristics of the instrument have been described in Chapter Two. The cell used in this experiment was the aluminium cell (Figure 2.10).

A schematic diagram demonstrating the mounting of the polymer film samples is shown in Figure 4.1. Discs of polymer film 18 mm in diameter were cut from the samples and fixed with the aid of double-sided adhesive tape to the underside of the thin-walled, highly polished stainless steel ring which was mounted together with the sample onto a similar thin-walled ring contained within the sampling tray. This arrangement was sealed by means of locking nuts inside the optoacoustic cell and the unnormalised spectrum of each polymer sample was recorded in the wavelength interval 250 nm to 350 nm. The magnitude of the signal at the peak of the absorption wavelength of 300 nm was measured from the chart recorder display. The polyester film samples examined were all of identical composition and of thickness, 6, 12, 25, 50, 125 and 250 x 10^{-4} cm. Each sample was examined at modulation frequencies of 10,

30, 120 and 280 Hz.

Transmission spectra of the samples in the ultraviolet region were obtained with the aid of a conventional UV/visible spectrometer.

As described in the Chapter One, Rosencwaig and Gersho [30] have developed a theoretical interpretation of the optoacoustic effect observed for solid samples in terms of the optical absorption coefficients of the sample and its heat transfer characteristics. For sinusoidal modulated radiation incident at the sample, the pressure variation in the gaseous atmosphere within the optoacoustic cell P is shown to be as in Equation 1.12

$$P = \frac{AB\beta}{k_s a_g(\beta^2 - \sigma_s^2)} \tag{4.1}$$

where β is the absorption coefficient (cm^{-1}) of the material under study and k_s is its thermal conductivity

$$\sigma_s = (1+j)a_s \tag{4.2}$$

a_s and a_g are thermal damping functions of an alternating temperature wave passing through the sample and gas respectively and are given by

$$a_i = \left(\frac{\omega}{2\alpha_i}\right)^{\frac{1}{2}} \tag{4.3}$$

with ω the frequency of the wave (i.e. the modulation frequency) and α_i, the thermal diffusivity of the material.

In Equation (4.1), A is a constant factor which is dependent upon the experimental arrangement and is proportional to the incident radiant energy at the sample surface and the ambient pressure within the cell.

$$B = \frac{(r-1)(b+1)\exp(\sigma_s x)-(r+1)(b-1)\exp(-\sigma_s x)+2(b-r)\exp(-\beta x)}{(g+1)(b+1)\exp(\sigma_s x)-(g-1)(b-1)\exp(-\sigma_s x)} \quad (4.4)$$

B is a complex function for the system and may be expressed as in Equation 4.4 where x is the thickness of the sample and other functions are given by,

$$r = \frac{(1-j)\beta}{2a_s} \quad (4.5)$$

$$b = \frac{k_b a_b}{k_s a_s} \quad (4.6)$$

$$g = \frac{k_g a_g}{k_s a_s} \quad (4.7)$$

The subscript "b" denotes the backing material of the sample and the product $k_i a_i$ may be considered as a thermal flux coefficient for the material.

To simplify Equation 4.1, it is necessary to apply assumptions which reduce Equation 4.4. The assumptions employed in this study of the magnitude of the optoacoustic signal, derived from polymer films may be considered.

Conventional transmission spectroscopy studies were undertaken for the thin film samples and these showed that even the thinnest material of 6×10^{-4} cm thickness, exhibited an optical density greater than 3.0 at 300 nm. Thus at this wavelength the samples may be considered opaque and β is thus very large i.e. $\exp(-\beta x) \simeq 0$ and $r >> 1$.

The experimental conditions employed, and shown in Figure 4.1, ensure that the backing material is air, and, hence, identical with the atmosphere above the sample top surface, i.e. b = g. Typical thermal characteristics

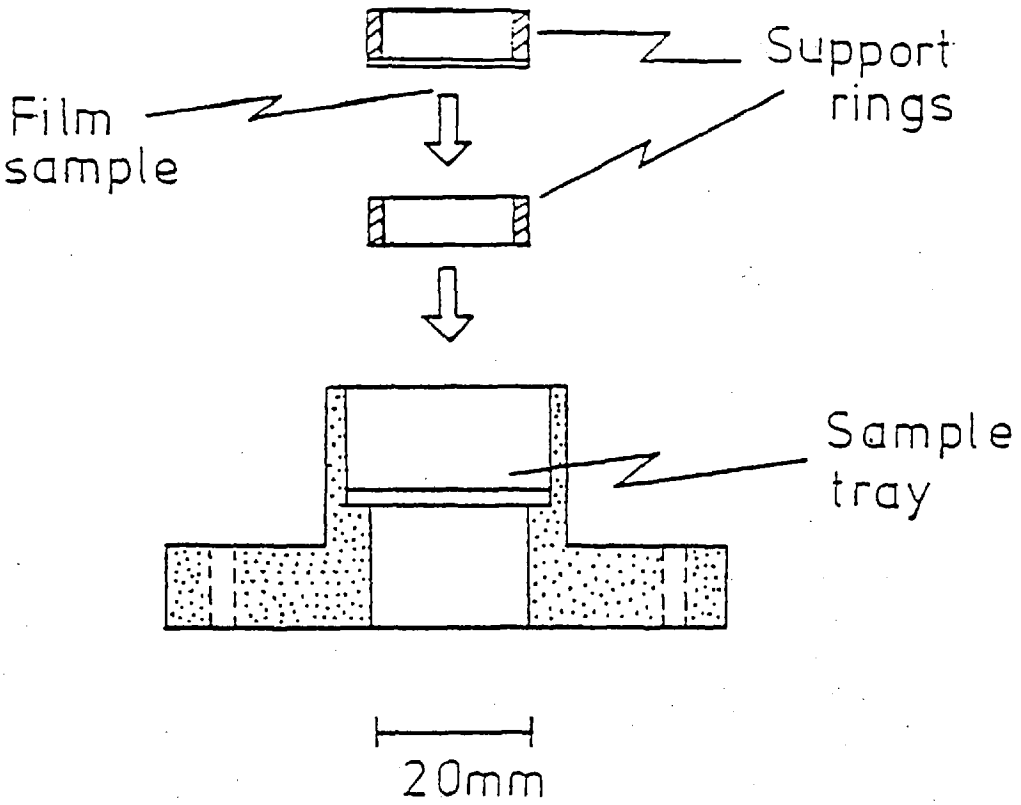

Figure 4.1: Sample holder and method employed to retain the polymer film

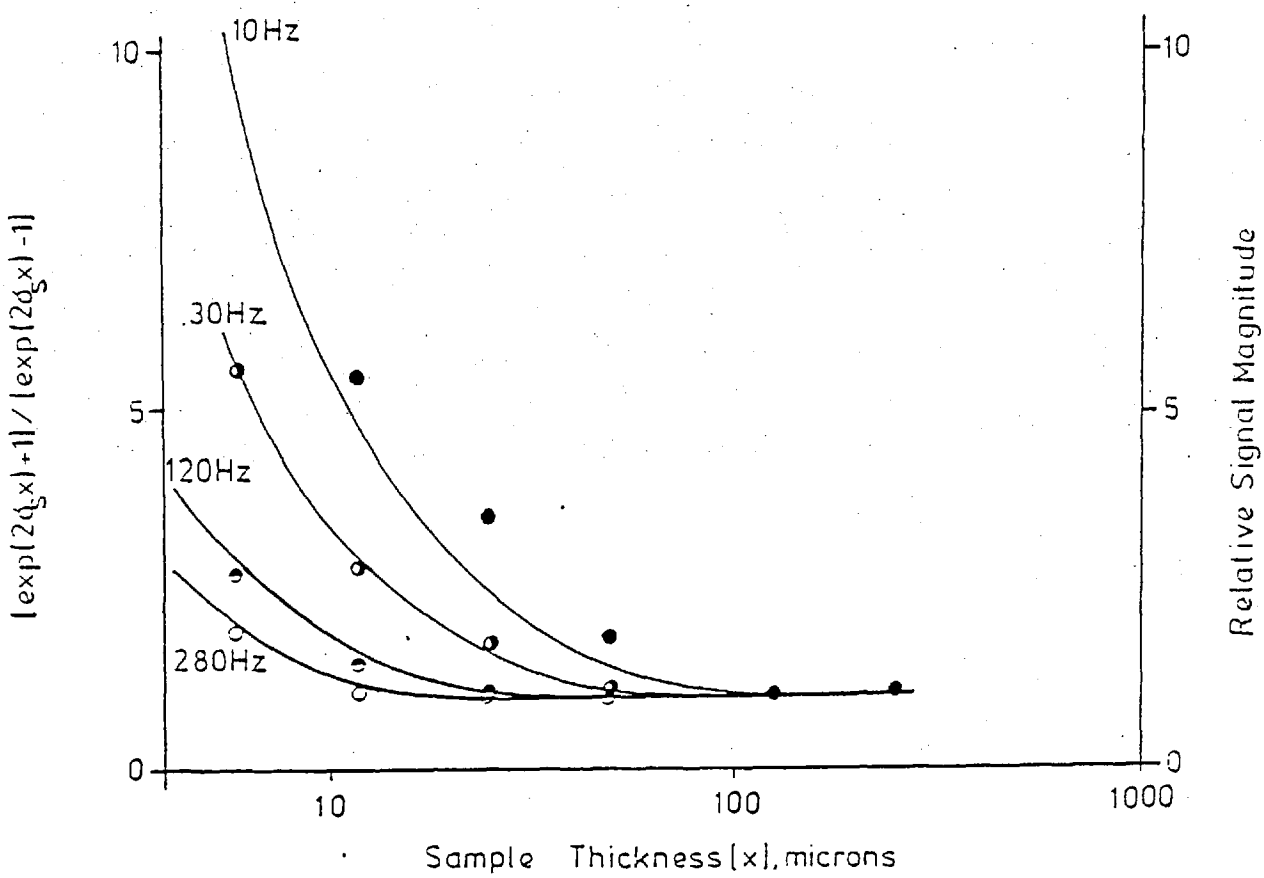

Figure 4.2: The function $[(\exp(2\sigma_s x)+1)/(\exp(2\sigma_s x)-1)]$ vs. x(solid lines) and the experimentally determined results for the relative optoacoustic signal magnitude for different values of sample thickness,x, as a function of modulation frequency; (a) ●, 10Hz; (b) ⊖ 30Hz; (c) ⊖ 120Hz; (d) ○ 280Hz. (The theoretical curves assume a value of 10^{-3} cm^2 s^{-1} for the thermal diffusivity of the polymer samples).

of polymers and air (nitrogen) are presented in Table 4.1 and allow the simplification to be made that b and g << 1. [127]

TABLE 4.1

THERMAL CHARACTERISTICS FOR NITROGEN AND POLYESTER SAMPLES [127]

	Air (N_2)	Polyester
$\alpha(cm^2\ sec^{-1})$	$200x10^{-3}$	1.0×10^{-3}
$k(cal.sec^{-1}cm^{-1}\ K^{-1})$	$6.4x10^{-5}$	3.4×10^{-4}
$\frac{A_i}{w^{\frac{1}{2}}}$ $(sec^{\frac{1}{2}}.cm^{-1})$	1.58	22.4
$g = \frac{K_g.A_g}{K_s.A_s} = \frac{K_b.A_b}{K_s.A_s} = 1.33 \times 10^{-2}$		

With these assumptions we may simplify equation 4.4 to provide,

$$B = r\,\frac{\exp(\sigma_s x) + \exp(-\sigma_s x)}{\exp(\sigma_s x) - \exp(-\sigma_s x)} \tag{4.8}$$

which may be rearranged

$$B = r\,\frac{\exp(2\sigma_s \cdot x) + 1}{\exp(2\sigma_s \cdot x) - 1} \tag{4.9}$$

Substituting equation (4.9) into equation (4.1) and applying the assumptions yields

$$P = \frac{A(1-j)}{2a_g a_s k_s}\,\frac{\exp(2\sigma_s x) + 1}{\exp(2\sigma_s x) - 1} \tag{4.10}$$

With the aid of equation (4.10) we may examine the effect of variation in sample thickness, x, on the magnitude of the optoacoustic signal. Examinations of

equations (4.9) and (4.10) indicate that for low values of x (i.e. for thermally thin samples) the signal magnitude should decrease with increasing thickness and reaches a limiting value when B, as expressed in equation (4.9), approximates to r; at high values of x (thermally thick samples) it should become independent of sample thickness.

The manner in which the signal, as given by $[\exp(2\sigma_s.x)+1][\exp(2\sigma_s.x)-1]$, should vary with the thickness x, of the sample shown in Figure 4.2, for a variety of modulation frequencies. Also shown in Figure 4.2 is the experimentally determined data. For comparison purposes the relative signal magnitude data is presented, i.e. the $1/\ell$ dependence predicted at large values of x in Equation 4.10 has been avoided by normalization for modulation frequencies. The two cases, thermally thin and thermally thick regions are clear from these results and good agreement is observed between the theoretical curves predicted from equations (4.9) and (4.10) and the experimental results determined from the examination of the optically opaque, thin polymer films.

It is interesting to consider the mechanisms of the heat-flow within the sample and cell in explaining the nature of the data shown in Figure 4.2. For any selected and fixed frequency of modulation we may assign to the sample under study a 'thermal diffusion length μs' i.e. a distance within the sample, from its upper surface, from which an alternating thermal signal may reach the upper surface without appreciable attenuation. Rosencwaig and Gersho [30] have assigned a value of $1/a_s$ (=μs) to this active depth. For an optically, opaque sample, any increase in sample

thickness has negligible effect on the amount of radiant energy absorbed and, providing the sample thickness is less than μs, an increase in thickness merely serves to increase the mass of the sample which may respond to alternating thermal wave produced in the sample. Indeed, to a first approximation, we may expect the thermal wave amplitude, hence the optoacoustic signal magnitude, to be inversely proportional to the sample thickness for a constant sample area, for values of thickness, x, less than μs. When the sample thickness is greater than μs, however, the sample mass, or volume, responding to the periodic thermal wave is constant as negligible alternating thermal energy is transferred to a depth greater than μs by definition of μs. Also, as μs is a function of modulation frequency, decreasing with increasing frequency, the point of inflexion of the two curves (inversely proportional to thickness and independent of sample thickness), moves to lower values of thickness with increasing modulation frequency.

A further observation may be made concerning equation (4.10). At high values of $\exp(2.\sigma_s.x)$ the optoacoustic signal magnitude is independent of sample thickness, as discussed above, and equation 4.10 reduces to,

$$P = \frac{A(1-j)\mu s}{2a_g k_s} \qquad (4.11)$$

which is identical with the expression derived by Rosencwaig and Gersho [30] for the case of optically opaque, thermally thick sample.

Unlike conventional spectrophotometric measurements by transmission, an optoacoustic measurement depends not

only on the optical properties of the sample but also its thermal characteristics. For the samples described in this work, little quantitative information concerning the samples could be gained from their ultraviolet absorption spectra due to their high opacity in this spectral region, even with relatively thin samples. The optoacoustic results however show very interesting trends with sample thickness and the advantage may betaken of the high opacity in the ultraviolet. Furthermore, as the optoacoustic effect is concerned with a periodic thermal wave, control of the thermal diffusion length may be achieved by the suitable control of the frequency of modulation of the incident radiation.

The experimental data presented above agrees well with the theoretical treatment derived from Rosencwaig and Gersho [30] and that it serves to illustrate the general applicability of their treatment of optoacoustic effect. My experimental results also show that for any thickness of sample above the thermal diffusion length, the signal magnitude is $\alpha\ 1/\omega$. It may be observed from my results that the greatest errors arise at low modulation frequencies (10Hz) and for thin samples (6×10^{-4} cm thickness). Although decreasing the frequency of modulation provides for an increase in signal magnitude (see equation 4.11), at frequencies below ca. 20Hz the experimental system employed for the studies described above suffers increasingly from "1/f" noise. Also with thin samples (less than ca 10^{-3} cm) the sample arrangement discussed may give rise to erroneous results by vibration of the sample due to the enclosed air volume below the sample.

With the increasing interest being shown in optoacoustic spectrometry for the examination of condensed phase samples not easily studied by conventional techniques, more quantitative data are certain to be produced to test the current theoretical treatments and expand the currently limited knowledge of the interrelation between the optical characteristics and thermal transfer properties of a wide variety of materials.

4.3 Effect of Sample Particle Size

The theories presented in the literature to-date concerning the production of optoacoustic signals from solid materials are general treatments and all assume a physically homogeneous sample such as a single crystal in thin film. None of these theoretical models adequately treat the common practical case of the sample being presented as a powder of random or selected particle size. It has been observed that the amplitude of the optoacoustic signal varies with the physical form of the sample, particularly the surface area. Therefore, a study was undertaken to examine the effect of the particle size for two strongly absorbing materials. The effect of the amount of sample and concentration of the absorbing species were also investigated.

Utilizing carbon black and dark blue cobalt glass the effect of particle size was studied. The instrument employed in this experiment was the double beam system described in Chapter Two and operated in the single beam mode. Optoacoustic signals were measured for carbon black at 479 nm and dark blue cobalt glass at 580 nm. The

modulation frequency employed in both cases was 30Hz with a monochromator bandpass of 20 nm and time-constant of 3 seconds. Sieving was carried out using standard BS 410 type sieves and an automatic sieve shaker for 1 hour. Equally weighed quantities of various particle sizes (38-63μm, 63-90μm, 90-125μm, 106-150μm, 125-180μm and 180-212μm) of carbon black and dark blue cobalt glasses were examined and the optoacoustic signal measured. The results are shown in Figures 4.3 and 4.4.

From Figures 4.3 and 4.4 it can be seen that the amplitude of the optoacoustic signal increases as the particle size of the sample decreases. Decreasing the particle size increases the surface area. This can be shown by assuming a model, say, having a space to accommodate 10 particles in each of two dimensions. Assuming the radius of each particle to be unity, the relative surface area of the particle in the model will be 200π. If the radius of the particles in the model is halved the relative surface area will increase to 400π, if the same area of a plane is covered. Hence, there are two phenomena occurring with regard to the optoacoustic signal due to the particle size: optical and thermal effects.

In the case of optical phenomena the total absorbed power which produces the optoacoustic signal is a function of the specular reflection which occurs at the sample-gas interface.

There are four major parameters which vary the magnitude of the specular reflectance. They are the particle size, the difference in the refractive index between

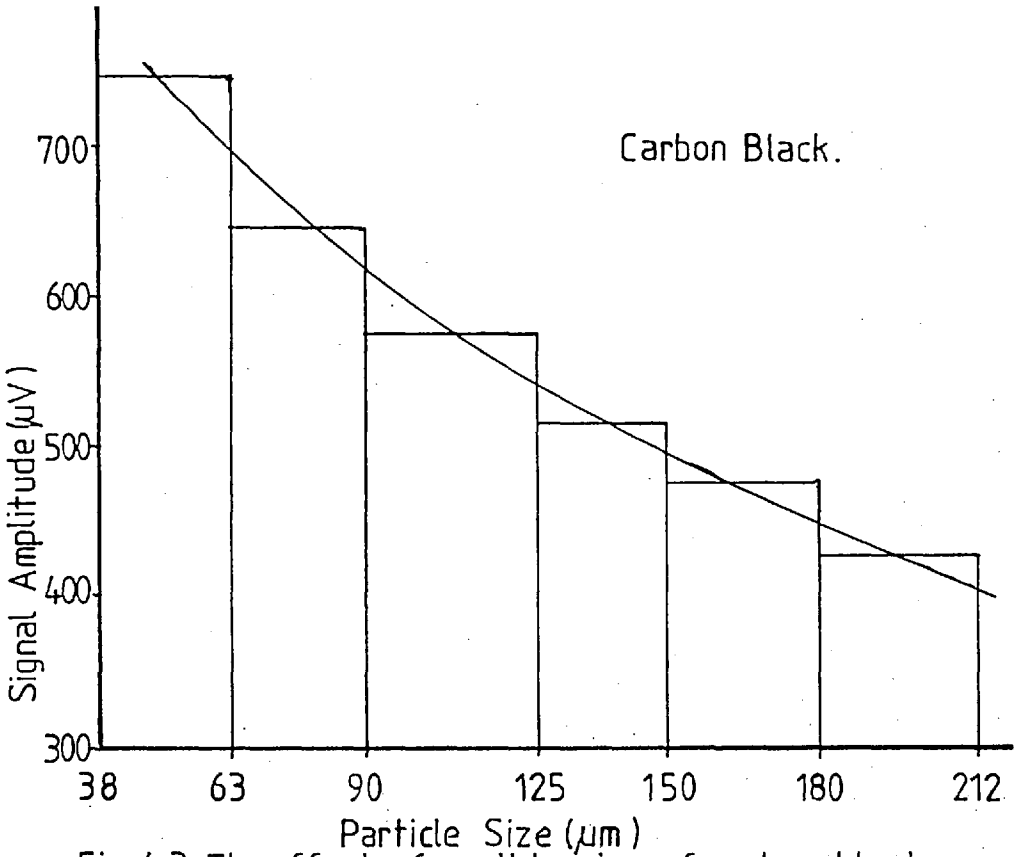

Fig.4.3. The effect of particle size of carbon black upon the OAS Signal.

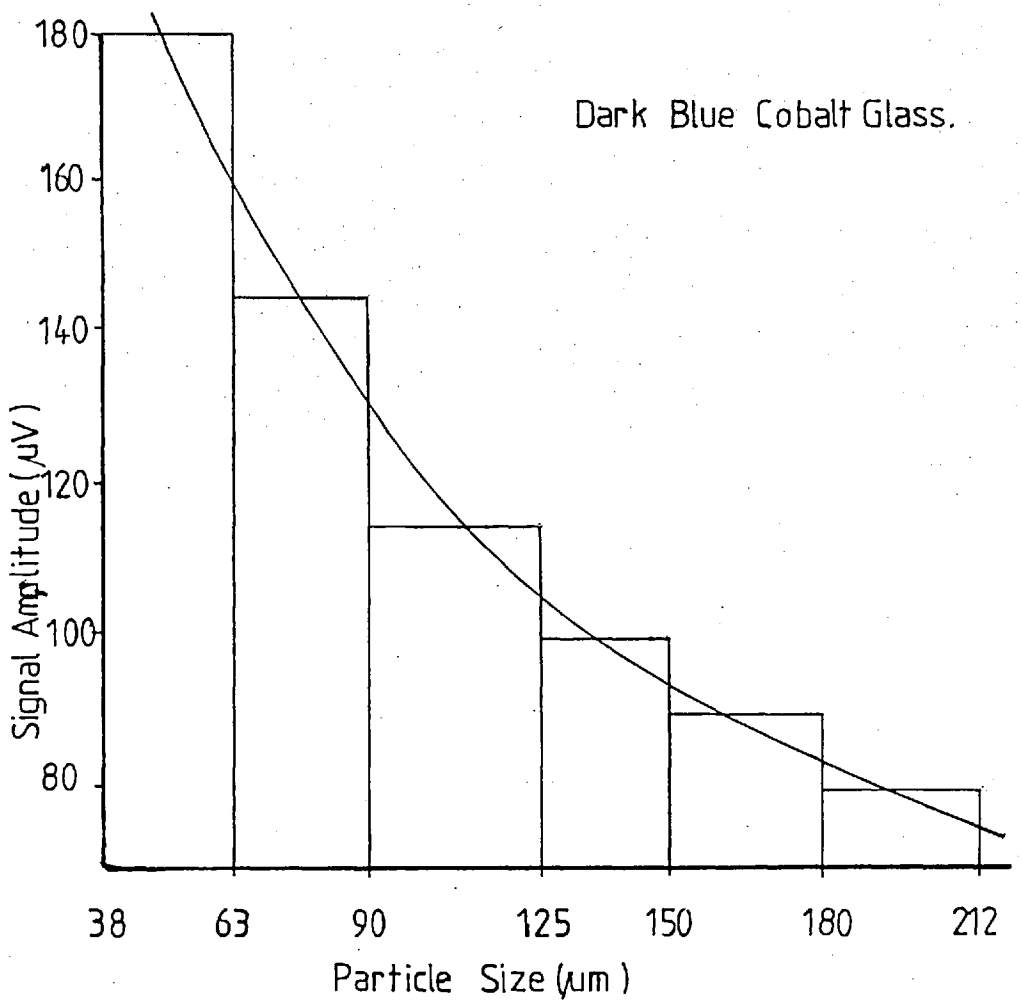

Fig.4.4. The effect of particle size of dark blue cobalt glass upon the OAS signal.

the gas and solid phase, β-the absorption coefficient and the geometry of the particle. As the particle size decreases there is more surface area exposed to illumination and the possibility of more specular reflection occurring.

With regard to the thermal effects in optoacoustic spectroscopy as explained in Chapter One, the important characteristic of the sample which determine the magnitude and the nature of the optoacoustic signal are its thermal transfer coefficients, in particular, the thermal diffusivity. The thermal transfer efficiency is greater for small particle sizes than for larger particle sizes because there is a greater area of contact between the gas and solid (i.e.efficient thermal coupling).

4.3.1 Effect of the amount of sample and concentration of absorbing species:-

Adams et al [29] have investigated the variation of signal magnitude with the sample size for a carbon black sample of particle size less than 76μm. The carbon powder was spread uniformly on to a 7 mm diamter disc of double sided clear adhesive tape. The mass of the sample was determined by weighing the adhesive tape with and without the powder sample. The optoacoustic signal was measured at 570 nm. The mass of the sample was then carefully decreased by removing some of the sample from the disc of tape and reweighing. A linear relationship was obtained for the variation of the signal amplitude with the sample mass [29]. As the sample mass and surface area decreases, the power absorbed from the incident beam of radiation become less so that the optoacoustic signal amplitude is

decreased. The minimum detectable mass of sample for carbon black, based on an estimation of the signal-to-noise ratio observed for the small background signal placed by the cell was about 10μg.

The effect on the concentration of the absorbing species was studied with two sets of carbon particles in the range 38-63μm and 180-212μm. Known concentrations of these carbon samples were mixed with Alumina (BDH Grade 5) of similar particle size.

The double beam instrument described in Chapter Two was employed in single beam mode for this experiment. Measurements were made at a wavelength of 479 nm with a modulation frequency of 28.5Hz and a monochromator bandwidth of 20 nm. The results are shown in Figure 4.5.

The graphs of carbon in alumina (Figure 4.5) were not linear over the entire concentration range of carbon in Alumina. The reason for this is not clear but may be due to the inhomogeneity of the powdered mixture, perhaps due to partial separation of particles according to their densities.

To overcome the above problem an identical experiment was carried out by mixing gently the carbon and alumina with a weighed quantity of glycerol (0.25g BDH grade) to produce a homogeneous paste. Glycerol was chosen because it is viscous, has a thermal conductivity of 7.03×10^{-4} cal/sec. cm^2 at $20^{o}C$ and is transparent to radiation at 479 nm. Optoacoustic signals were measured at 479 nm with a modulation frequency of 75Hz and a monochromator bandwidth of 20 nm. Good linearity was now observed for two different particle sieve ranges (i.e. 38-63μm, and 180-

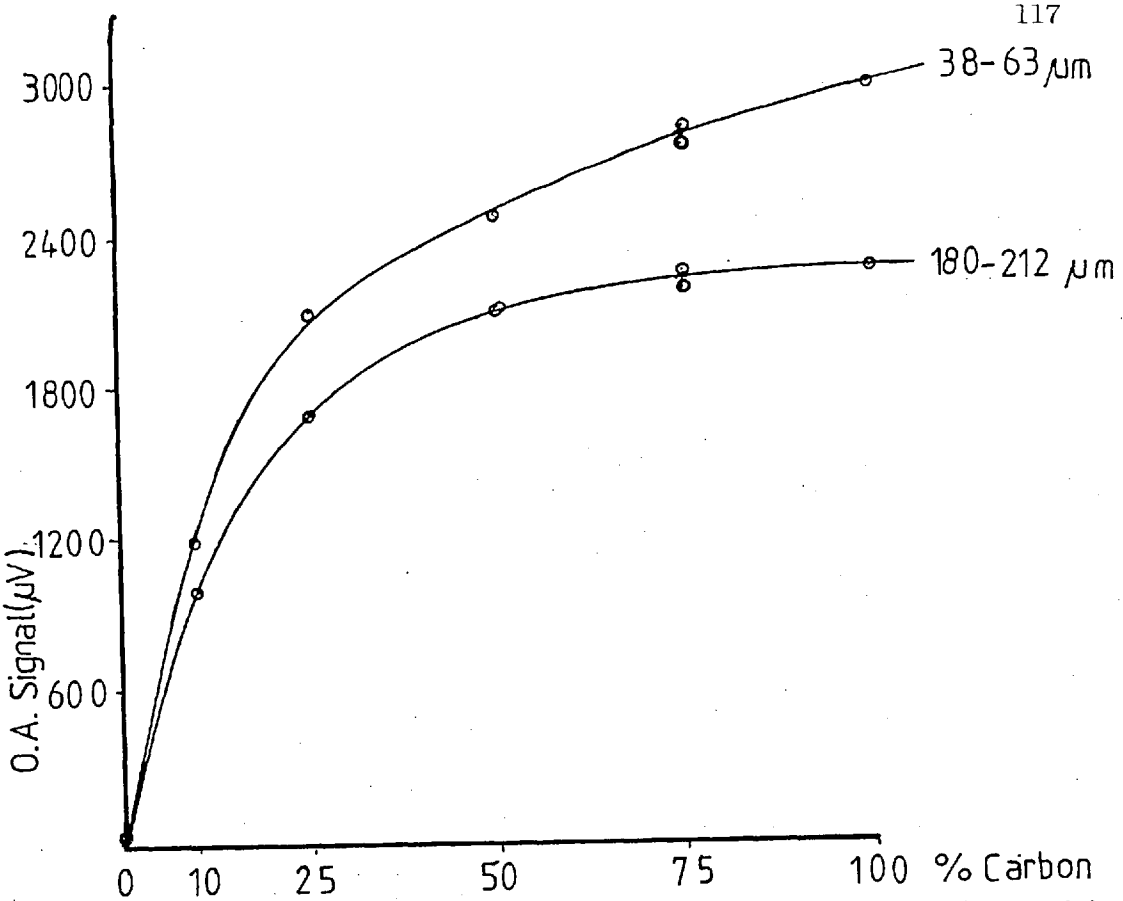

Fig.4.5.The effect of the concentration of carbon, with matched particle size of carbon and alumina, upon the OAS signal.

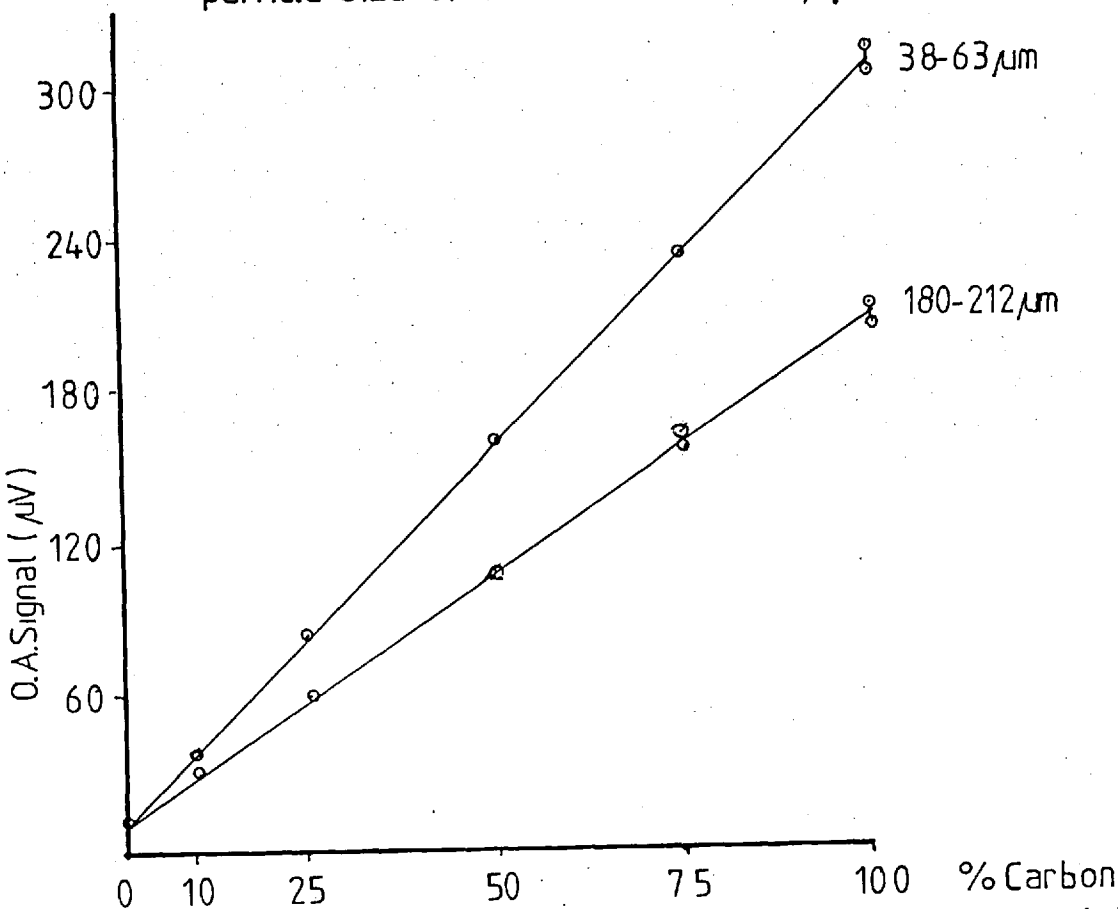

Fig.4.6. The effect of the concentration of carbon, with matched particle size of carbon and alumina with glycerol, upon the OAS signal.

212μm) of carbon black (Figure 4.6). Presumably the high viscosity of the glycerol inhibits the settling out of the components of the solid in the mixture.

4.4 Conclusion

In this chapter a quantitative derivation for the production of the optoacoustic signal with respect to optically opaque samples of polymer films of differing thickness is detailed. As mentioned earlier the experimental results obtained agree well with the Rosencwaig and Gersho's [30] theoretical prediction on the special cases of optically opaque, thermally thin and also optically opaque, thermally thick samples. Although Rosencwaig [30] claims that his theory gives an adequate physical picture of the process, he has not published so far any experimental results to support his theoretical model.

For quantitative application of optoacoustic spectroscopy to powdered samples the particle sizes normally have to be controlled. In the complementary technique of diffuse reflectance spectroscopy the signal variation due to particle size is also very complicated [11]. Although optoacoustic spectroscopy is susceptible to particle size effect as in diffuse reflectance spectroscopy, the scattering effects in optoacoustic spectroscopy is less severe as discussed in Chapter Three of this thesis.

CHAPTER FIVE

SOME QUANTITATIVE MEASUREMENTS IN THE NEAR-INFRARED REGION

5.1 Introduction

In this chapter the quantitative determination of moisture in single cell protein (Pruteen) and the determination of polyvinylacetate (PVAc) in vinylchloride/vinylacetate copolymer in the near-infrared region by optoacoustic spectroscopy is described. The optoacoustic technique used for the determination of moisture in Pruteen is also compared with another method using wide-line n.m.r. The technique employing optoacoustic spectroscopy for the determination of polyvinylacetate in vinylchloride/vinylacetate copolymer is compared with the complementary technique of diffuse reflectance spectroscopy.

Near-infrared spectroscopy covers the region of the electromagnetic spectrum from 0.75μm to 2.5μm. The practical reason for this spectral region being separated from the UV-visible and infrared regions is that for optimum performance it is necessary to change the instrumental optics, sources, detectors and sample handling techniques. Absorption bands observed in the infrared region are due to vibrational transitions rather than to the electronic transitions which are observed in the UV-visible region and, therefore, spectra require to be interpreted differently. The absorption bands that are observed in the near-infrared are due largely to the overtone and combination of hydrogenic stretching and bending fundamentals. Therefore, near-infrared spectroscopy can be defined as the study of low energy electronic transitions, overtones and combinations of hydrogenic (C-H, N-H, O-H, etc.) stretching and bending vibrations [128].

Table 5.1: Spectra-structure and molar absorptivity data for near-infrared regions [136]

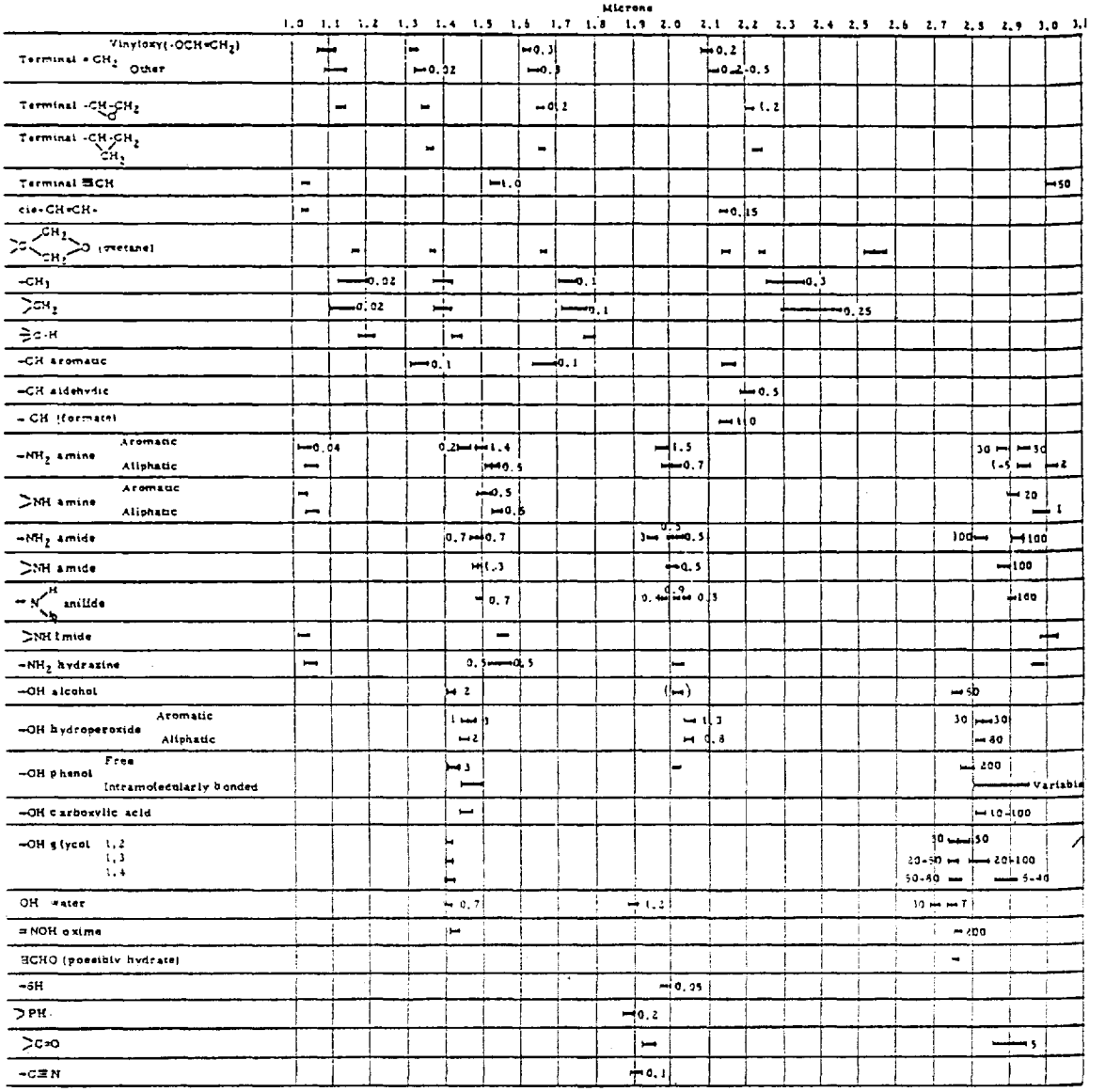

Table 5.2: Approximate theoretical wavelengths of overtones [133]

Group	Overtone	λ	Intensity*	Group	Overtone	λ	Intensity*
		μ				μ	
C—H	1	1.7	s	C—C	3	1.75	vw
	2	1.1	m		4	1.4	n
	3	0.85	w	C—O	3	1.85	w
	4	0.7	vw		4	1.5	vw
O—H	1	1.4	s	C=C	3	1.5	vw
	2	0.95	m		4	1.2	n
	3	0.7	w	C=O	2	1.9	m
	4	0.55	vw		3	1.45	w
N—H	1	1.4	m		4	1.15	vw
	2	0.95	w	C≡C	2	1.6	m
	3	0.7	vw		3	1.15	vw
	4	0.55	n	C≡N	2	1.5	w
S—H	1	1.95	w		3	1.1	vw
	2	1.3	vw	C—F	4	1.6	vw
C—D	2	1.55	s	C—Cl	6	1.9	n
	3	1.15	m	Si—H	2	1.5	s
O—D	2	1.45	m		3	1.15	m
	3	1.1	w	P—H	2	1.4	w
N—H	2	1.35	w		3	1.05	vw
	3	1.0	vw				

*Relative intensities: s, strong; m, medium; w, weak; vw, very weak; n, not desirable or extremely difficult to detect.

Near-infrared spectroscopy is primarily a quantitative rather than a qualitative technique [128]. However, it is particularly useful in the characterisation of rare earth and transition metal ions. It is well suited for the quantitative determination of water, alcohols, phenols, amines, unsaturated hydrocarbons or ester carbonyls and other compounds containing O-H, N-H or C-H groups.

The history of near-infrared spectroscopy date back to 1800 [129] and the first near-infrared spectrum of an organic compound recorded photographically (0.7μm to 1.2μm) was obtained by Abney and Festing [130]. Thereafter, this region was neglected forsometime until 1928 when Bracket [131] revived the technique. In 1954 Kaye [132] published his review of the near-infrared region and since then several papers have been published on applications in this region [133-135]. The theory of spectroscopy in the near-infrared region is reported elsewhere [128].

Analytical applications

Kaye [132] in his review has presented a Colthup-type group frequency chart for overtones and combination bands between 0.6μm and 3.4μm. This chart has been included in the most recently published review of near-infrared absorption bands and is shown in Table 5.1. [136] The approximate wavelengths of some overtone bands (Table 5.2) are also given by Wheeler [133].

Carbon-Hydrogen groups

The C-H group is characterised by fundamental stretching bands in the range of 3.0-3.6μm, combination bands between 2.0 and 2.4μm, first overtone stretching bands between 1.6 and 1.8μm and second overtone stretching bands in the region 1.1 - 1.2μm. Higher order combinations give rise to other weak bands throughout the near-infrared region [128].

Oxygen-Hydrogen groups

The fundamental oxygen-hydrogen vibrations occur at ca 2.8μm and the first and the second overtone bands near 1.4μm and 1.0μm respectively. A combination band exists near 2.0μm. These bands have been used invariably in the determination of water, alcohol and phenol [128]. The combination band 1.9μm is favoured in most of the studies of water because the molar absorptivity at this band is twice the value of the molar absorptivity of the overtone band 1.39μm [132].

Nitrogen-Hydrogen groups

The fundamental N-H stretching bands of amines, amides and related compounds occur at ca. 2.8-3.0μm. The first overtone stretching bands are near 1.5μm and the second overtone stretching band are near 1.0μm. The $-NH_2$ group also exhibits a highly characteristic combination band near 2.0μm[128].

Carbonyl group

The carbonyl group has a high intensity fundamental stretching vibration at about 5.8μm and its second

overtone occurs in esters at about 2.0μm [137]. Haslam *et al* [138] have reported an ester carbonyl band at 2.15μm in the analysis of polyvinylacetate in vinylchloride/ vinylacetate copolymer.

The above studies were carried out utilising a transmission method. Recently, reflectance techniques have been reported in the near-infrared region for the analysis of milk fat in milk powders using the first overtone of C-H stretching vibration of the methylene group at 1.742μm [139]. A method for the determination of moisture in wheat by near-infrared diffuse reflectance spectroscopy has been reported by Law *et al* [140].

5.2 DETERMINATION OF MOISTURE IN PRUTEEN

5.2.1 Introduction

The "Pruteen" examined in this project is the trade name of a single cell protein marketed by ICI. This material is manufactured by microbial fermentation utilizing products obtained from natural gas. At the moment there are few rapid instrumental techniques which can be used as a routine quality control for the determination of moisture in single cell protein.

Near-infrared optoacoustic spectroscopy has been investigated for this purpose and the results obtained compared with an approach employing wide-line n.m.r.

Frequently, water is present in a sample matrix in various forms ranging from physically adsorbed molecules to chemisorbed molecules and the elements of water present as hydroxyl groups. Usually moisture is described as free

water or bound water depending upon the nature of adsorption occurring.

Amongst the methods available for the determination of moisture include gravimetric analysis and this technique is the most common for food stuffs. In the gravimetric method the weighed sample is placed in an oven at atmospheric pressure and heated to 100 ±1°C [141]. Total weight-loss is taken as a measure of the amount of water present in the sample. The titrimetric method of determining water developed by Karl Fischer is described in BS 2511-1970. This is based upon the non-stoichiometric reaction of water with iodine and sulphur dioxide in pyridine-methanol solution. The reagent is standardised against a weighed trace of water and the end-point is subsequently determined by back titration with a solution of water in absolute methanol. Other methods for the determination of water include (Dean & Stark) reflux distillation of the food with an immiscible solvent, having a higher boiling point and lower specific gravity than water e.g. toluene, xylene etc. [142]. A technique employing gas chromatography [143] has also been described.

Several workers [144-146] have described the use of low resolution (wide-line) nuclear magnetic resonance spectroscopy for the determination of the moisture content of food stuffs.

5.2.2 Establishment of standards

The determination of moisture in Pruteen by near-infrared optoacoustic spectroscopy and wide-line n.m.r. required standard calibration graphs to be obtained.

In the procedure used to obtain calibration standards samples of unsieved Pruteen, Pruteen ground in a pestle and mortar and sieved Pruteen were tried. Sieving was carried out with an automatic time-controlled siever. The sieves were of the standard BS 410 type. The sieved materials used in these moisture determination studies were all sieved for an hour prior to their analysis. In order to provide controlled humidity atmospheres eleven desiccators each containing 250 ml of an appropriate saturated aqueous salt solution were set up as described in Table 5.3.[147] Before placing the Pruteen for equilibration in the desiccators it was dried by keeping it in an oven 105°C ±1°C to constant weight. 200 mg of the dried Pruteen was weighed in a watch glass and left in the desiccators overnight in a room at constant temperature (20±1°C). Equilibration of the moisture was ascertained by rechecking the weight of increase of the sample every day. It was found that some of the Pruteen sample attained equilibration by the seventh day and the remainder by the ninth day in the desiccator. Hence, Pruteen standards were equilibrated for ten days before the spectra were scanned. In the case of sieved Pruteen samples the particle sizes examined were of diameter 38-63μm and 125-180μm. While studying the equilibration of moisture in the initial stage of the experiment it was noticed that any sudden fall in the temperature resulted in great variations in the moisture content of the Pruteen samples. Hence, the storage of the desiccators in a temperature controlled room is of considerable importance.

For the preparation of the standards employed for the wide-line n.m.r. 23g for the unsieved Pruteen and 2g for

TABLE 5.3 [147]

The percentage humidity at the given temperature at equilibrium within a closed space when a saturated solution* of the given substance is present (*The concentrations indicated for the sulphuric acid and phosphoric acid solution)

SOLID PHASE	t^{o}(C)	% HUMIDITY
H_2SO_4 conc.	20	0
H_3PO_4 ½ H_2O	24	9
LiCl. H_2O	20	15
$CaCl_2.6H_2O$	20	32.3
KCNS	20	47
$Ca(NO_3)_24H_2O$	18.5	56
$NaNO_2$	20	66
$NaClO_3$	20	75
$Na_2S_2O_35H_2O$	20	78
NH_4Cl	20	79.5
$ZNSO_47H_2O$	20	90

the sieved Pruteen were taken for the equilibration. The procedure adopted was the same as for the standards employed for the optoacoustic method.

5.2.3 Methods employing optoacoustic spectroscopy

After the establishment of standards the moisture eqilibrated Pruteen was examined in the near-infrared region using optoacoustic spectroscopy.

5.2.3.1 Experimental

The instrument employed in the study was the single beam instrument with a tungsten filament source described in Chapter Two. All spectra were scanned with a wavelength scan rate of 300 nm min^{-1}, a monochromator bandwidth of 30 nm, a time-constant of 1 second and a modulation frequency of 22.6Hz. Wavelength calibration was performed with holmium, erbium, europuim and praeseodymium oxides.

The first experiments were performed with unsieved Pruteen. After equilibration for 10 days as described in section 5.2.2 the sample was re-weighed and transferred quickly and very carefully with a camel hair brush into the aluminium sample cup, sealed into the optoacoustic cell and the spectrum scanned between 1μm and 2.5μm. Figure 5.1 shows the poorly resolved spectrum obtained with unsieved Pruteen containing 8% moisture. It is likely that the lack of resolution in Figure 5.1 could be caused by a mixture of particles of different sizes being present. As described in Chapter One of this thesis, optoacoustic signals are dependent upon the surface area of the sample and this, in

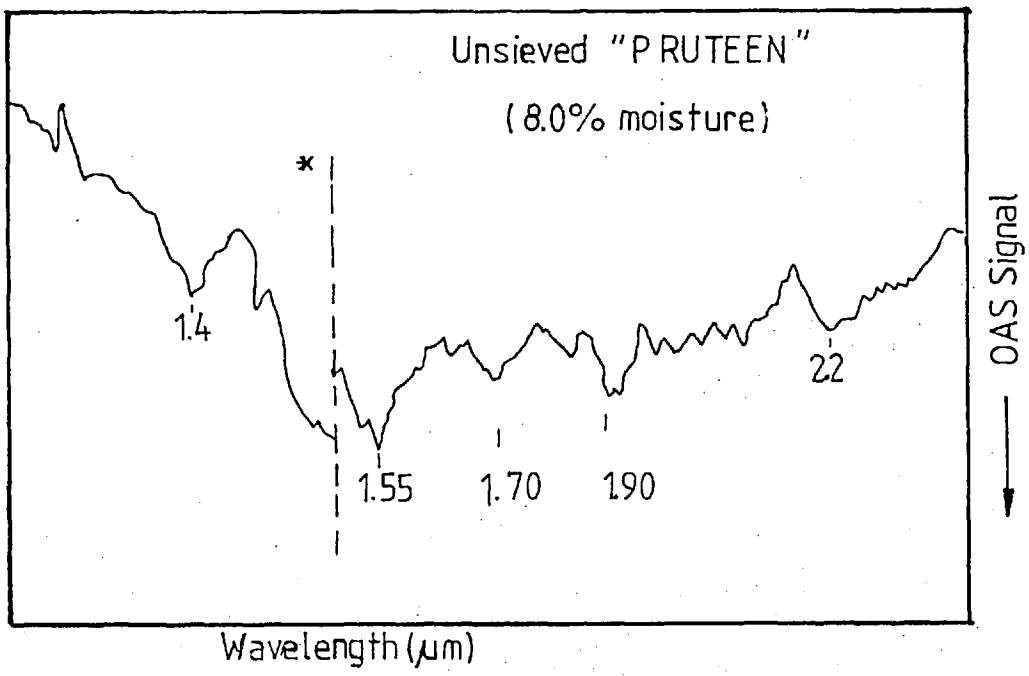

Fig.5.1. Near-IR Spectra Unsieved "PRUTEEN" (Uncorrected Spectrum).

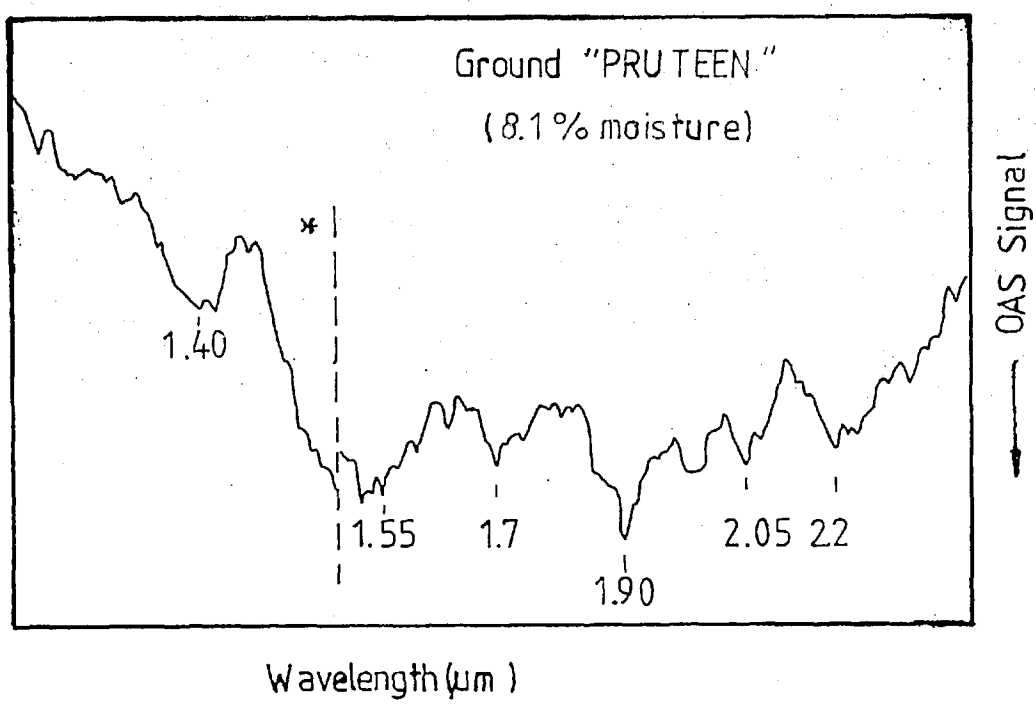

Fig. 5.2 Near-IR Spectra Ground "PRUTEEN" (Uncorrected Spectrum)

* filter change

turn, depends upon the particle size. In order to standardize the particle size of the sample it was ground in a pestle and mortar for about five to ten minutes. Figure 5.2 shows the spectrum obtained with a sample of ground Pruteen containing 8.1% moisture. It may be observed that although the resolution is improved the spectrum is still unsatisfactory. It was found not to be possible to obtain any useful quantitative data from spectra of unsieved or ground Pruteen. Greater control of the particle size of the sample was employed by sieving the sample of Pruteen for an hour in standard BS 410 sieves. The particle diameters of the Pruteen samples examined were 38-63μm and 125-180μm. Figure 5.3 shows manually corrected (i.e. with carbon black) 125-180μm particle size spectra of Pruteen containing 11.6%, 8.4% and 0% moisture.

5.2.3.2 Results and Discussion

The Pruteen spectra (Figure 5.3) shows six clear bands. The band at 1.4μm is the first overtone band and bands at 1.9μm and 2.2μm are combination bands of the fundamental OH vibration at ca. 2.8μm. The band at ca. 1.55μm is the first overtone and the band at 2.05μm is the combination band of the N-H stretching band at ca. 2.8-3.0μm. The 1.7μm band is the first overtone of the C-H stretching of the fundamental at 3.0 to 3.8μm.

As described earlier the bands at 1.4μm and 1.9μm are characteristic of the free, undissociated water and the bands at 1.4μm and 2.2μm [101,148] are characteristic of the bonded hydroxyl group. Hunt et al [149-152] have discussed

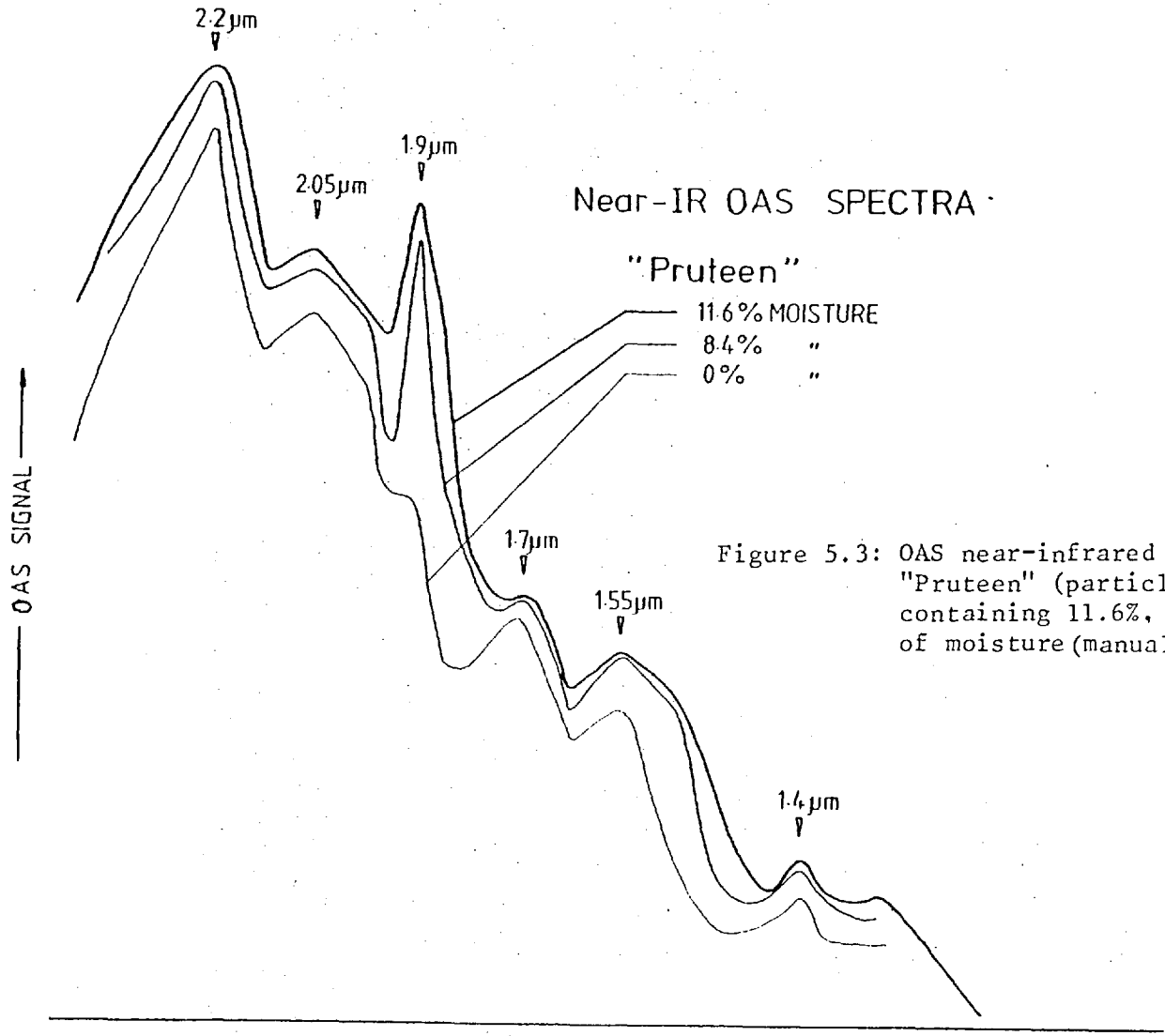

Figure 5.3: OAS near-infrared spectra of "Pruteen" (particle size 125-180µm) containing 11.6%, 8.4% and 0% of moisture (manually corrected).

extensively the OH absorption bands in the case of the diffuse reflectance spectra (Visible and near-infrared) of minerals and rocks. In the case of water there are three vibrational modes e.g. (V_1), (V_2) and (V_3). (V_1) is the symmetric vibrational mode, (V_2) is the H-O-H band and (V_3) is the asymmetric stretching vibration. These three fundamental vibrations occur in the region (V_1) ca. 2.89μm to 2.70μm (3450 to 3700 cm^{-1}), (V_2) ca 6.26μm to 6.06μm (1595 to 1650 cm^{-1}) and (V_3) ca 2.81μm to 2.66μm (3550 to 3750 cm^{-1}). Overtones are $2V_1$ and $2V_3$ at about 1.42μm (7000 cm^{-1}), $2V_2$ at about 3.12μm (3200 cm^{-1}). Combination bands include V_1+V_2 at about 1.92μm (5200 cm^{-1}), $2V+V_2$ at about 1.17μm (8500 cm^{-1}), V_3+V_2 at about 1.92μm (5200 cm^{-1}), $V_1+V_2+V_3$ at about(8300 cm^{-1}) and $2V_1+V_3$ at about (10,000 cm^{-1}) [143].

To get a working calibration graph the uncorrected spectra of different moisture content Pruteen samples of 125-180μm particle diameter were examined. First, calibration was tried by plotting peak heights of the 1.9μm band against moisture content (Figure 5.4). As there was no correlation of the signal and moisture content, it was decided to try and find a suitable band as an internal standard to correct for possible variations in the background. Ratios of 1.9/1.55μm, 1.9/1.4μm, 1.9/1.7μm and 1.9/2.2μm bands against moisture content were plotted (Figures 5.5 and 5.6). The ratios of the 1.9μm/1.55μm bands for the particle diameter ranges 38-63μm and 125-180μm are also shown in Table 5.4.

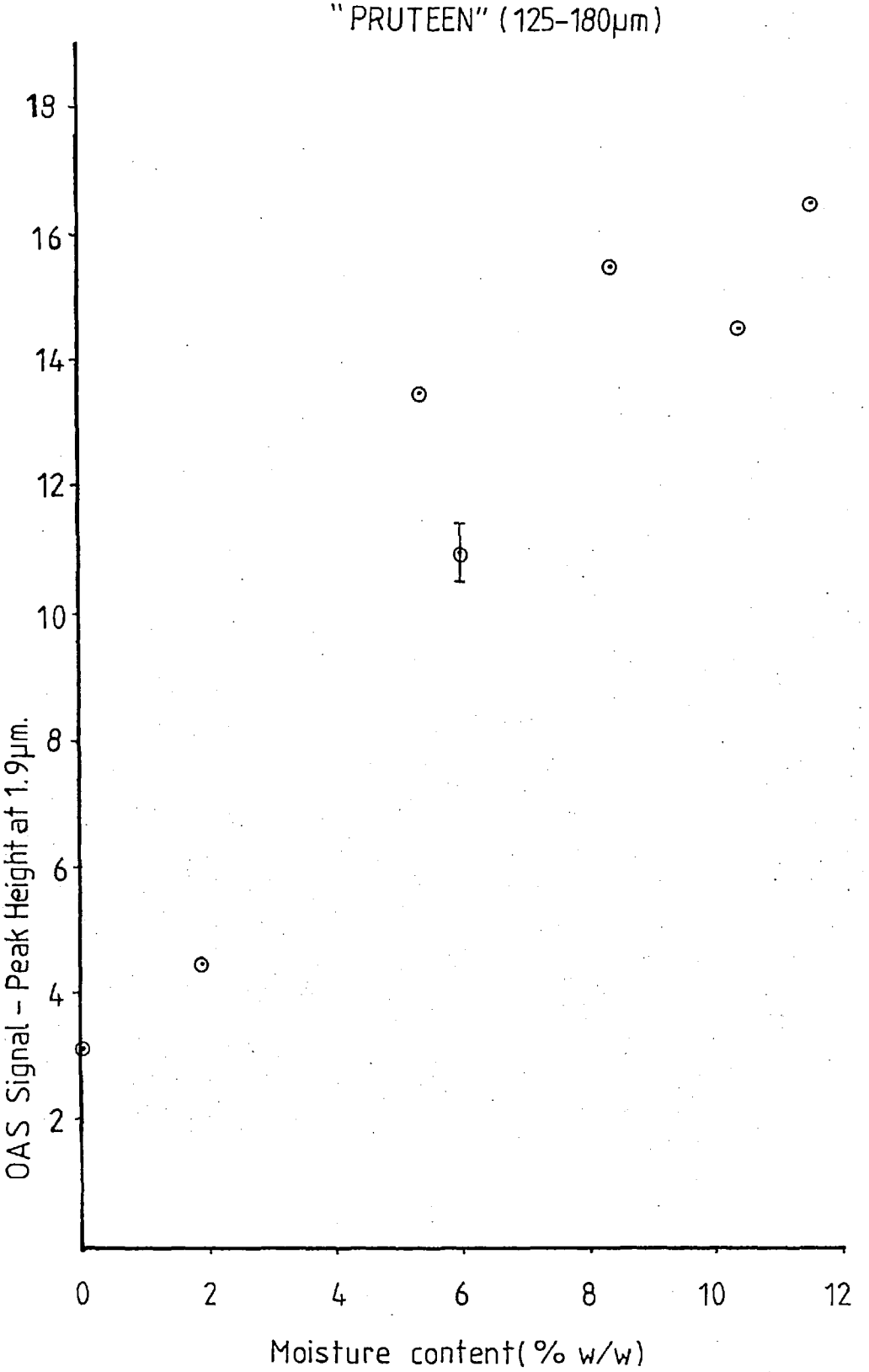

Figure 5.4. OAS Near-IR calibration graph of moisture in "Pruteen" (particle size 125-180μm) by taking the signal peak height at 1.9 μm.

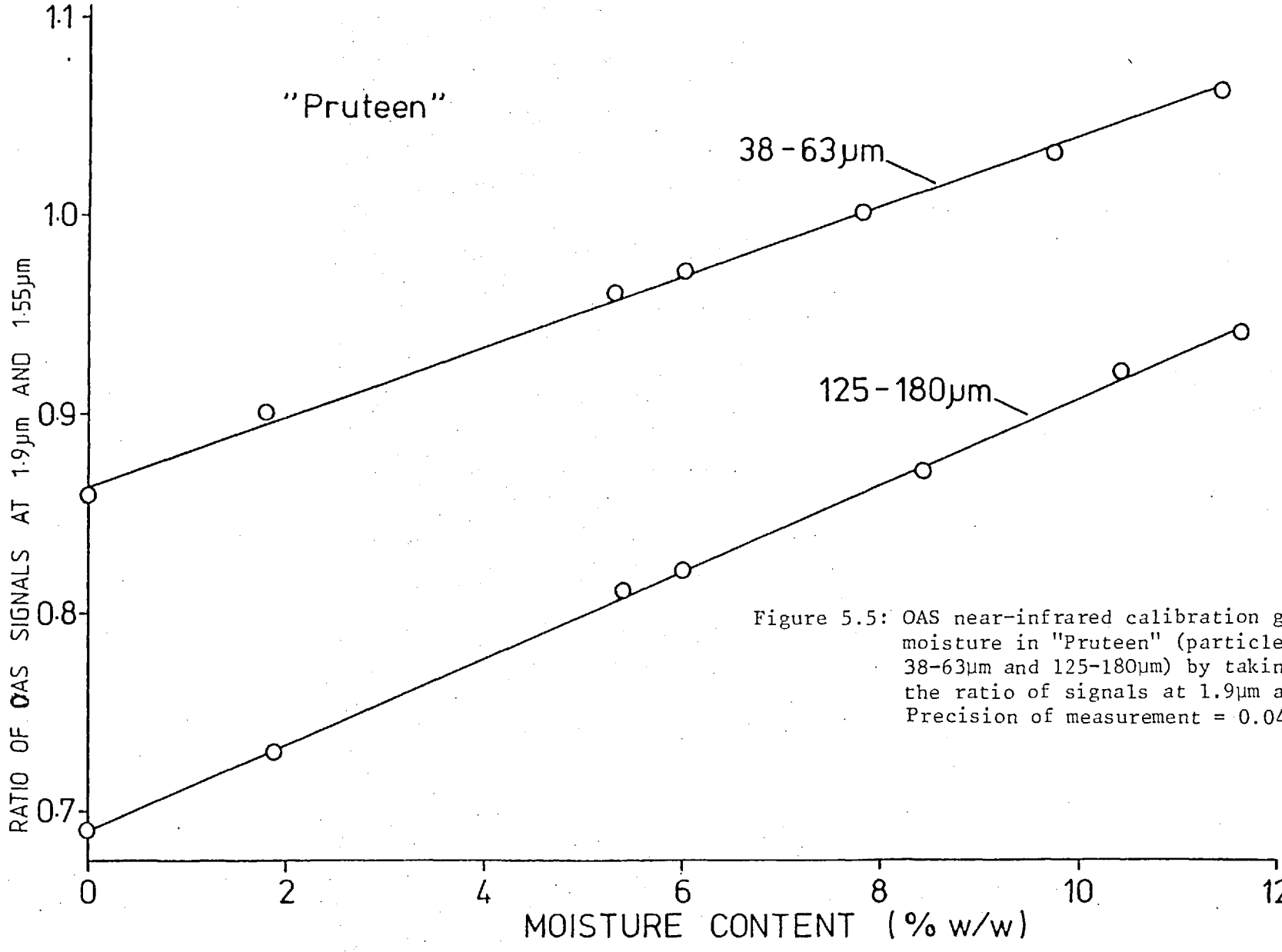

Figure 5.5: OAS near-infrared calibration graph of moisture in "Pruteen" (particle size 38-63µm and 125-180µm) by taking the ratio of signals at 1.9µm and 1.55µm. Precision of measurement = 0.04.

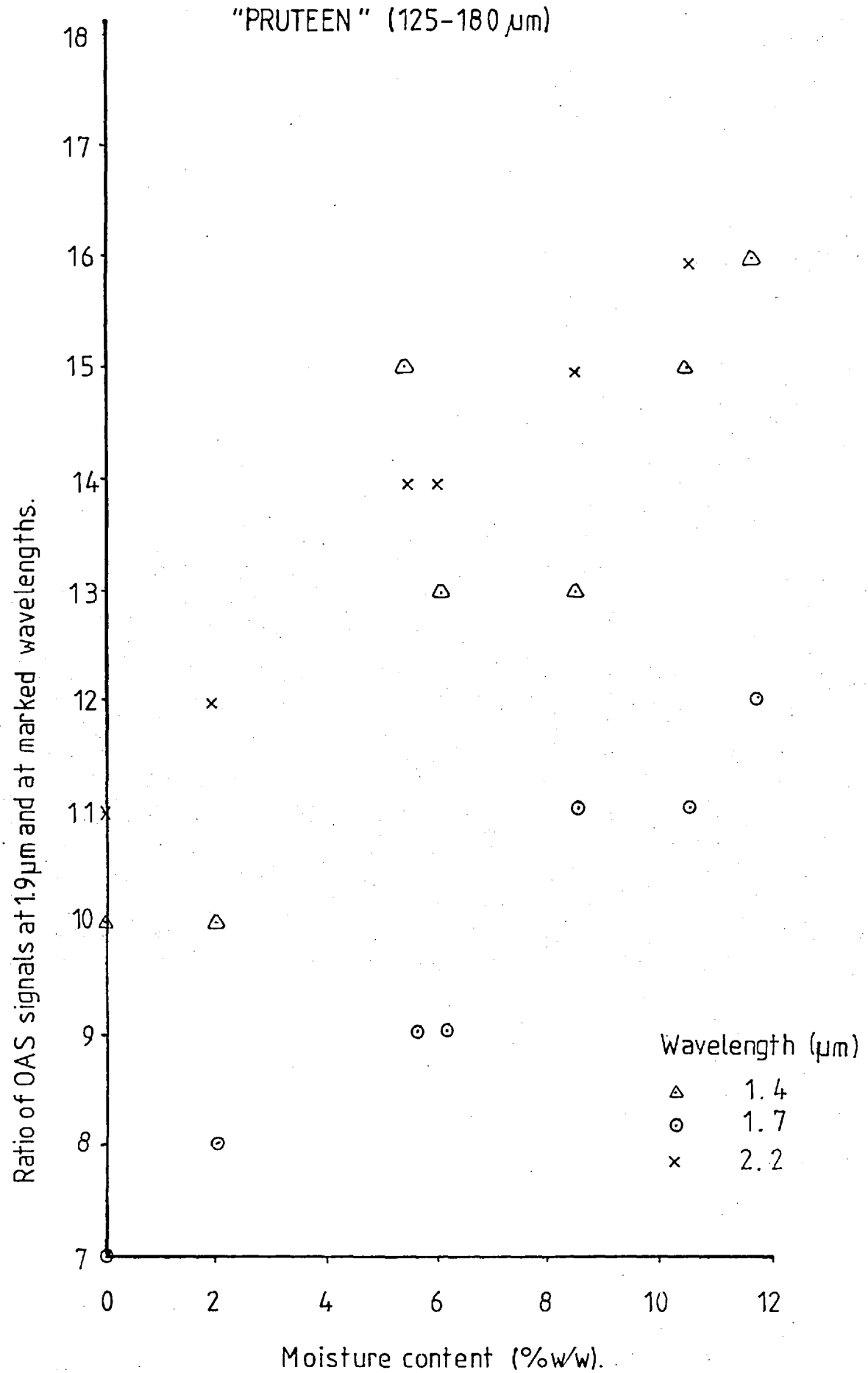

Fig.5.6. OAS Near-IR calibration graph of moisture in "Pruteen" (particle size 125-180um) by taking ratios of the signal at 1.9µm to the signals at 1.4µm, 1.7µm and 2.2µm.

TABLE 5.4: OAS near-infrared signal ratio of moisture in sieved "Pruteen" (particle size 38-63μm and 125-180μm) at 1.9μm/1.55μm.

DESICCANTS	% MOISTURE 38-63μm	RATIO 1.9μm/1.55μm 38-63μm	% MOISTURE 125-180μm	RATIO 1.9μm/1.55μm 125-180μm
H_2SO_4 conc.	0	0.86	0	0.69
LiCl H_2O	2.3	0.90	1.9	0.73
H_3PO_4 $\frac{1}{2}H_2O$	5.8	0.96	5.4	0.81
$CaCl_2$ $6H_2O$	6.3	0.97	6.0	0.82
KSCN	7.8	1.00	8.4	0.87
$Ca(NO_3)_2$ $4H_2O$	9.7	1.03	10.4	0.92
$NaNO_2$	11.4	1.06	11.6	0.94
$NaClO_3$	14.8	1.08	15.9	0.88
NH_4Cl	16.6	1.01	16.9	0.84
$Na_2S_2O_3$ $5H_2O$	17.5	1.03	19.0	0.84
$ZnSO_4$ $7H_2O$	25.3	1.01	27.1	0.83

Figure 5.5 shows the ratio of 1.9μm/1.55μm bands for particle diameter 38-63μm versus moisture content. The graph is linear up to 11.4% moisture. A similar calibration graph for the large particle size, 125-180μm is also shown and is also linear up to 11.6% moisture. It was not possible to obtain any linear relationship with the moisture content by plotting the other ratios describe . From the results shown in Figure 5.5 it is evident that the control of particle size is important in the moisture determination of Pruteen. In the case of Pruteen of particle diameter 38-63μm there is a larger optoacoustic signal than for the Pruteen particle size 125-180μm. This increase in optoacoustic signal with decrease in particle size is apparently due to the increase in the surface area of the sample in contact with the gas phase., but as can be noticed from the slope of the graphs the sensitivity is comparatively lower than for the Pruteen particle size 125-180μm. Very little information is available at the moment to establish this phenomenon.

As the OA signal has a dependence upon the modulation frequency as a result of the varying thermal depth, the spectrum was measured initially at the three different modulation frequencies of 18.6Hz, 22.6Hz and 30Hz. At 18.6Hz, although the spectrum was resolved well, the signal-to-noise ratio was very poor. In the case of measurements made at 30Hz although the signal-to- noise ratio was good, the bands were not resolved well. The modulation frequency of 22.6Hz was chosen because well resolved bands were obtained with a good signal-to-noise ratio. The reproducibility of the technique was also

investigated by taking spectra of each of 15 sets of the same sample.

Experiments were also carried out to determine the effect of the sample mass on the optoacoustic signal. This was studied by taking 15 different samples ranging from 50 mg to 400 mg as shown in Table 5.5.

TABLE 5.5: "PRUTEEN" - effect of sample mass

MASS OF SAMPLE (mg)	RATIO OF MEASUREMENTS MADE AT 1.9 & 1.55μm
50	0.99
75	1.00
100	0.98
125	1.00
150	1.00
175	0.99
200	0.99
225	0.93
250	0.98
275	0.96
300	0.96
325	0.97
350	0.99
375	0.97
400	1.00

A statistical evaluation of the calibration graph of Pruteen particle diameter 38-63μm shows it has a regression coefficient (linearity coefficient) value of 0.9996, the slope is 0.0176 (±0.0002) and the intercept is 0.8596 (±0.0012). The calibration graph for the Pruteen of particle diameter of 125-180μm has a regression coefficient of 0.9993, the slope is 0.0128 (±0.0002) and the intercept is 0.6899 (±0.0019). The result of these calculations indicate the existence of a significant difference and sensitivity between the calibration graphs for the Pruteen of different particle size.

With regard to the reproducibility of the technique the relative standard deviation is 0.04.

Once the calibration graph is determined it is desirable that the moisture in the unknown Pruteen can be determined by sieving and taking the sample at random without any pre-weighing. Table 5.5. shows the ratio of the optoacoustic signal (1.9μm/1.55μm) with respect to the mass of Pruteen. It is necessary to determine whether or not a correlation exists between the mass of sample and the ratio of the optoacoustic signals at 1.9μm and 1.55μm. There are different measures of correlation but the most generally accepted one is called the Pearson Product-moment coefficient of correlation, commonly symbolised as r [153]:

$$r = \frac{\Sigma xy - n\overline{xy}}{n\sigma_x\sigma_y}$$

where n = number of samples
x = the mass of sample
y = the ratio of the optoacoustic signal (1.9/1.55μm) with respect to mass
σ = standard deviation.

The value of r for the data in Table 5.5 has been calculated to be -0.2 which is near to zero. Hence it can be concluded that there is no correlation of optoacoustic signal to

the mass of the sample.

5.2.4 TECHNIQUE EMPLOYING WIDE-LINE N.M.R.

5.2.4.1 Introduction and Instrumentation

Nuclear magnetic resonance spectroscopy was first observed in 1946 by two teams of physicists, Purcell, Torry and Pound at Harvard and Block, Hanser and Packard at Stanford who shared the Nobel Prize for their work. This was followed by the development of high resolution NMR for elucidiating molecular structures. Wide-line low resolution NMR follows the same theoretical principles as the high resolution technique, which is described elsewhere [154]. The performance of low resolution NMR instrumentation has been improved considerably in recent years and the total hydrogen content of liquids can be determined with an accuracy of ca. 0.1%. The resolution of a low resolution spectrometer, is about six orders of magnitude less than for high resolution instruments. The signal obtained from a sample utilizing low resolution NMR spectroscopy is a function of the total hydrogen content of the sample and is not a function of the chemical shifts present in the molecule.

The Newport Instruments MK IIIA spectrometer is designed for the determination of the amount of a proton-containing liquid present in various solid materials. The bandwidth of the nuclear magnetic resonance spectrum of hydrogen in liquids is relatively narrow in comparison with the bandwidth of the nuclear magnetic resonance spectrum of hydrogen in crystalline solids. The sample

FIGURE 5.7: NMR INSTRUMENT MK IIIA (Field Value 635 Gauss)[155]

to be analysed is placed in a strong magnetic field and radio-frequency energy is applied in a direction perpendicular to the magnetic field. When the applied magnetic field strength and the radio-frequency energy fulfil certain criteria, some of the radio-frequency energy is absorbed by the protons in the sample. The absorbed energy is measured and the information is displayed in digital form.

The wide-line NMR measurements were made using a MK IIIA Newport Analyser of R.F. frequency 2.7MHz (Fig. 5.7)(Newport Instruments Ltd., Milton Keynes MK14 4AW) equipped with a 40cm^3 capacity glass sample tube [155]. The instrument is composed of two modules: the magnet/sample assembly, into which the material under test is inserted, and the electronic console, which contains all the control instrumentation required for setting up and measuring the NMR signals. A simplified block diagram of the instrumental assembly is shown in Figure 5.8.

The bandwidth of the resonance signal obtained from the sample depends upon the relative mobility of the protons. The resonance bandwidth of protons in the liquid phase is relatively narrow compared with the resonance bandwidth of protons in the solid phase. An analogue gate can be set to pass signals of various bandwidths between 0.25G and 10G. The narrow bandwidth resonance from liquid phase protons passes through the gate at all gate bandwidths, but signals from solid phase protons pass through the gate to a progressively lesser extent as the gate bandwidth is reduced. Generally, measurements made with a small gate width (1.5G) correspond largely to the amount of liquid

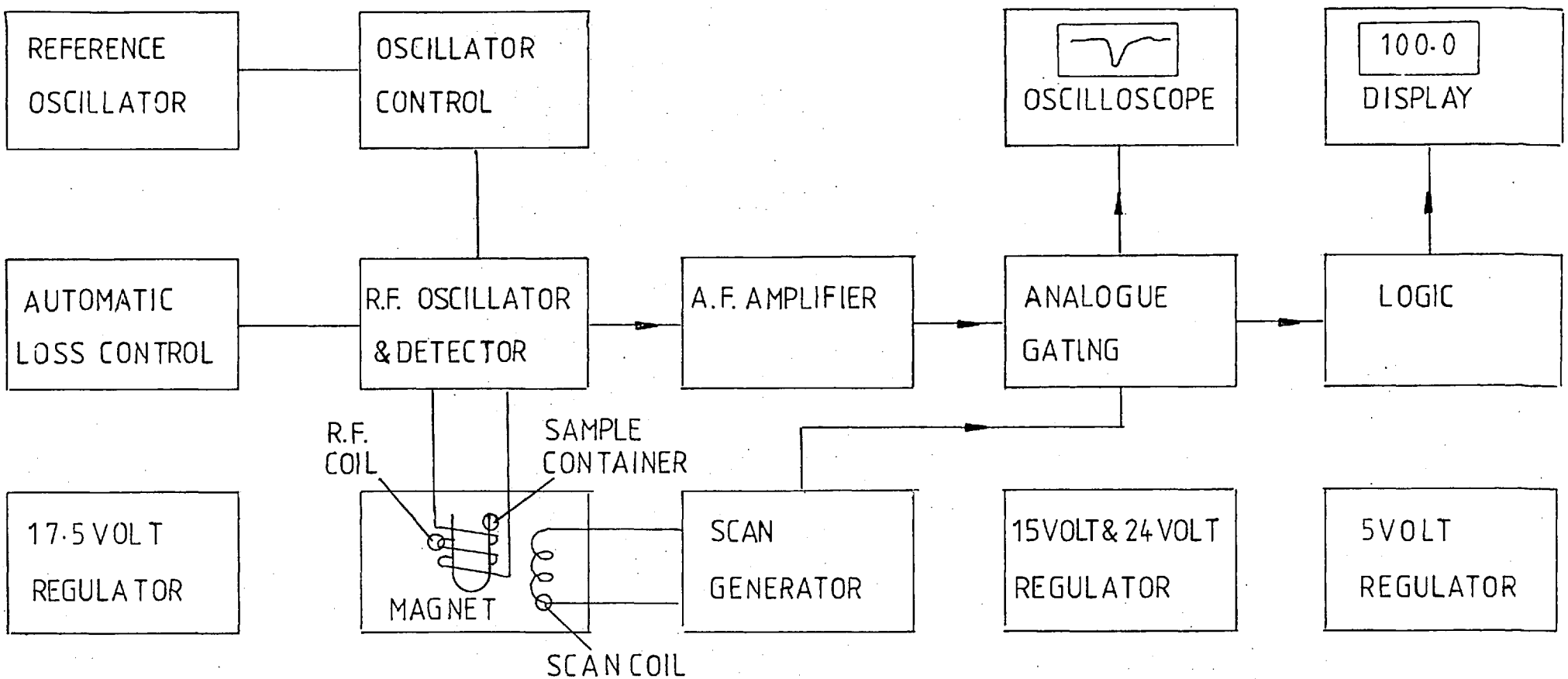

Fig.5.8. Block Diagram of Newport Analyser MK IIIA (155)

phase protons present, whereas, signals measured at wide gate widths (10G) correspond to the amount of solid and liquid phase protons present.

The signal obtained is proportional to the area of the resonance signal within the gate width. As the gate width is increased the resonance signal occupies a smaller proportion of the gate bandwidth and gives a lower signal. At small gate widths, the tuning of the resonance signal becomes very critical whereas at large gate widths the signal obtained is reduced and a lower precision in the measurement results.

The signal is measured by taking the train of resonance signal pulses to an analogue-to-digital convertor. The NMR signal even from a 100% liquid sample is relatively small and susceptable to noise from the electronics. In order to reduce the effects of this noise the signal is integrated over a period of time selected from the range 1, 8, 32 and 128 seconds. Following the insertion of the sample into the coil the reset button is pressed. An audio alarm is fitted to give an indication of the end of each integration period and a small oscilloscope is fitted to allow the position of the resonance signal in the gate to be adjusted.

5.2.4.2 Results and Discussion

A calibration graph was obtained as described in 5.2.2 for samples of Pruteen containing moisture in the range of 0-21%. The equilibrated pruteen samples were in turn transferred to a 40 cm^3 sample tube fitted with a PTFE stopper and the NMR signals measured at ambient

temperatures. Three readings of each pruteen sample were taken at each of the gate widths of ½G, 1½G and 10G after the instrument had been tuned with the sample containing the greatest amount of moisture. The instrument settings are given in Table 5.6.

TABLE 5.6: NMR settings for measurement of moisture in unsieved "Pruteen"

R.F. level	150μA
A.F. gain	600
Integration time	32s
Loss control	Low

The mean of the three measurements made were corrected to give the signal per gram of Pruteen. This value was then multiplied by the gate width and plotted against the percentage moisture content of the Pruteen sample. The results are shown in Figure 5.9.

In order to investigate the effect of the particle size of the sample upon the horizontal portion of the calibration for moisture contents less than 5%, calibration graphs were constructed using sieved samples of Pruteen. The calibration graph for the Pruteen of particle sizes in the range 125-180μm and 38-63μm are shown in Figures 5.10 and 5.11. The instrument settings are given in Table 5.7.

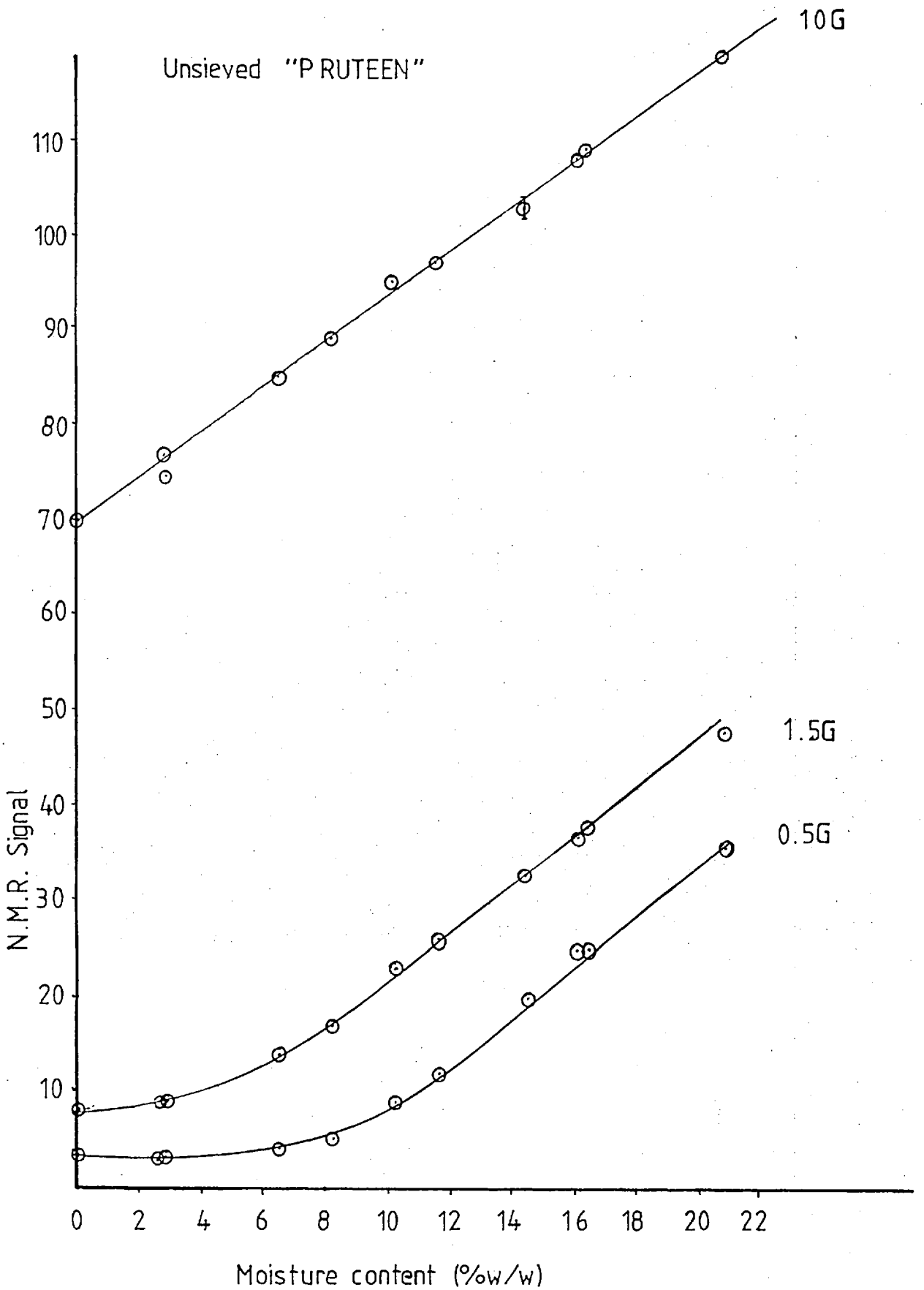

Fig.5.9. NMR Calibration graph of moisture in unsieved "Pruteen" using gate widths of 0.5G, 1.5G and 10G.

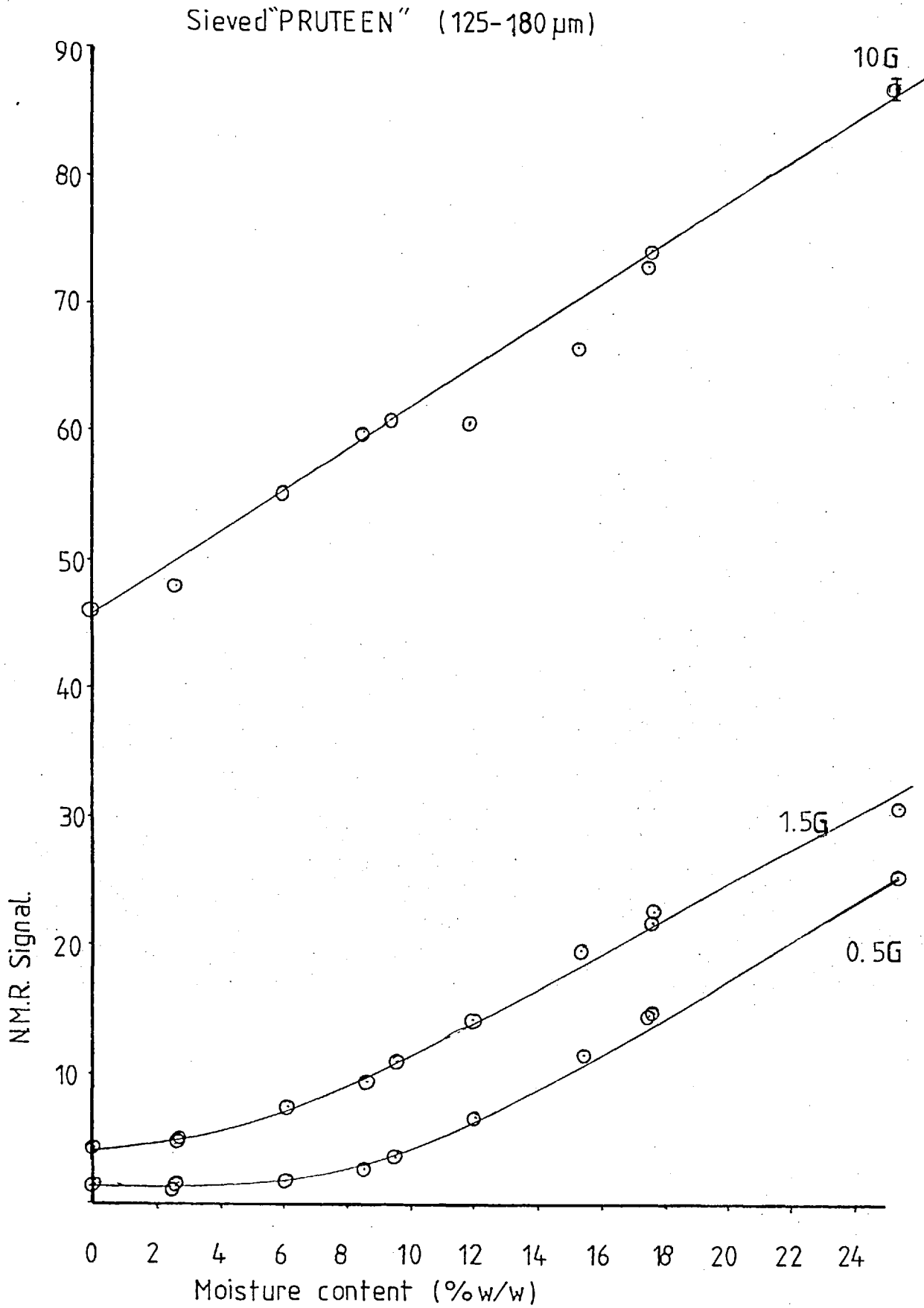

Fig.5.10. NMR Calibration graph of moisture in sieved "Pruteen" of particle size 125 -180µm using gate widths of 0.5G, 1.5G and 10G.

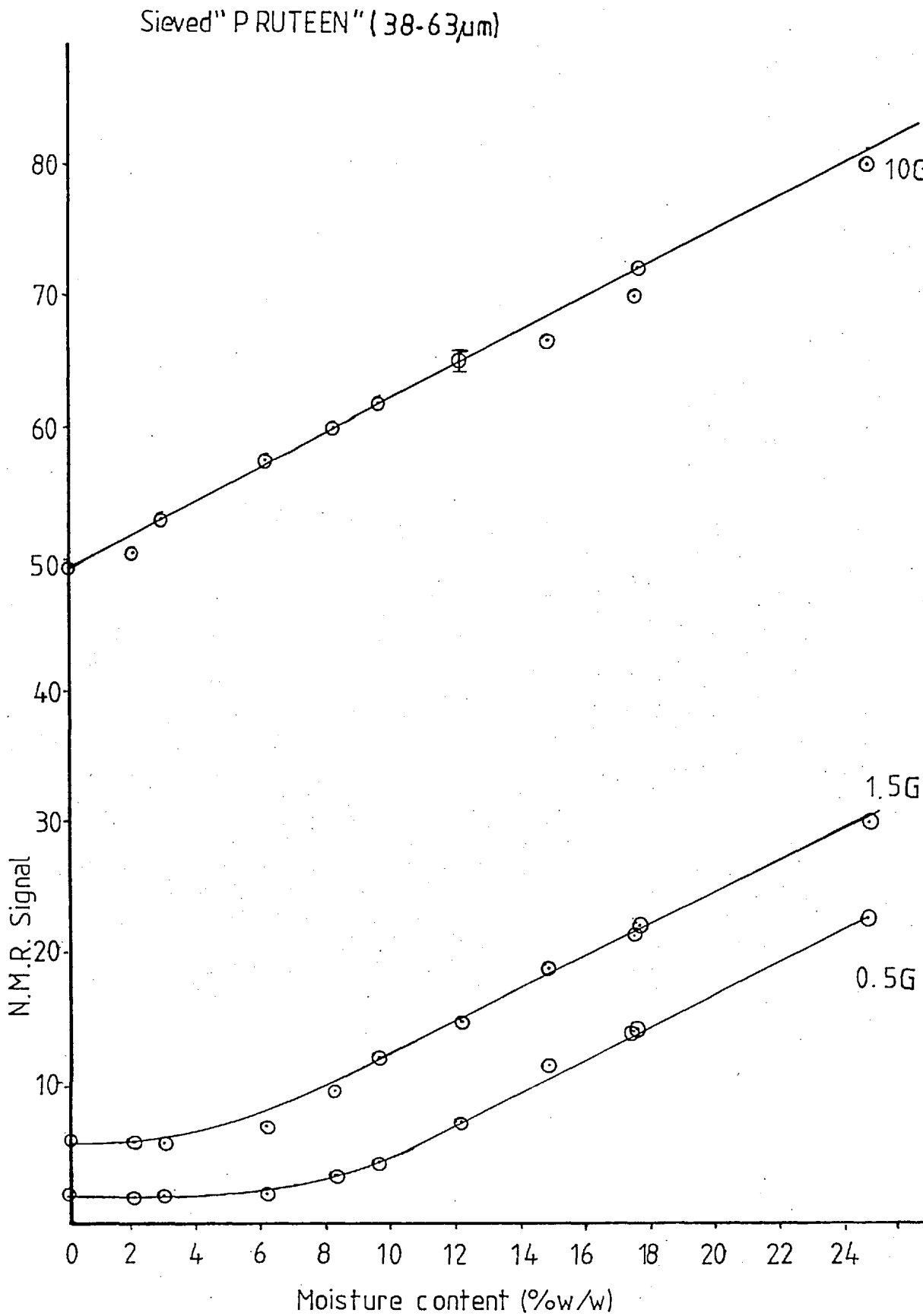

Fig. 5.11. NMR Calibration of moisture in sieved "Pruteen" of particle size 38 - 63 μm using gate widths of 0.5G, 1.5 G and 10G.

TABLE 5.7: NMR settings for measurement of moisture in sieved "Pruteen"

R.F. level	500μA
A.F. gain	1000
Integration time	32s
Loss control	low

The calibration graph for the corrected NMR signal of the unsieved samples of Pruteen is shown in Figure 5.9. For the measurements made at small gate widths, corresponding largely to the liquid phase proton present, the graph is linear for moisture contents greater than ca.6%. The linear calibration graph obtained at the gate width of 10G corresponds to the total proton content of the sample. The horizontal portion of the calibration graph obtained using a gate width 0.5G and 1.5G is attributable to the liquid phase component being very small compared with the signal due to the solid phase component. This is probably the result of moisture below the 5% level being more strongly held to the protein material. Therefore, the horizontal portion of the calibration graph can be attributed to the presence of bound water.

From the experiments involving the variation of the particle size of the Pruteen (Figures 5.10 and 5.11) it may be observed that the existence of the horizontal portion of the calibration graph for moisture contents less than ca. 5% appears not to be effected by rigorously controlling the particle size of the sample. The precision of the n.m.r. measurements was found to be ca. 0.01.

5.3 DETERMINATION OF POLYVINYL ACETATE (PVAc) IN POLYVINYL CHLORIDE AND POLYVINYL ACETATE COPOLYMER

5.3.1 Introduction

The wide variety of copolymers produced from vinyl chloride and vinyl acetate represent by far the most important commercial class of polyvinyl chloride copolymers [156]. The resins produced range from about 3% to 40% polyvinyl acetate. The most important subclass of vinyl chloride/vinyl acetate copolymers are low molecular weight resins containing 10-15% polyvinyl acetate. These resins are widely used for preparing phonograph records and floor tiles. Other copolymers having similar compositions and molecular weights are used for the solution application of protective coatings. The copolymers having less than 10% acetate content are often used for films and sheet. The structural formula of PVAc/PVC copolymer can be written as

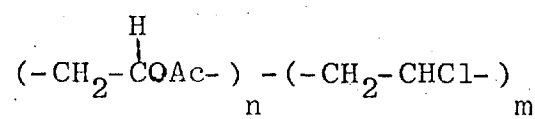

Haslam et al [138] have reported a near-infrared transmission method for the quantitative determination of vinyl acetate in vinylchloride/vinylacetate copolymer. This method depends upon the measurement of an absorption band occurring at about 2.15μm due to a vibration mode of the ester carbonyl group in vinylacetate. A series of laminates is made each with three layers of PVC with a different known thickness (between 0.25 and 2mm) of polyvinyl acetate and a set of calibration samples obtained. The

absorbance at 2.15μm is plotted against the thickness of PVAc in the calibration sample. This graph may be used to estimate the equivalent thickness of PVAc in the unknown test specimen. The percentage of combined vinyl acetate in the unknown is then calculated using the formula

$$\frac{1.20 \times 100}{1.40(T-t)+1.20t}\ \%$$

where 'T' is the thickness of test specimen,
't' the determined equivalent thickness of PVAc
1.20 and 1.40 g/cm^3 are the assumed densities vinyl acetate and combined vinyl chloride.

5.3.2 Technique employing OAS

In this section the quantitative determination of PVAc in vinyl chloride/vinyl acetate copolymer by near-infrared OAS is discussed.

Five samples (both sieved and unsieved) ranging between 0. and 15% of PVAc (0%, 2.1%, 7.8%, 9% and 15%) in vinyl chloride/vinyl acetate copolymer were supplied by ICI Plastics Division, Welwyn Garden City, Herts.

The sieved samples supplied were as follows. The finer one was passed through a 200 mesh sieve and the coarser one was that retained on the 100 mesh sieve. The < 200 mesh sample had a range of particle diameter of 8 to 90μm, of which the bulk was between 25 and 90μm. The ≥100 mesh sample had a range of particle diameter 20 to 250μm of which the bulk was equal or greater than 100μm.

5.3.2.1 Experimental

The instrument employed in this experiment was the same one used in the moisture determination of Pruteen i.e. the single beam instrument with a tungsten halogen source. The cell used was also the same one that was employed for the studies of Pruteen. All spectra were scanned at a rate of 300 nm min^{-1}, a monochromator bandwidth of 30 nm a time-constant of 1 second and a source modulation frequency of 22.6Hz. Wavelength calibration was performed using holmium, erbium and praeseodymium oxides.

First the unsieved samples were examined. These gave poor unresolved ester carbonyl bands at about 2.1μm (Figure 5.12). It is possible that the lack of resolution is caused by a mixture of different particle sizes as previously observed in the studies of Pruteen. Therefore, the experiment was repeated with the two sieved sets of vinyl chloride/vinyl acetate copolymer. This gave a reasonably good ester carbonyl band at ca. 2.1μm as shown in the uncorrected spectra of Figure 5.13 for 15%, 7.8% and 0% of PVAc of <200 mesh particle size.

5.3.2.2 Results and Discussion

The vinyl chloride/vinyl acetate copolymer uncorrected spectrum (Figure 5.13) shows five bands. These bands are at ca. 1.2μm, 1.4μm, 1.75μm, 2.1μm and 2.4μm. The bands at 1.2μm, 1.75μm, and 2.4μm are second overtone, first overtone, combination band, respectively, of C-H stretch of the fundamental at 3.0 - 3.6μm. The 1.4μm and 2.1 μm bands are the third and second overtones of the ester carbonyl band fundamental at 5.8μm.

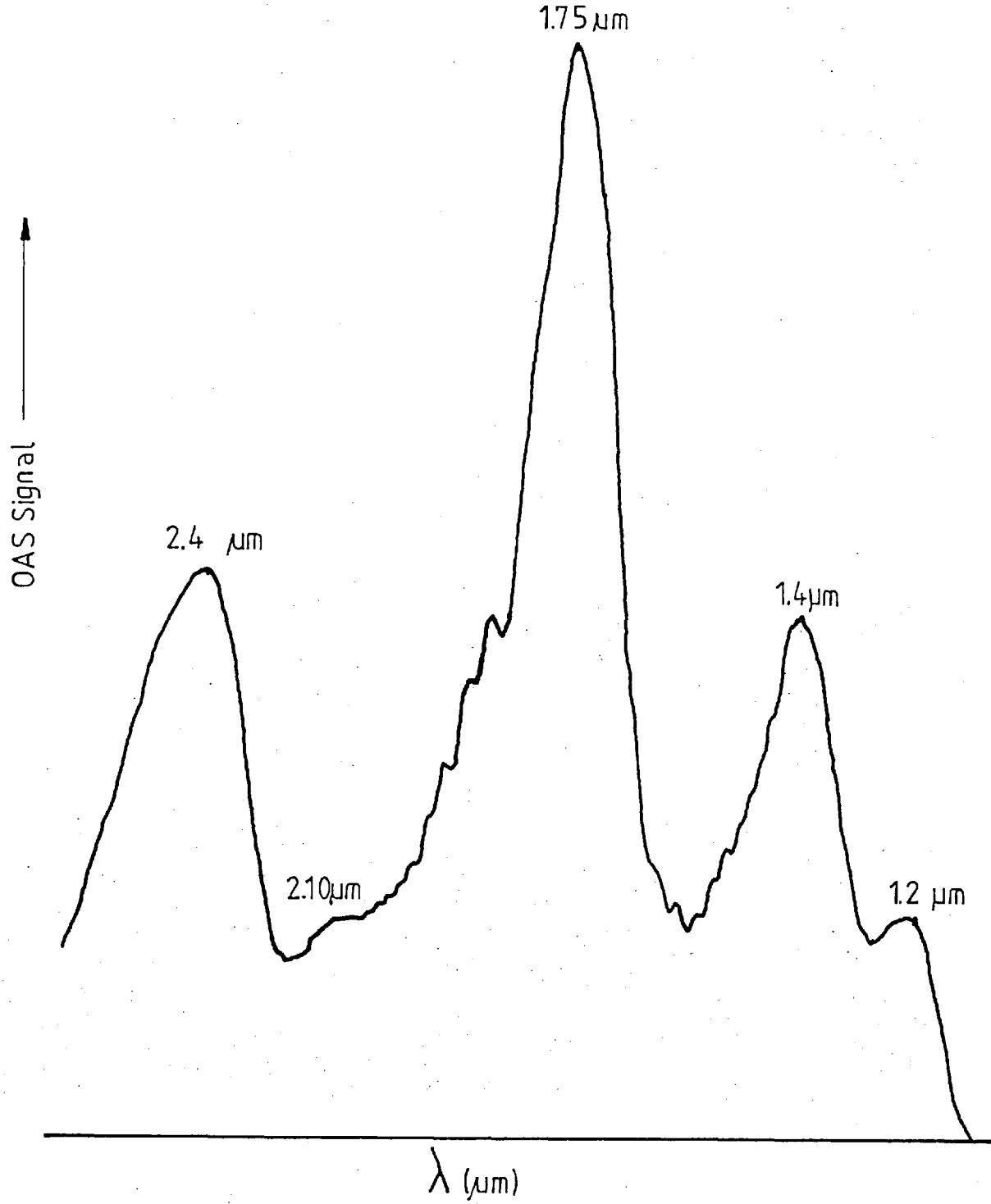

Fig.5.12. OAS Near-I.R. Spectrum of Unsieved PVAc /PVC Copolymer containing 15% PVAc.(Uncorrected Spectrum).

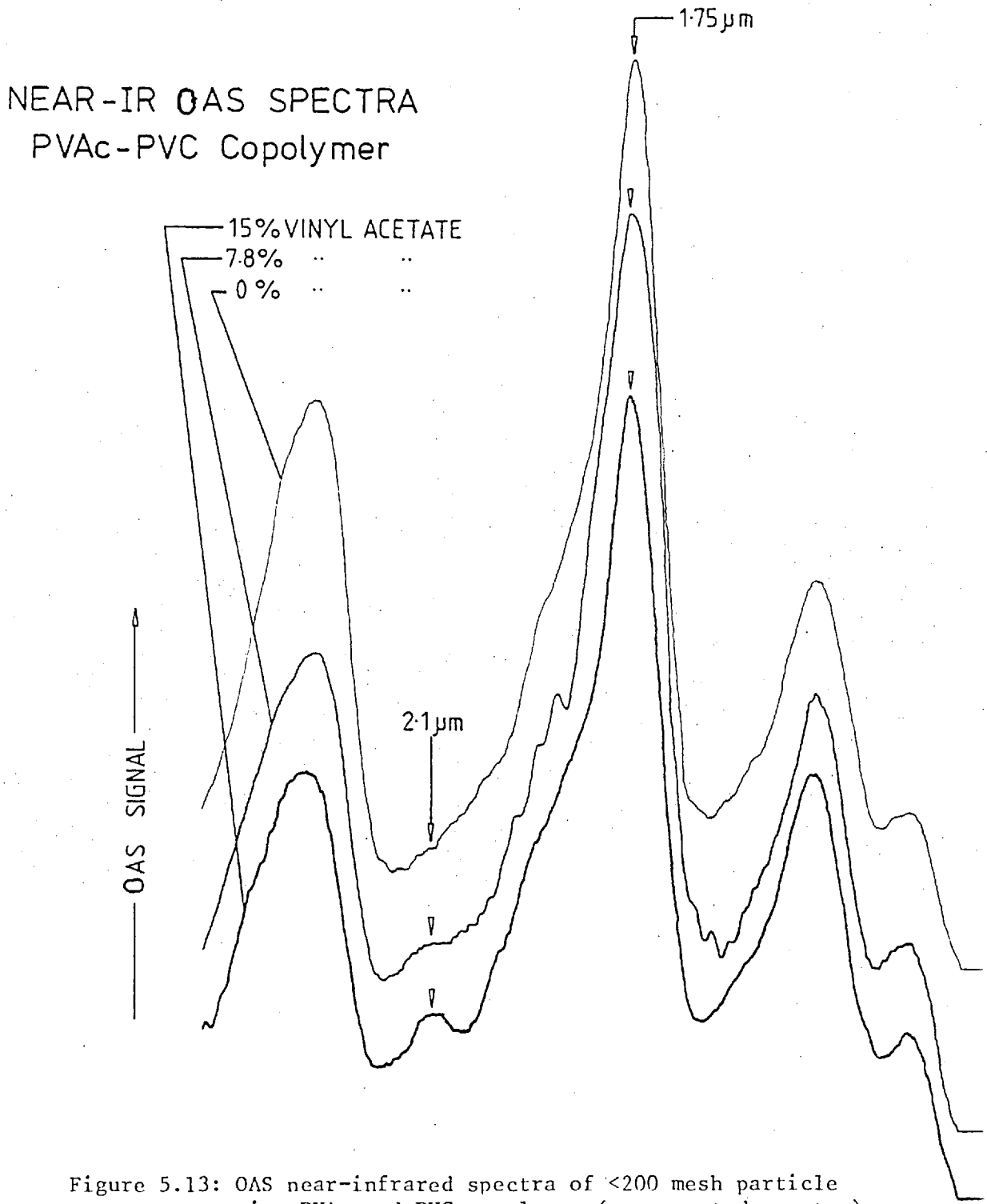

Figure 5.13: OAS near-infrared spectra of <200 mesh particle size PVAc and PVC copolymer (uncorrected spectra)

For a working calibration graph a suitable band was chosen as an internal standard to correct for possible variation in the background. The ratios of the opto-acoustic signal obtained at the carbonyl band (ca 2.1μm) to the reference C-H band (ca.1.75μm) when plotted against the concentration of polyvinyl acetate gave a linear calibration as shown in Figure 5.14. It can also be seen that the smaller particle diameter (i.e. < 200 mesh) is less sensitive than the coarser (i.e. ≥ 100 mesh) particle size. As described in the section on Pruteen, very little information is available at the moment to establish this phenomenon.

The spectrum was measured initially with two other modulation frequencies of 18.6Hz and 30Hz. In terms of signal-to-noise ratio and resolution only the modulation frequency of 22.6Hz was found to be most suitable.

A statistical analysis of the results in Figure 5.14 shows that the PVAc/PVC with smaller particle sizes (i.e. < 200 mesh) has a regression coefficient of 0.994; the slope is 0.0045 (±0.0002) and the intercept is 0.131 (±0.0018). In the case of PVAc/PVC with the large particle size (i.e.≥100 mesh), the regression coefficient is 0.992; the slope is 0.0067 (±0.0003) and the intercept is 0.132 (±0.0029). The results indicate that there is a significant difference between the slopes of <200 mesh and ≥100 mesh sample.

With regard to the reproducibility of the measurement, the relative standard deviation was found to be 0.05.

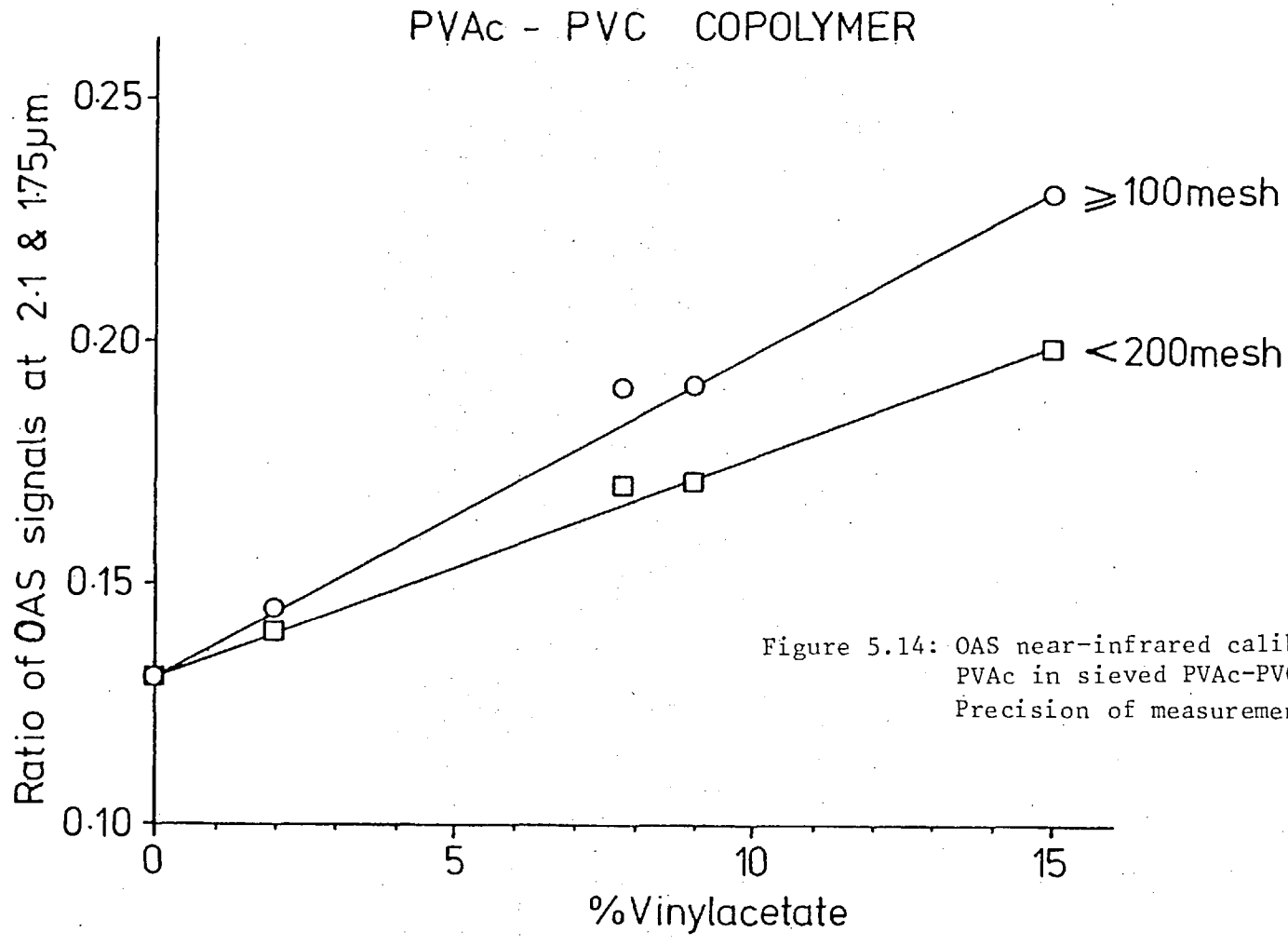

Figure 5.14: OAS near-infrared calibration graph of PVAc in sieved PVAc-PVC copolymer. Precision of measurement = 0.05.

5.3.3 Technique employing Diffuse Reflectance

A full account of diffuse reflectance spectroscopy is presented, including the details of the instrumentation, in Chapter One of this thesis. Being a complementary technique to OAS the use of diffuse reflectance spectroscopy was tried for the analysis of PVAc in the vinyl chloride/ vinyl acetate copolymer samples.

5.3.3.1 Experimental

A Beckman DKA double beam spectroreflectometer instrument with a lead sulphide detector described in Chapter One was used for the analysis. For making the discs a KBr press was used. Before the measurements with the polymer sample were made, zero and 100% reflectance were set with MgO in the exit ports. The spectra were scanned between 0.8μm and 2.5μm.

When the unsieved vinyl chloride/vinyl acetate copolymer samples were scanned a very poorly resolved carbonyl band was obtained. The poor resolution of the carbonyl band could have been due to the non-uniform particle size of the powder. Therefore the powder was prepared in the form of pressed disc of 30 mm diameter and 1 mm thickness and after the initial zero and 100% were set with the MgO standard, the spectra were scanned as previously described. Discs were made with the KBr press by applying a pressure of $1.4 \times 10^7 N/m^2$. The results are shown in Figure 5.15. A further study with two sets of the sieved samples (<200 mesh, and ≥.100 mesh) showed a better resolved carbonyl band than that of the pressed disc technique as shown in the spectra of Figure 5.16 for

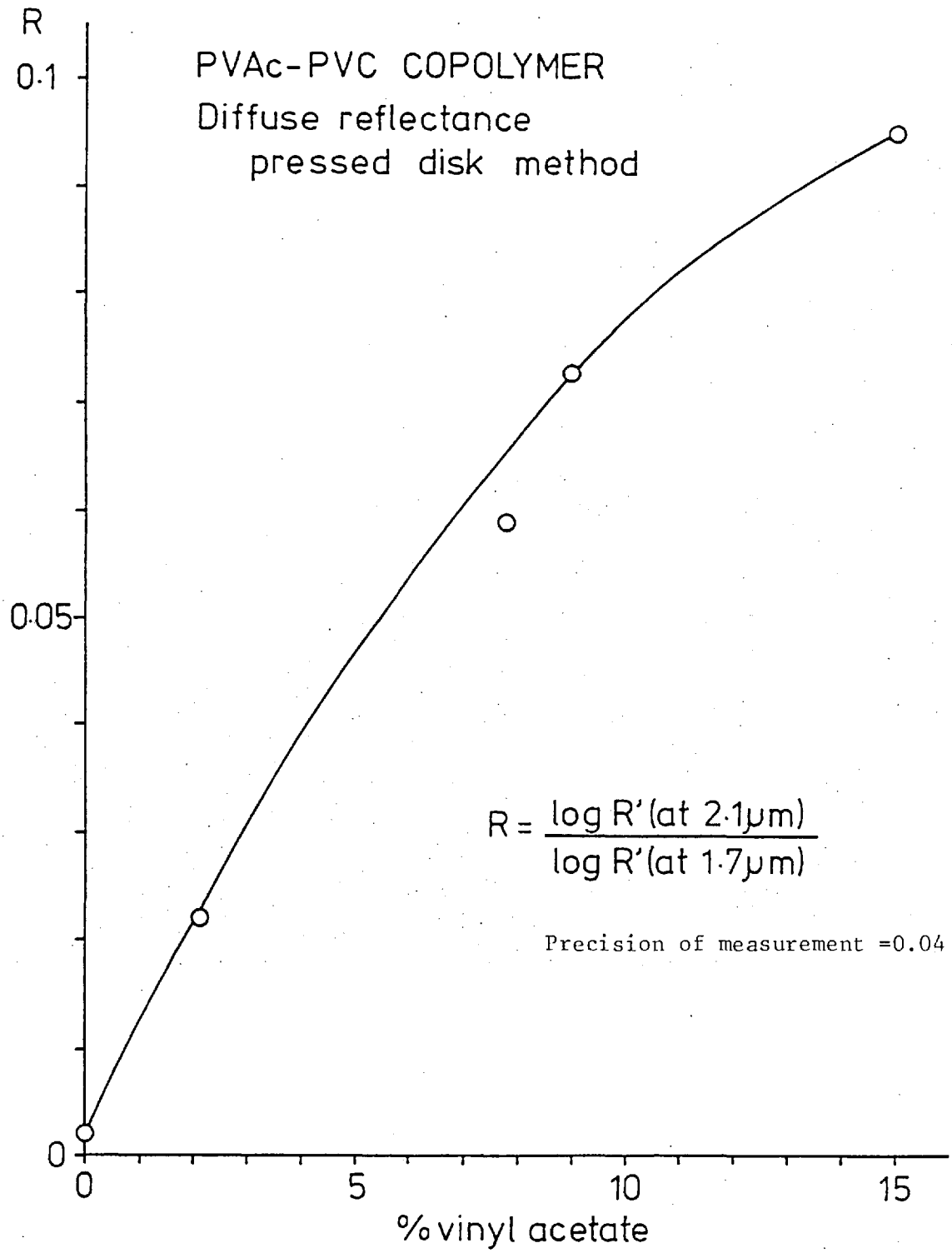

Figure 5.15: Diffuse reflectance near-infrared calibration graph of PVAc in unsieved PVAc-PVC copolymer by the pressed disc method. R in the graph is the ratio shown and R' is obtained as shown in Figure 5.16.

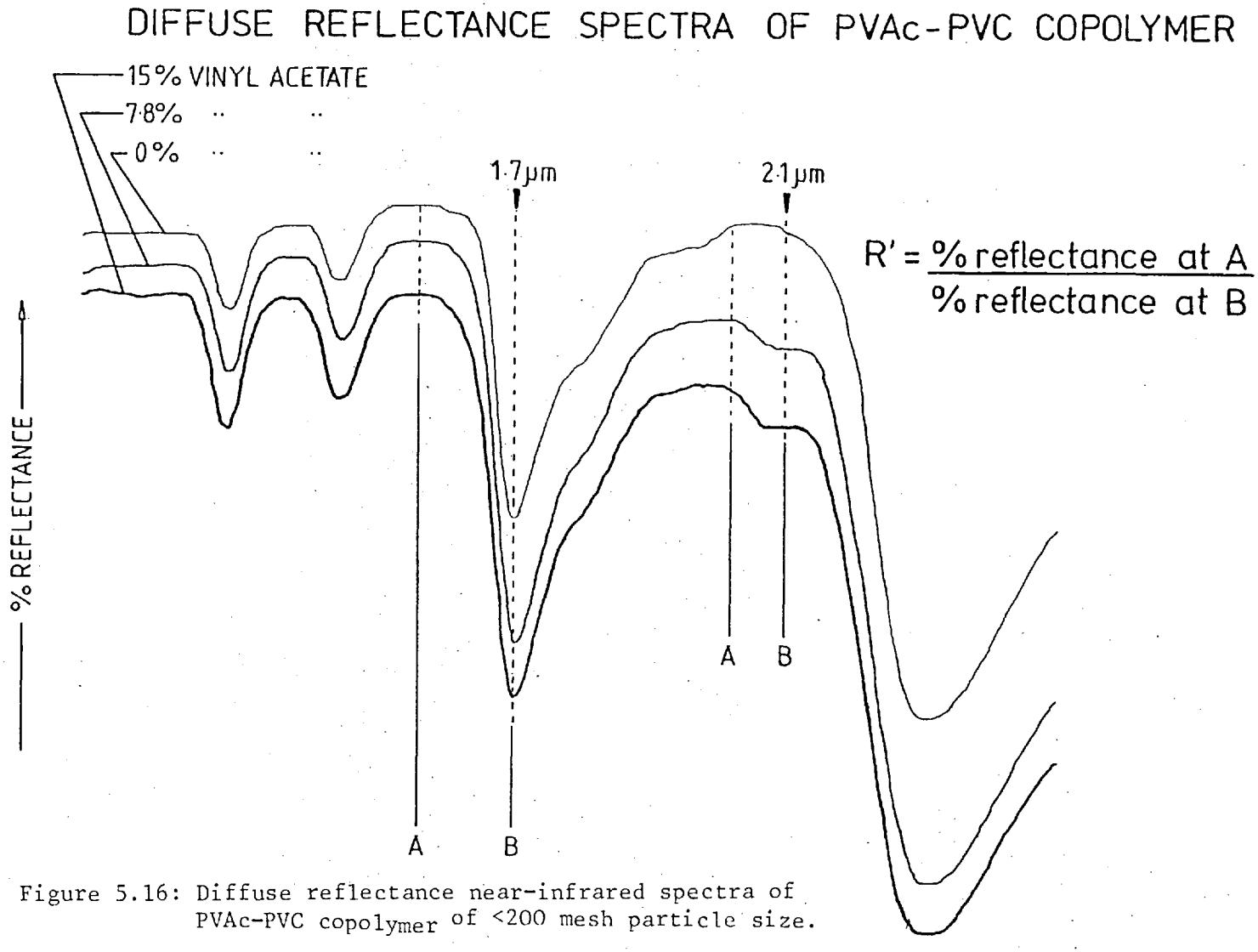

Figure 5.16: Diffuse reflectance near-infrared spectra of PVAc-PVC copolymer of <200 mesh particle size.

15%, 7.8% and 0% PVAc of <200 mesh particle size

5.3.3.2 Results and Discussion

The diffuse reflectance spectra shown in Figure 5.16 have five bands as observed in the optoacoustic spectra.

The calibration graphs of Figure 5.17 were plotted by dividing the log ratio at 2.1μm band by the ratio at 1.7μm against %PVAc in the vinyl chloride/vinyl acetate copolymer.

A statistical analysis of <200 mesh sample, (Figure 5.18) gives a regression coefficient of 0.997; a slope of 0.0050 (±0.0002) and an intercept of 0.017 (±0.0013). With regard to the ≥100 mesh samples, the result (Figure 5.18) have a regression coefficient of 0.987; a slope of 0.0061 (±0.0004) and an intercept of 0.019 (±0.0035). The results indicate that there is a significant difference between the two slopes.

The results of the pressed disc technique (Figure 5.15) show a poor linearity coefficient (i.e. 0.973) compared with the results obtained with the sieved samples. Although the results for the <200 mesh sieved sample have a better linearity than the results for the ≥100 mesh samples the latter is more sensitive than the former. It is well known in diffuse reflectance spectrometry that as the particle size decreases the amount of specular reflectance increases and probably this explains the poorer sensitivity of the technique for the <200 mesh particle size.

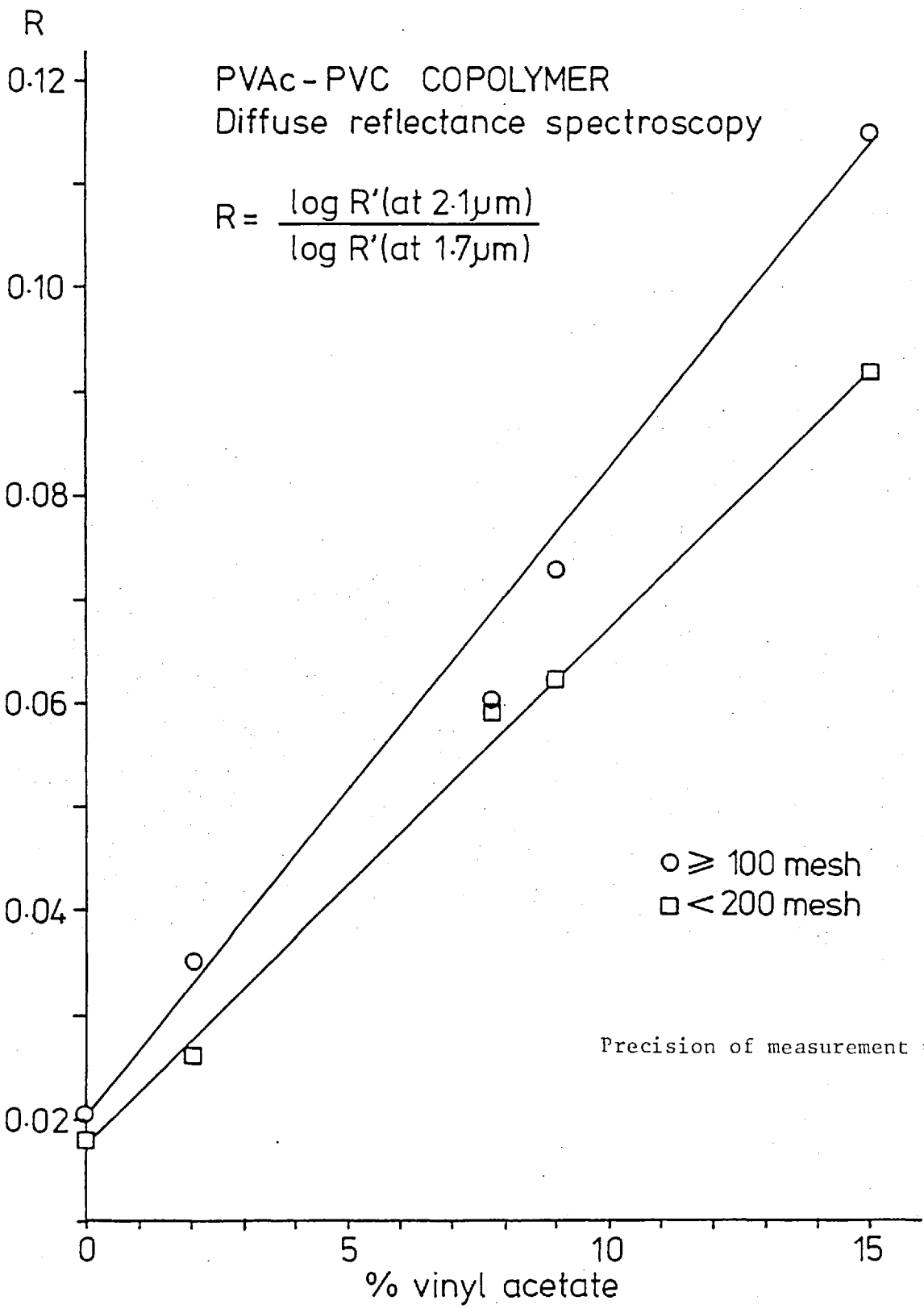

Figure 5.17: Diffuse reflectance near-infrared calibration graph of PVAc in sieved PVAc-PVC copolymer . R in the graph is the ratio shown and R' is obtained as shown in Figure 5.16.

The precision of measurements made using the pressed disc technique was found to be 0.04 and for the sieved samples 0.015.

5.4 CONCLUSION

In the determination of moisture in Pruteen by optoacoustic near-infrared spectroscopy, the bands of the bound hydroxyl groups and the mobile hydroxyl groups are well resolved and distinct. In the Pruteen spectrum the band of $-NH_2$ (1.55μm) is also observed which could be used as a band for the determination of protein in the material. Pruteen being opaque, conventional transmission methods are unsuitable. In the case of optoacoustic spectrometry as only the absorbed photons produce the optoacoustic signal, the scattering effect is very much minimised. Once the calibration graph is prepared, the amount of moisture can be determined without any sample preparation or preweighing and with relatively small amounts of sample. Additionally, the technique is non-destructive. The only major disadvantage of the technique employing OAS is the effect of the particle size. In the complementary technique of diffuse reflectance spectrometry the need to control the particle size is also reported [157]. The alternate wide-line method also provides a non-destructive method for the analysis of water in Pruteen. Although no control of particle size is needed, the method holds good only for moisture contents above ca. 6%. Below this the effect of the bound water interferes in the measurement. In wide-line n.m.r. the method determines protons in the liquid phase and therefore, is likely to give a total value for

protons in solution. Before applying the method to the determination of water in any new material, it is necessary to determine whether other hydrogen containing compounds are present in the liquid. These might be either other low viscosity liquids or solids in solution. Often suitable corrections can be made for contribution by other constituents but this means it is a time consuming technique.

The ester carbonyl band of the PVAc optoacoustic spectrum is better resolved than the diffuse reflectance spectrum. The sample preparation and calibration of results in optoacoustic spectrometry is very simple compared with the diffuse reflectance method. In the diffuse reflectance technique the results of the pressed disc method have a very poor signal-to-noise ratio compared with the use of a sieved sample.

The results obtained using diffuse reflectance spectroscopy with sieved samples are also poor compared with the results obtained using optoacoustic spectroscopy.

Although the particle size and distribution of the sample is an important parameter for obtaining quantitative results using both diffuse reflectance and optoacoustic spectroscopy, the nature of the measurements made in diffuse reflectance spectroscopy mean that for this technique the particle size of the sample is particularly critical.

CHAPTER SIX

MISCELLANEOUS QUALITATIVE ANALYSIS

6.1 Introduction

This chapter describes some of the spectral information obtained in the ultraviolet, visible and near-infrared regions of the spectrum using optoacoustic spectroscopy for some of the many ICI samples examined.

The samples studied are grouped under five different headings according to the nature and the details available:

1. Examination of Tin and Antimony oxide catalysts
2. Evaluation of Quinoline as a Flotation agent for mineral extraction
3. Dye formulations and dye pigments
4. Miscellaneous

Other than the quantitative aspects of the study of tin/antimony oxide catalysts, the remaining investigations were of a purely qualitative nature as part of the preliminary exercise for ICI to assess the potential of optoacoustic spectroscopy to their industrial applications.

6.2.1 Examination of Tin/Antimony Oxide Catalysts

Catalysts based upon mixed oxides of tin and antimony have been developed industrially for the selective oxidation of hydrocarbons [158].

Six samples of varying composition of Antimony oxide in Tin oxide were received, as shown in Table 6.1. Out of the six, five were calcined at 600°C and the sixth one calcined at 700°C.

TABLE 6.1: Details of antimony in tin oxide catalyst.

	Sample	Calcination Temperature	Percentage of Sb in Tin oxide
(1)	21c Sn/Sb	600°C	4%
(2)	27B Sn/Sb	600°C	20%
(3)	26 Sn/Sb	600°C	40%
(4)	26 Sn/Sb	700°C	40%
(5)	46A Sn/Sb	600°C	65%
(6)	29 Sn/Sb	600°C	83%

The objective of this experiment was to investigate whether the optoacoustic ultraviolet visible spectral information could be correlated quantitatively with the Antimony present in the catalyst.

Experimental

The instrument employed was the double beam instrument with the 300 watt xenon arc source described in Chapter Two. The samples were ground and the spectrum scanned in the UV-visible region (λ 270 nm - 700 nm). The scan rate used was 50 nm min^{-1} at a spectral half-bandpass of 10 nm with a time-constant of 3 seconds. The modulation frequency employed was 28Hz.

Results and Discussion

The optoacoustic spectrum of Sn/Sb catalysts containing 83% Sb is shown in Figure 6.1. From the spectrum it can be seen that absorption is greater in the ultra-violet region than in the visible region of the spectrum. Because of the variation in particle size of the original sample, the calibration was not obtained by an absolute

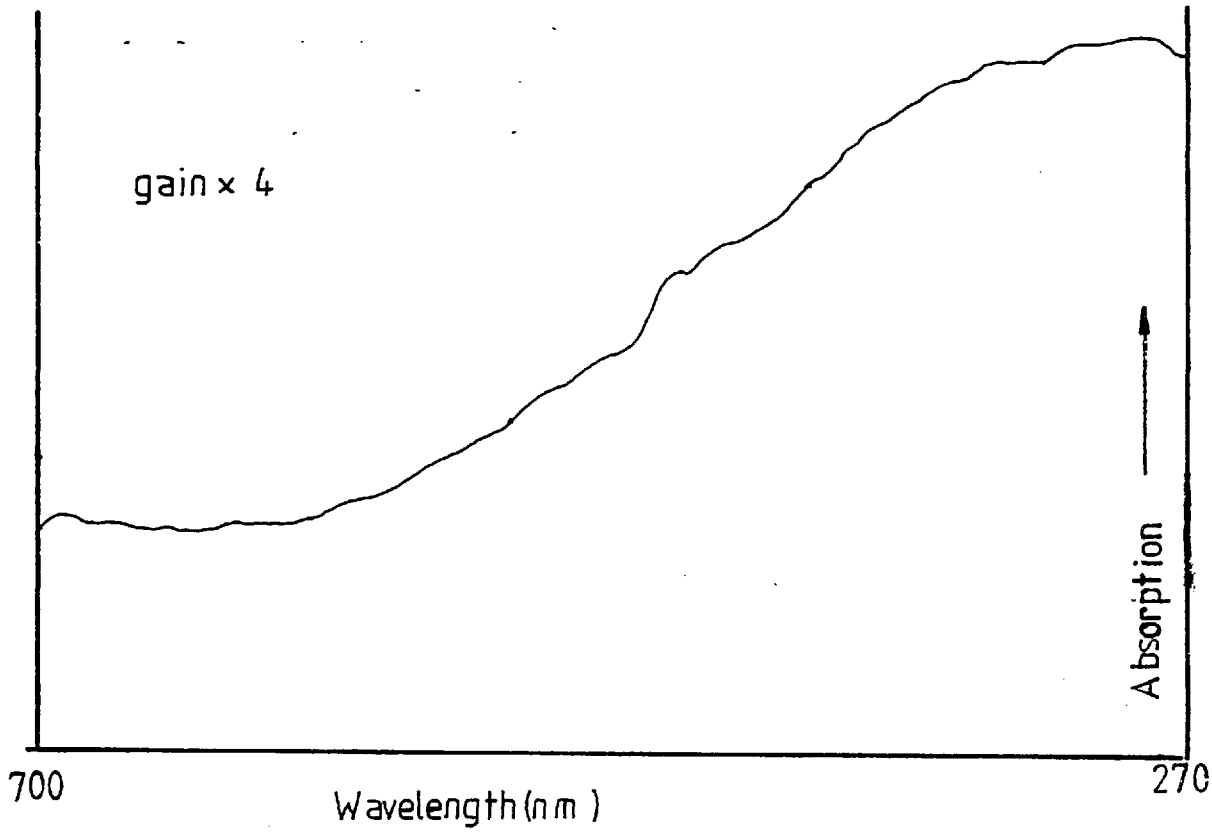

Fig.6.1. UV-Vis OAS Spectrum of Sn/Sb sample calcined at 600°C containing 83% Sb.

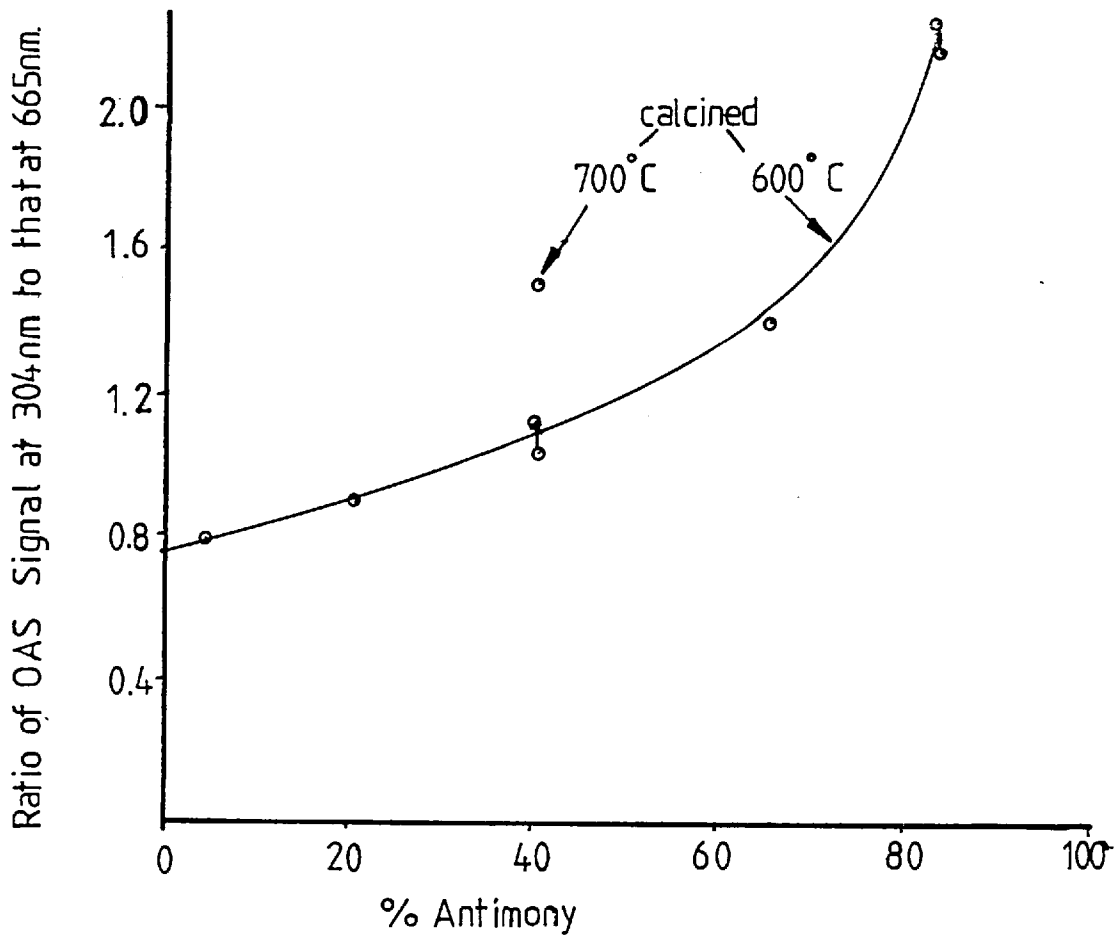

Fig.6.2. OAS Calibration graph of Antimony in Tin Oxide.

signal magnitude measurement. Instead a two wavelength ratio technique was employed. Figure 6.2 shows the variation in the ratio of absorption at 304 nm to that at 665 nm. The lack of linearity at higher concentration could be attributed to compound formation. The variation of the ratio for sample No.4 appears to be due to the difference in the calcining temperature of the sample. No other wavelength combination examined produced fully linear curves.

6.2.2 Evaluation of Quinoline as a Flotation agent for Mineral Extraction

The three samples examined were (1) untreated Malachite, (2) Malachite with 1% Quinoline derivative and (3) Quinoline derivative complexed to copper ions (84% Quinoline/16% Cu^{2+} w/w).

The aim of this experiment was to obtain information about the mechanism of binding (Physical or Chemical) between the Quinoline and the malachite particles from the ultraviolet, visible and near-infrared spectra

Experimental

For the production of UV-visible spectra the instrument employed was a single beam instrument and a digital scan recorder was employed for the sequential correction of spectra as detailed in Chapter Two. The same single beam instrument may be used for studies in the near-infrared region by changing the grating and source as described in Chapter Two. The UV-visible spectral range employed was from 290 nm to 700 nm with a modulation frequency of 28Hz, a monochromator bandwidth of 10 nm and a scan rate of 100 nm min^{-1}. For

studies in the near-infrared the wavelength region examined was from 1μm to 2.5μm with a modulation frequency of 28Hz, a monochromator bandwidth of 30nm and wavelength scan rate of 300 nm min^{-1}.

Results and Discussion

The spectra of the samples in the UV-visible and near infrared regions are given in Figures 6.3 and 6.4.

The UV-visible spectra of Malachite (Figure 6.3A) and Quinoline on malachite (Figure 6.3B) are identical. The quinoline-copper ions (Figure 6.3C) absorption maxima are more in the wavelength range of 290 nm to ca 490nm and absorption decreases towards a wavelength of 700nm.

The near-infrared spectra are quite interesting. The malachite (Figure 6.4A) and Quinoline/Malachite spectra (Figure 6.4B) are similar, whereas the Quinoline/copper ions sample spectrum (Figure 6.4C) exhibits the absorption bands characteristic of aromatic C-H overtones at ca 1.7μm and the combination bands at ca 2.2μm. No evidence of these bands with the Quinoline/Malachite sample exists.

6.2.3 Dye formulations and dye pigments

The sample of dyes received were (1) yellow reactive dye on cotton, (2) yellow disperse, (3) yellow disperse-Parent dye, (4) yellow disperse dye formulations and (5) blue azoic dye on cotton and (6) blank cotton for blue azoic dye on cotton.

The dye pigments received were (1) WED/C/9723 copper

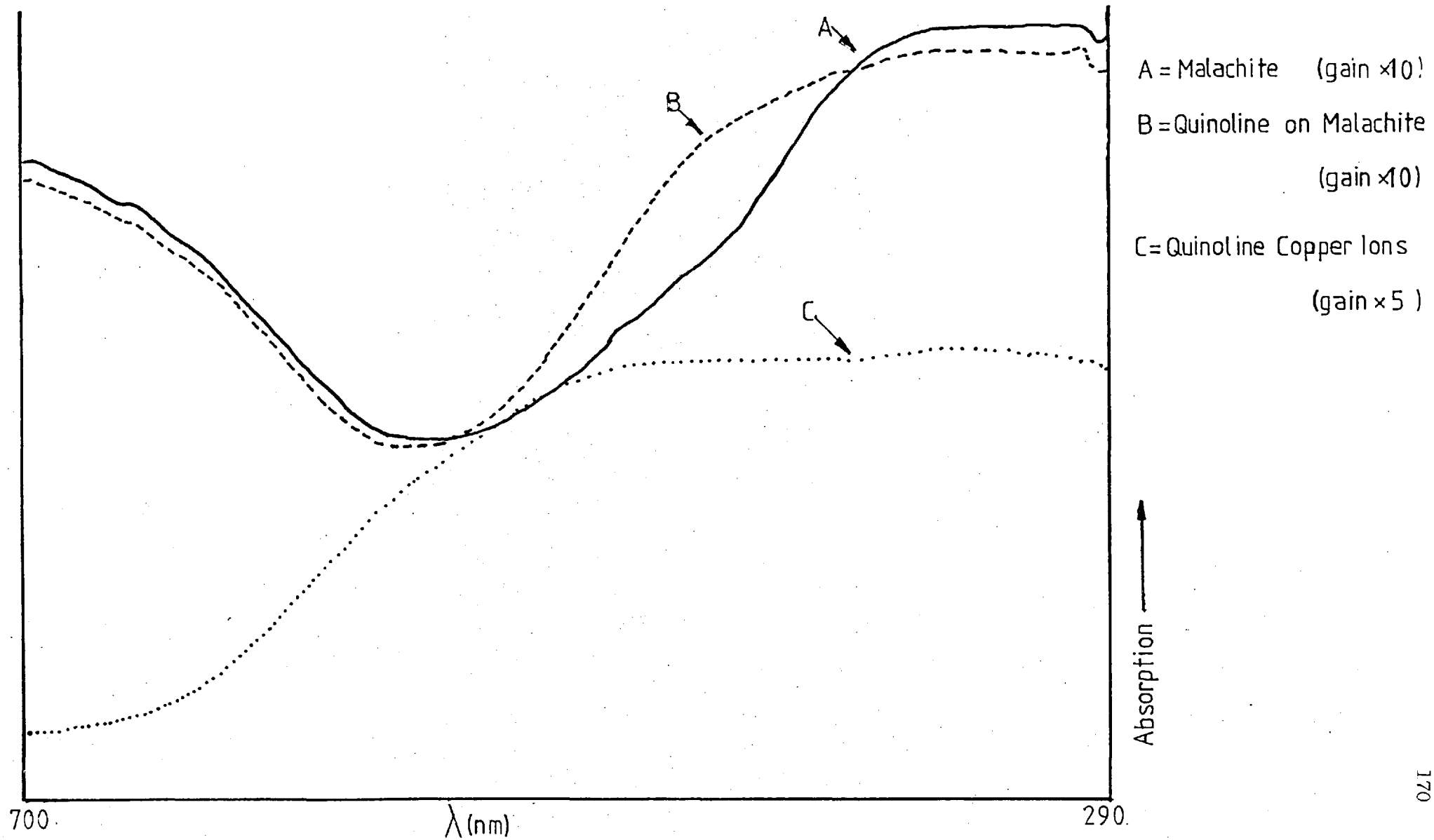

Fig.6.3. OAS UV-Vis Spectra

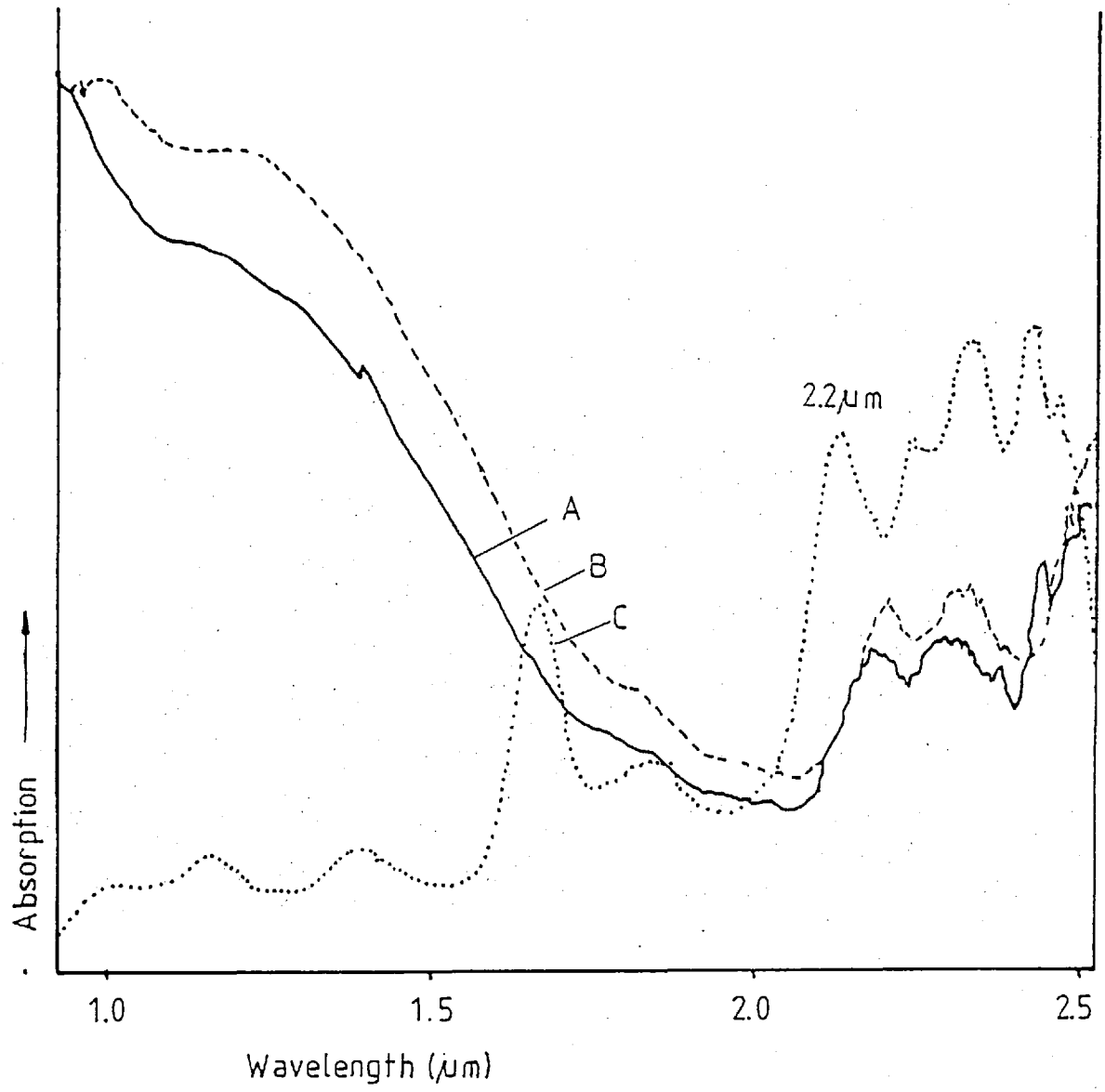

Fig. 6.4. OAS Near-IR Spectra of

A - Malachite (gain ×1)

B - Quinoline on Malachite (gain ×1)

C - Quinoline Copper Ions (gain ×2)

phthalocyanine dye works quality, (2) WED/C/9724 copper phthalocyanine dye obtained from another source, (3) WED/C/9725 copper phthalocyanine dyes obtained from a third source, (4) WED/G/9726 Monastral Green GN-Chlorinated copper phthalocyanine, (5) WED/G/9727 halogenated copper phthalocyanine derived from 9725 and (6) WED/C/9729 Monastral Green 6Y standard chlorinated and brominated copper phthalocyanine.

The aim of this experiment was to get some information from the UV-visible spectra and thereby to probe further into the possible application of optoacoustic spectroscopy to dye characterisation in colour matching and colour comparison.

In the case of copper phthalocyanine pigments the samples were examined to assess their quality and to find significant differences if any through UV-visible spectra of the samples. Copper phthalocyanine dyes are used in printing inks, also in lacquers, emulsion paints, distempers, rubber plastics, leather cloth and paper. The structural formula of a typical phthalocyanine dye is shown below [159]:

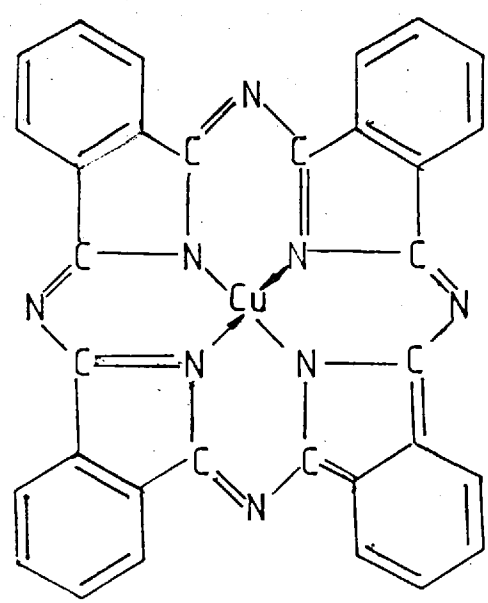

Phthalocyanine.

Experimental

The instrument employed for this investigation in the UV-visible region was the double beam instrument described in Chapter Two operated with the 300 watt xenon arc source. The scan rate used was 50 nm min^{-1} with a monochromator bandwidth of 10nm, modulation frequency of 28Hz and a time-constant of 3 seconds.

Results and Discussion

The spectra of dyes are shown in Figures 6.5 and 6.6. Although the absorption maxima of all the yellow dyes (1) to (4) were at ca 480 nm each one had its own characteristic difference in the shape of the absorption bands. Sample (5) the blue azoic dye, was found to absorb mainly in the visible region towards 700 nm.

Spectra of normal quality copper pthalocyanine (sample 1) and of poor quality halogenated copper phthalocyanine (sample 2) are shown in Figure 6.7. The UV-visible spectra of copper phthalocyanine dyes were not well resolved because of signal saturation effects and all the spectra looked alike. Fuchsman and Silversmith [160] have recently reported that these signal saturations can be avoided by grinding with alumina.

6.2.4 Miscellaneous

Copper carbonate ageing experiment

Copper carbonate has been used as a fungicide for the control of plant diseases and as a catalyst in an admixture with metal carbonate in the hydrogenation of fatty oils and as a catalyst in the oxidation of naphthalene

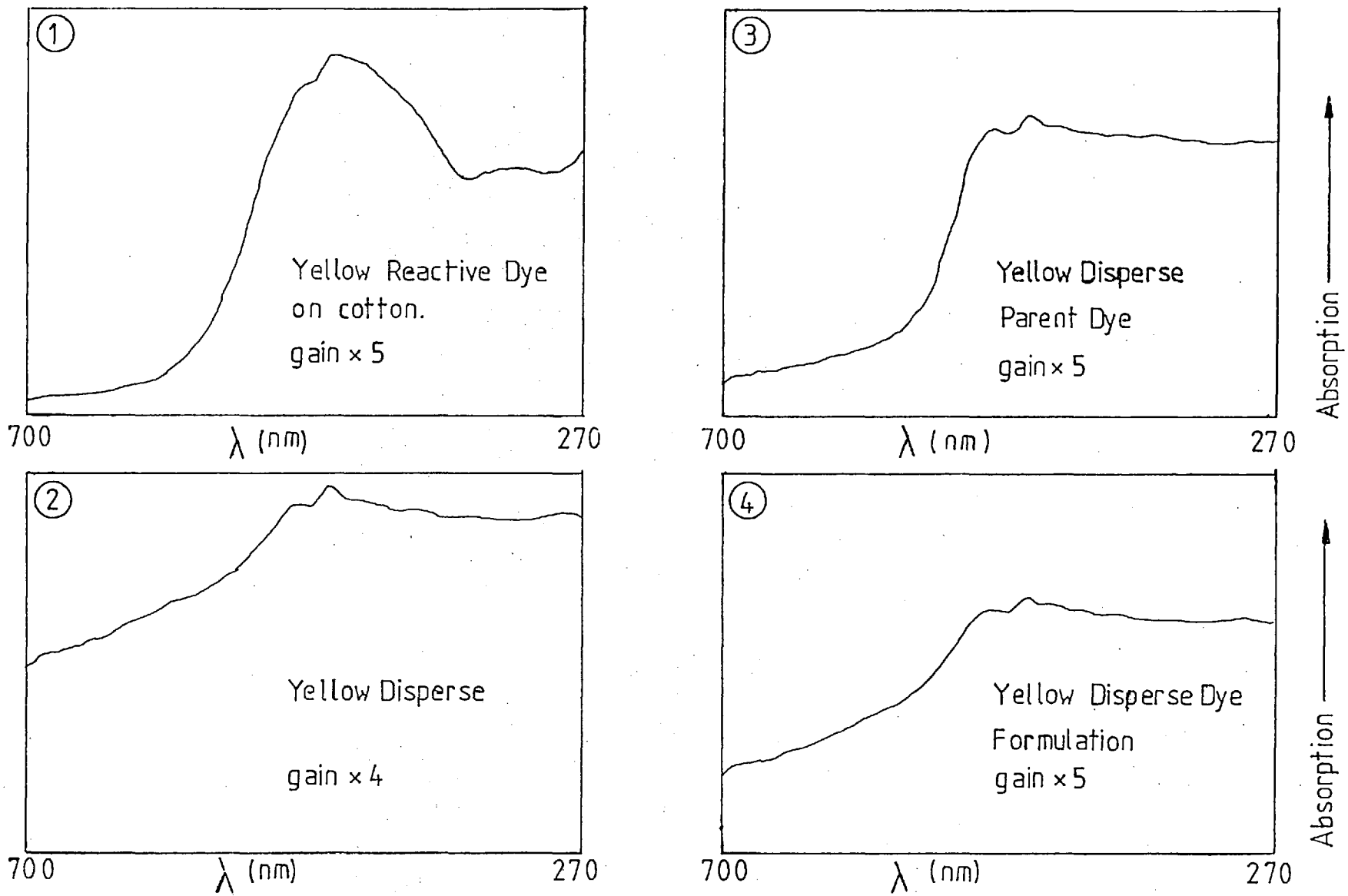

Fig.6.5. OAS UV-Vis spectra of yellow dyes.

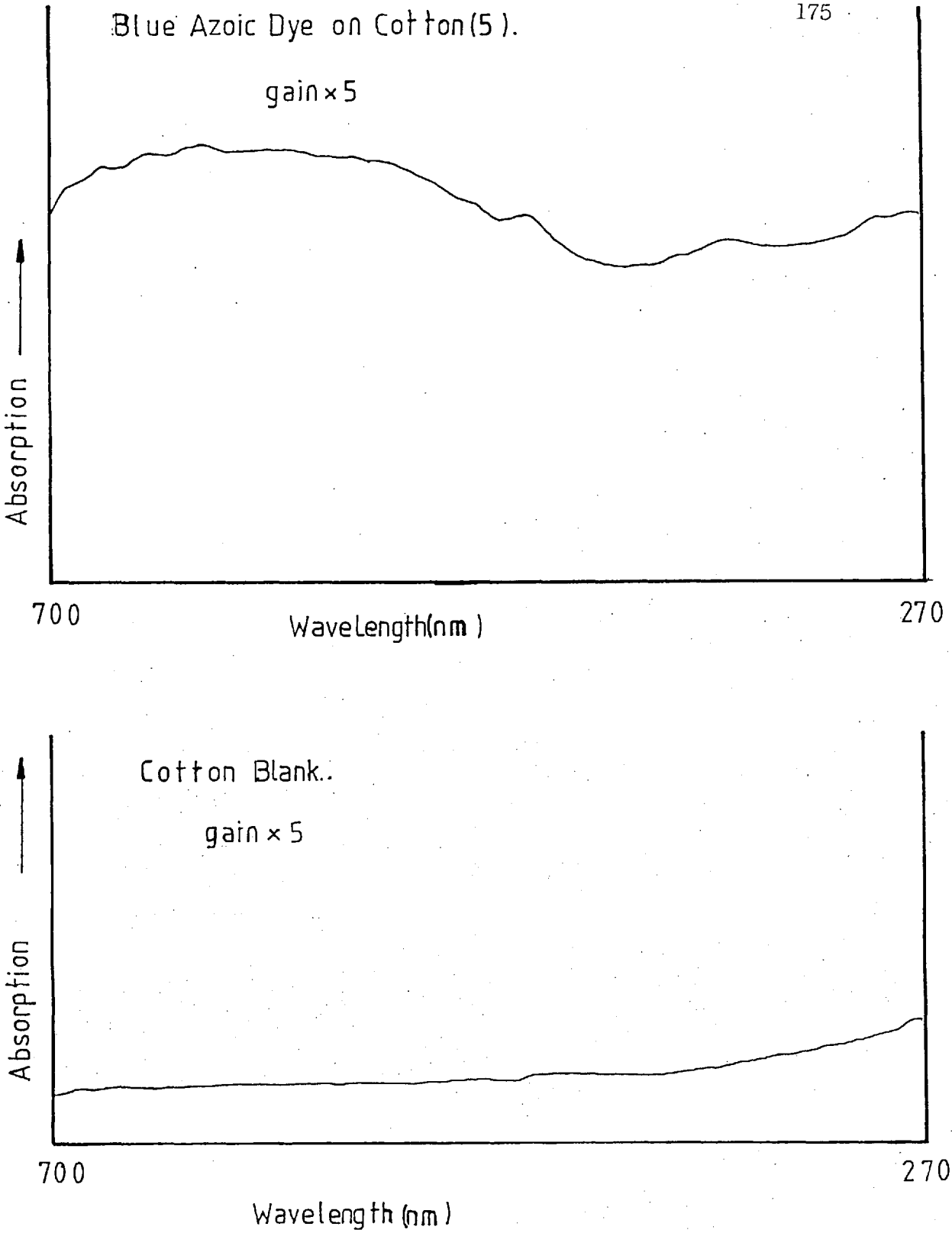

Figs.6.6. OAS UV-Vis spectra of a blue azoic dye(5).

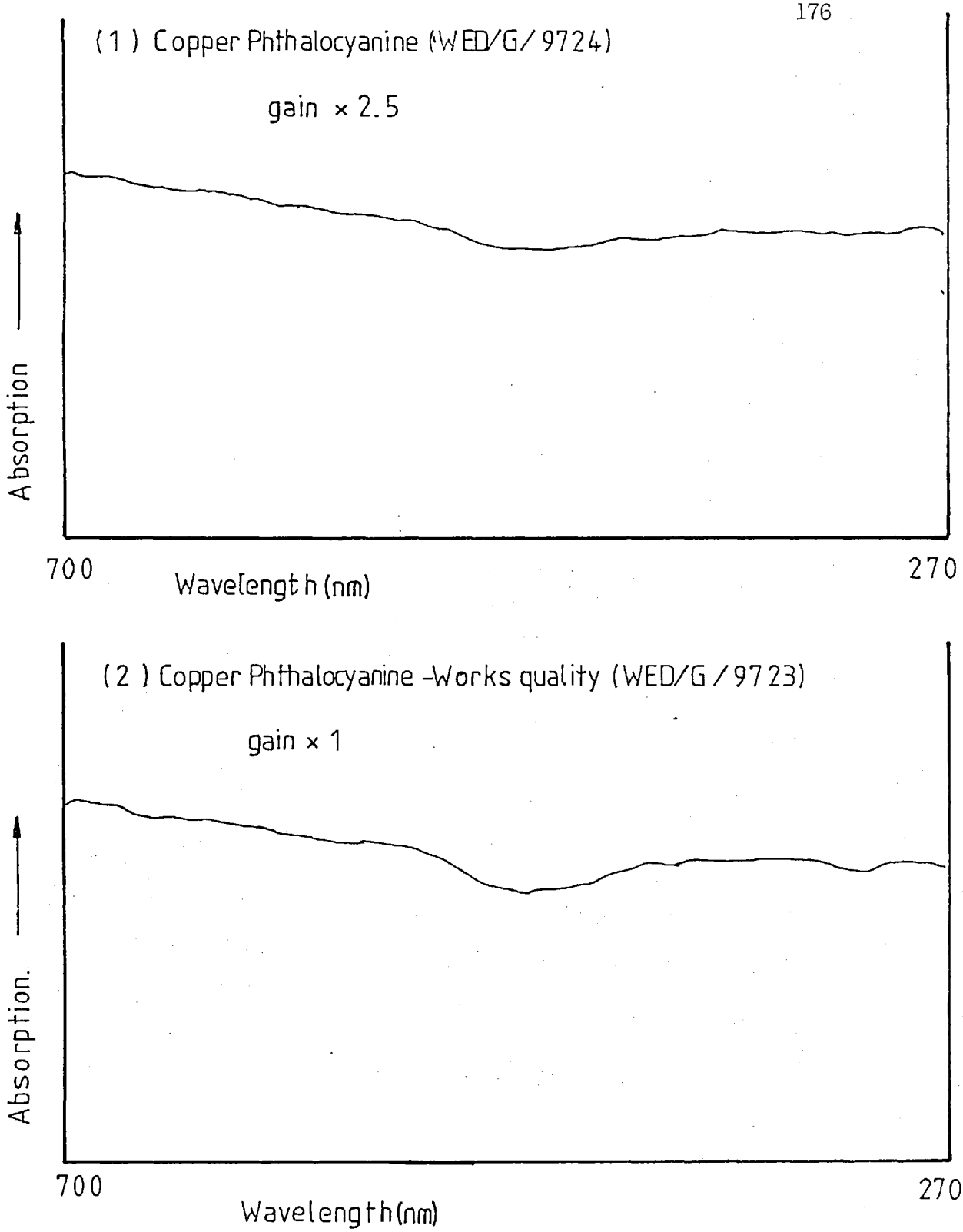

Figs.6.7. OAS UV-Vis Spectra of Phthalocyanine Dyes.

derivatives [161].

The aim of this experiment was to observe the transformation change from a blue gelatinous precipitate to green malachite when copper nitrate and sodium carbonate are mixed together at a particular molar ratio (1.5:1) at ca 65°C by scanning the UV-visible spectrum.

It was thought at first that it would be possible to monitor the changes which occur during ageing processes, but the optoacoustic signal obtained from an aqueous slurry was too heavily damped out by the water present. An attempt to avoid these effects was made by spreading the precipitate over anhydrous alumina and scanning the spectrum. Although alumina absorbed some of the water, there was still signal dampening and no meaningful spectrum was obtained. Centrifugation of the sample was also investigated. A poor spectrum was also obtained with the centrifuge precipitate. Drying the sample was the only effective means of getting an OAS signal, but this was incompatible with the objective of the experiment.

6.3 Conclusion:

The samples examined in this chapter were part of a general evaluation for ICI of the possible industrial applications of optoacoustic spectrometry. The results of the experiments investigating tin/antimony oxide catalysts appears promising and the experiments have to be repeated with sieved samples. The concentration of quinoline in the quinoline malachite sample and quinoline spectra are essential for any meaningful comment.

With regard to the dyes and dye formulations, although good spectra were obtained a number of comparative examinations of the original dyes and related samples would be essential for any useful assessment of possible applications.

CHAPTER SEVEN

CONCLUSIONS AND SUGGESTIONS FOR FUTURE WORK

From the studies made of samples of laser mirrors it has been shown that optoacoustic spectroscopy offers several distinct advantages over conventional calorimetric techniques for the measurement of the absorption coefficient. As the change in the temperature of the sample is monitored indirectly the problem of maintaining efficient transducer contact with the sample is eliminated. As a calorimetric technique optoacoustic spectroscopy has also been employed previously in the study of luminescence quantum efficiencies[32].

A particular advantage of optoacoustic spectroscopy compared with other spectroscopic techniques is the ability to provide information about the thermal characteristics of the sample as well as the radiative absorption occurring.

The studies made of photochromic substances have shown that measurement made using optoacoustic spectroscopy are relatively free from interferences caused by scattered light. With other complementary techniques radiation scattering has been shown to result in a relatively poor signal-to-noise ratio being obtained.

The studies made of polymer film samples have demonstrated experimentally the optoacoustic theory of Rosencwaig and Gersho applied to the special cases of optically opaque, thermally thin and optically opaque, thermally thick samples.

For quantitative studies of powdered samples, particle size plays an important role in determining the magnitude of the optoacoustic signal. In the complementary technique of diffuse reflectance the particle size is an even more

critical parameter in determining the signal magnitude. From the studies made of carbon black and dark blue cobalt glass it has been observed that there is a greater opto-acoustic signal and presumably increased thermal transfer efficiency at the sample/gas interface with finer particle size. The role of specular reflectance in determining the magnitude of the optoacoustic signal is also important. The magnitude of the specular refelctance occurring would be expected to increase as the particle size is decreased; an effect also observed in diffuse reflectance spectroscopy. However, it appears that the change in the efficiency of thermal transference is a more important parameter in determining the magnitude of the optoacoustic signal than is the change in the amount of specular reflectance occurring.

Studies of moisture in Pruteen and polyvinyl acetate in the vinyl chloride/vinyl acetate copolymer have demonstrated that optoacoustic spectroscopy is a better technique compared with some other competing spectroscopic technique in terms of the ability to produce a well resolved spectrum. Although NMR is independent of particle size effects, the method investigated is successful only when the moisture has to be determined at concentration greater than 6%. Also the elimination of any other hydrogen containing liquids present is vital in order to ensure that only the water is detected. The results of studies made using diffuse reflectance spectroscopy for the determination of polyvinyl acetate in vinylacetate/vinyl chloride copolymer have exhibited relatively poor signal-to-noise ratio compared with the results obtained using optoacoustic spectroscopy.

The results obtained for the determination of water in Pruteen and of polyvinylacetate in vinyl chloride/vinyl acetate copolymer have demonstrated for the first time that optoacoustic spectroscopy is capable of being used in quantitative applications as well as for qualitative analysis in the near-infrared region of the spectrum.

The design of the sample cell is a very important parameter in the design of any optoacoustic spectrometer. Some criteria governing the design of the cell has been discussed in Chapter Two of this thesis. Presently many of the limitations of optoacoustic spectroscopy are due to the attainment of poor signal-to-noise ratios in the cell. It appears that an improved signal-to-noise ratio can be obtained by incorporating the microphone preamplifier within the cell. The type of microphone transducer used in this work appears to be the most satisfactory for use with a wide variety of sample types. However, several workers [68,69] have described the use of piezoelectric transducer for making measurements of liquid samples. Such piezoelectric transducers could be usefully employed, for example, in the studies of phase transformation in the ageing of copper carbonate mentioned in Chapter Six.

With improvements in the instrumentation, especially in the design of the cell, studies of the mechanism involved in the colour change of photochromic substances such as salicylidene-2-chloroaniline should be possible. The study of phototransformations of phytochrome [162] is another possible area of research. Phytochrome is the photoreversible chromoprotein that controls many aspects of plant growth.

Little information is currently available which describes the effect of changes in the particle size of the sample upon the magnitude of the optoacoustic signal. This is an area which may be usefully investigated to establish the requirements for quantitative analysis.

Quantitative studies of milk fat by near-infrared OAS is a promising application that may be investigated.

Optoacoustic spectroscopy is a very promising technique and should find many useful applications especially for solid samples which are diffcult to examine using alternative techniques.

REFERENCES

1. Ewing, G.W., Instrumental Methods of Analysis, 4th Edition, McGraw-Hill Kogakusha Ltd, London, (1975).

2. Newton, Sir Isaac, Optiks, Dover Publication Inc., New York (1952), Reprint of 4th edition of 1730.

3. Kirchhoff, G., Philosophical Magazine, 20, (1860), 1.

4. Kirchhoff, G., and Bunsen, R., Philosophical Magazine, 20, (1860), 89.

5. Kirchhoff, G. and Bunsen, R., Philosophical Magazine, 22, (1861), 329.

6. Thorne, A.P., Spectrophysics, Chapman & Hall, London, (1974).

7. Cheng, K.L. and PratherII, J.W. "Ultraviolet and Visible Spectroscopy", in Instrumental Analysis (ed. Bauer, H.H., Christian, G.D. and O'Reilly, J.E.), Allyn and Bacon, London (1978).

8. Skoog, D.A. and West S.D., Fundamentals of Analytical Chemistry, 3rd Edition, Holt, Rineheart and Winston, New York, (1976).

9. Willard, H.H., Merritt, L.L. and Dean, J.A., Instrumental Methods of Analysis 5th Edition, D. Van Nostrand, London (1974).

10. Fahrenfort, Spectrochem. Acta., 17, (1961), 698.

11. Wendlandt, W.W. and Hect, H.G., Reflectance Spectroscopy, Interscience, London, (1966).

12. Taylor, A.H., J. Optical Soc. Am., 4, (1920), 9.

13. Benford, F., Gen. Elec. Rev., 23, (1920), 72.

14. Frei, R.W. and MacNeil, J.D., Diffuse Reflectance Spectroscopy in Environmental Problem Solving, C.R.C. Press, Ohio, (1973).

15. Kortüm, G., Reflectance Spectroscopy - Principle Methods and Applications, Springer-Verlag, New York, (1969).

16. Beckmann Instrumental Manual (1220A), Beckmann Instruments, Inc., Fullerton, California, (1963).

17. Schenk, G.H., "Molecular Fluorescence and Phosphorescence" in Instrumental Analysis (Ed. Bauer, H.H., Christian, G.D. and O'Reilly, J.E.). Allyn and Bacon, London (1978).

18. Parker, C.A. Photoluminescence of Solutions with Applications to Photochemistry and Analytical Chemistry, Ellsevier, London, (1968).

19. Becker, R.S., Theory and Interpretations of Fluorescence and Phosphorescence, Wiley-Interscience, London, (1969).

20. Cowan, D.O. and Drisko, R.L., Elements of Organic Photochemistry, Plenum Press, London (1976).

21. Cundall, R.B. and Gilbert, A., Photochemistry, Nelson,London (1970).

22. Wells, C.H.J., Introduction to Molecular Photochemistry, Chapman & Hall, London, (1972).

23. Brown, G.H., Technique of Chemistry, Volume III, Photochromism, Wiley-Interscience, London, (1971).

24. Callis, B.J., J. Res. Nat. Bur. Standards (US) 80A, (3),(Phys. and Chem), (May-June 1976), 413.

25. Gelernt, B., Findeisen, A., Stein, A. and Poole, A.J., J. Chem. Soc., Faraday Trans. II, (1974), 939.

26. Demas, J.N. and Crosby, G.A., J. Phys. Chem., 75, (1971), 991.

27. Crosby, G.A., Demas, J.A., and Callis, J.B., J. Res. Nat. Bur. Standards (US), 76A, (6), (Phys. and Chem.) (Nov-Dec. 1972), 561.

28. Callis, J.B., Gouterman, M. and Danielson, J.D.S., Rev. Sci. Inst. 40 (12) (1969), 1599.

29. Adams, M.J., King, A.A. and Kirkbright, G.F., Analyst, 101, (1976), 73.

30. Rosencwaig, A. and Gersho, A, J. Appl. Phys., 47, (1976), 64.

31. Lahmann, W. and Ludwig, H.J., Chem. Phys. Lett., 45, (1977), 177.

32. Adams, M.J., Highfield, J.G. and Kirkbright, G.F., Anal. Chem., 49, (1977), 1850.

33. Bell, A.J., Proc. Amer. Assoc. Adv. Sci., 29, (1880), 115.

34. Röntgen, W.C., Phil. Mag. 11, (5), (1881), 308.

35. Tyndall, J., Proc. Roy. Soc. (London) 31, (1881), 307.

36. Bell, A.J., Phil. Mag, 11(5), (1881), 510.

37. Rayleigh Lord, Nature (London), 23, (1881), 274.

38. Mercadier, M.E. Phil. Mag, 11(5), (1881), 78.

39. Preece, W.H., Proc. Roy. Soc.(London), 31, (1881), 506.

40. Veingerov, M.L., Doklady Akad. Nauk, USSR, 19, (1938), 687.

41. Pfund, A.H., Science, 90, (1939), 326.

42. Luft, K.F., Zeit, Techn. Phys., 24, (1943), 97.

43. Veingerov, M.L., Doklady. Akad. Nauk. USSR, 46, (1945), 182.

44. Gorelik, G., Doklady, Akad. Nauk. USSR, 54, (1946), 779.

45. Read, A.W., Adv. in Mol. Relaxation Processes, 1, (1967), 257.

46. Cottrel, T.L., Macfarlane, I.M., Read, A.W., and Young, A.H., Trans. Faraday Soc., 62, (1966), 2655.

47. Kerr, E.L. and Atwood, J.G., Appl. Opt., 7, (1968), 1915.

48. Kreuzer, L.B., J. Appl. Phys., 42, (1971), 2934.

49. Kreuzer, L.B., and Patel, C.K.N., Science, 173, (1971), 45.

50. Kreuzer, L.B., Kenyon, N.D. and Patel, C.K.N., Science, 177, (1972), 347.

51. Dewey, C.F., Jr., Kamm, R.D. and Hackett, C.E. Appl. Phys. Lett., 23, (1973), 1633.

52. Claspy, P.C., Pao, Y.H., Kwong, S., and Nodov, E., Appl. Opt., 15, (1976), 1506.

53. Hayes, H.V., Rev. Sci. Instrum., 7, (1936), 202.

54. Golay, M.J.E., Rev. Sci. Instrum., 18, (1947), 347.

55. Golay, M.J.E., Rev. Sci. Instrum., 18, (1947), 357.

56. Weber, P.F., Optik, (1950), 152.

57. Luchin, S.M., Zhur. Tech. Fez., 16, (1946), 1115.

58. Terenin, A.N. and Yaroslavkie, N.G. IZVEST. Ak. Nauk. SSSR, 9, (1945), 203.

59. Golay, M.J.E., Rev. Sci. Instrum., 20, (1949), 816.

60. Houghton, A.V. and Acton, R.V., AIAA, 2, (1964), 120

61. Parker, J.G., Appl. Opt., 12, (1973), 2974.

62. Kerr, E.L., Appl. Opt., 12, (1973), 2520.

63. Harshbarger, W.R. and Robin, M.B., Acc. Chem. Res., 6, (1973), 329.

64. Rosencwaig,A., Opt. Commun., 7, (1973), 305.

65. Rosencwaig, A., Science, 181, (1975), 657.

66. Rosencwaig, A. and Hall, S.S., Anal. Chem., 47, (1975), 548.

67. McClelland, J.F. and Kniseley, R.N., Appl. Optics, 15, (1976), 2658, and 15, (1976), 2967.

68. Lahmann, W., Ludewig, H.J. and Welling, H., Anal. Chem., 49, (1977), 549.

69. Tam, A.C., Patel, C.K.N. and Kerl, R.J., Opt. Lett. 4, (3), (1979), 81.

70. Patel, C.K.N. and Tam, A.C., Appl. Phys. Letters, 34, (1979), 467.

71. Adams, M.J. and Kirkbright, G.F., European Spectroscopy News, 14, (1977), 22.

72. Adams, M.J. and Kirkbright, G.F., Analyst, 102, (1977), 281.

73. Kaiser, R., Can. J. Phys, 37, (1959), 1499.

74. Rosengreen, L.G., Infrared Phys., 13, (1973), 109.

75. Aamodt, L.C., Murphy, J.C., and Parker, J.G., J. Appl. Phys., 48, (1977), 927.

76. Aamodt, L.C. and Murphy, J.C., J. Appl. Phys, 49, (1978), 3036.

77. Bennet, H.S. and Forman, R.A., Appl. Opt., 15, (1976), 347.

78. Bennet, H.S. and Forman, R.A., Appl. Opt., 15, (1976), 2405.

79. Bennet, H.S. and Forman, R.A., Appl. Opt., 16, (1977), 2834.

80. Bennet, H.S. and Forman, R.A., J. Appl. Phys., 48, (1977), 1432.

81. Rosencwaig, A. and Gersho, A., Science, 190, (1975), 556.

82. Monahan, E.M. and Nolle, A.W., J. Appl. Phys., 48, (1977), 3519.

83. Melamid, N.T., J. Appl. Phys., 34, (1963), 560.

84. Afromowitz, M.A., Yeh, P. and Yee, S.J., J. Appl. Phys., 48, (1977), 209.

85. Wetsel, G.C. and McDonald, F.A., Appl. Phys.Lett., 30, (1977), 2521.

86. McClelland, J.F. and Knisely, R.N., Appl. Phys. Lett., 28, (1976), 467.

87. McClelland, J.F. and Knisely, R.N., Appl. Optics, 15, (1976), 2658.

88. Gelbwachs, J.A., 'Tunable Radiation Sources in the Ultraviolet and Visible Spectral Regions' in Optoacoustic Spectroscopy and Detection. (ed. Pao, Y.H.) Academic Press, London, (1977).

89. Cann, M.W.P., Appl. Opt., 8, (1969), 1645.

90. Baum, W.A. and Dunkelman, L., J. Opt. Soc. Am., 40, (1950), 782.

91. Anderson, W.T., J. Opt. Soc. Am., 41, (1951), 385.

92. Brewer, R.G. and Mooradian, A. (eds) 'Laser Spectroscopy', Plenum, New York (1974).

93. Schäfer, F.P., "Principles of Dye Laser Operation", in Topics in Applied Phys., Vol. I, Springer-Verlag, (1973).

94. Bradley, E.G., (ed. Bauer, H.H., Christian, G.D., and O'Reilly, J.E.) Allyn and Bacon, London, (1978).

95. Rosencwaig, A., "Solid State Photoacoustic Spectroscopy" in Optoacoustic Spectroscopy and Detection, (Ed. Pao, Y.H), Academic Press, London (1977).

96. Claspy, P.C. "Infrared optoacoustic spectroscopy and detection" in Optoacoustic Spectroscopy and Detection (ed. Pao, Y.H.), Academic Press, London (1977).

97. Brüel Kjaer, Instruction Manual 4166, Microphone Cartridge, (1971).

98. Malmstadt, H.V., Enke, C.G., Crouch, S.R. and Horlick, G., Electronic Measurement for Scientists, Benjamin, W.A. Inc., London (1973).

99. Adams, M.J. Beadle, B.C., King, A.A., and Kirkbright, G.F., Analyst, 101, (1976), 553.

100. Beadle, B.C., Ph.D. Thesis, University of London, (1978).

101. Adams, M.J. Beadle, B.C., and Kirkbright, G.F., Anal. Chem., 50,(9), (1978), 1371.

102. Adams, M.J., Beadle, B.C. and Kirkbright, G.F., Analyst, 102, (1977), 569.

103. Marckwald, W., Z. Phys. Chem., (Leipzig), 30, (1899), 140.

104. Livingston, R. "Behaviour of Photochromic System", in Techniques of Chemistry, Vol. III, Photochromism (ed. by Brown, G.H.) Wiley-Interscience, London, (1971).

105. Termeer, E., Ann. Chem., 181, (1876), 1.

106. Phipson, T.L., Chem. News, 43, (1881), 283.

107. Bertelson, R.C. "Photochromic process involving heterolytic cleavage" in Techniques of Chemistry, Vol. III, Photochromism (ed. by Brown G.H.) Wiley-Interscience, London, (1971).

108. Eigemann, G."Photochromic process by homolytic cleavage"in Techniques of Chemistry, Vol. III, Photochromism (ed. by Brown, G.H.) Wiley-Interscience, London, (1971).

109. Ross, D.L. and Blank, J., "Photochromism by cis-trans isomerization" in Techniques of Chemistry, Vol. III, Photochromism, (ed. by Brown, G.H.) Wiley-Interscience, London, (1971).

110. Margerum, J.D. and Miller, L.J.,"Photochromic process by Tautomerism" in Techniques of Chemistry, Vol. III, Photochromism (ed. by Brown, G.H.) Wiley-Interscience, London (1971).

111. Deb, S.K. and Forrestal, L.J. "Photochromism in inorganic systems" in Techniques of Chemistry, Vol. III, Photochromism, (Ed. by Brown, G.H.), Wiley-Interscience, London, (1971).

112. Cohen, M.D. and Schmidt, G.M.J., J. Phys. Chem., 66, (1962), 2442.

113. Dessauer, R. and Paris, J.P. Advances in Photochemistry, Vol. I, (ed. by Albert, W., Noyles, J.R. Hammond, G.S. and Petts, Jr, J.N.) Interscience, London, (1963), 275.

114. Cohen, M.D., Hershberg, Y., and Schmidt, G.M.J., J. Chem. Soc., (1964), 2051.

115. Cohen, M.D., Schmidt, G.M.J., and Flavin, S., J. Chem. Soc., (1964), 2041.

116. Becker, R.S. and Richey, W.F., J. Amer. Chem. Soc., 89, (1967), 1298.

117. Ottolenghi, M. and McClure, D.S., J. Chem. Phys., 46, (1967), 4613, 4620.

118. West, W. and Saunders, V.I., J. Phys. Chem., 63, (1959), 45.

119. Nail, N.R., Moser, F., Goddard, P.E. and Urbach, F., Phys. Rev., 98, (1955), 1557.

120. Moser, F., Nail, N.R. and Urbach, F., Phys. and Chem. Solids, 3, (1957), 153.

121. Armistead, W.H. and Stookey, S.D,Science, 144, (1964), 150.

122. Malkin, S. and Cohen, D., Photochem., and Photobiology, 29, (1979), 803.

123. Chance-Pilkington,, "Reactolite Rapide", Technical Information, Note. R.1. (1977).

124. Rosencwaig, A., Anal. Chem., 47(6), (1975), 592A.

125. Adams, M.J. and Kirkbright, G.F., Analyst, 102, (1977), 678.

126. Hordvik, A. and Skolnik, L., Appl. Opt., 16, (1977), 2919.

127. Touloukian, L.R., Powell, R.W., Ho, C.Y., and Nicolasu, M.C., Thermal Diffusivity, IFI/Plenum, New York,(1973) .

128. Whetsel, K.B. "Near-infrared spectrometry" in Applied Spectroscopy Reviews, Vol.II, (Ed. Brame, E.G.), Marcel Dekker, New York, (1969).

129. Herschel, W., Phil. Trans., 90, (1800), 225.

130 Abney, W.and Festing, E.R., Phil. Trans. 172, (1881), 887.

131. Bracket, F.S., Proc. Natl. Acad. Sci., U.S.; 14, (1928), 857.

132. Kaye, W., Spectrochem. Acta, 6, (1954), 257.

133. Wheeler, O.H., Chem. Rev., 59, (1959), 629.

134. Goddu, R.F., Adv. Anal. Chem. Inst., 1, (1960), 347.

135. Goulder, J.D.S., Chem. and Ind., (1957), 142.

136. Goddu, R.F. and Delker, D.A., Anal. Chem., 32, (1), (1960), 140.

137. Holman, R.T. and Edmondson, P.R., Anal. Chem., 28, (1956), 1533.

138. Haslam, J., Willis, H.A., and Squirrell, D.C.M., Identification and Analysis of Plastics, Second Edition, Butterworth, London, (1972).

139. Ahmed, W. and Goldstein, M., Lab. Practice, 25, (1976), 385.

140. Law D.P, and Tkachuk, R., Cereal Chem., 54(4), (1977), 874.

141. The Statutory Instruments, No. 840, The Fertilisers and Feeding Stuffs, (Amendment) Regulations, Her Majesty's Stationary Office, London, (1976).

142. Pearson, D. The Chemical Analysis of Foods,6th Edition, J&A Churchill, London (1970).

143. Mitchell, J.J. and Smith, D.M., Aquametry, Part I, 2nd Edition, John Wiley Sons, London (1977).

144. Mansfield, P.B. and Horn, C.A., J. Fd. Technol., 7, (1972), 53.

145. Kern, P., Sieber, R. and Rust, P. "Analysis of Fat and Water Content of Cheese", Swiss Dairy Research Station, CH-3097, Liebefeld-Berne, (1974).

146. Moisture in Grain, Flour, Dough, and Finished Cereal Products - Special Application Report, New Port Instruments Ltd, Blakeland North, Milton Keynes, MK14 5AW (1970).

147. CRC Handbook of Physics and Chemistry, 58th Edition, (1977-78), E-46.

148. Hunt, G.R. and Salisbury, J.W., Modern Geology, 1, (1970), 283.

149 Hunt, G.R., and Salisbury, J.W., Mod. Geol., 2, (1971), 22.

150. Hunt, G.R., Salisbury, J.W. and Lenhoff, C.J., Mod. Geol., 2, (1971), 195.

151. Hunt, G.R., Salisbury, J.W. and Lenhoff, C.J., Mod. Geol., 3, (1971), 1.

152. Hunt, G.R., Salisbury, J.W. and Lenhoff, C.J., Mod. Geol., 4, (1973), 217.

153. Harper, W.M., Statistics , 2nd Edition, Macdonald and Evans, Estover, Plymouth, (1976).

154. Jackman, L.M., and Sternhill,S., Applications of NMR Spectroscopy in Organic Chemistry, 2nd Edition, Pergamon Press, Oxford, (1969).

155. User Handbook - New Port Analysis, MK IIIA, New Port Instruments Ltd., Blakelands North, Milton Keynes, MK14 5AW (1978).

156. Encyclopaedia of PVC (edited by Nass, L.I.) Marcel Dekker Inc., New York, (1976).

157. Private Communication from Dr Becconsall, J.K; Corporate Laboratory, ICI Limited, Runcorn, Cheshire.

158. Cross, Y.M. and Pyke, D.R. Journal of Catalysts, 58, (1979), 61.

159. Allen, R.L.M., Colour Chemistry , Nelson, London, (1971).

160. Fuchsman, W.H. and Silver Smith, A.J., Anal. Chem., 51(4), (1979), 589.

161. Hsu, C.T., J. Appl. Chem., 6, (1956), 84.

162. Kendrick, R.E. and Sprutt, C.J.P., Photochemistry and Photobiology, 26, (1977), 201.

LIST OF PUBLICATIONS

1. Adams, M.J., Beadle, B.C., Kirkbright, G.F. and Menon, K.R. 'Optoacoustic Spectrometry of Surfaces: Dielectric coatings for Laser Mirrors'
APPLIED SPECTROSCOPY, 32, (1978), 430.

2. Adams, M.J., Kirkbright, G.F. and Menon, K.R., 'Effect of sample thickness on the magnitude of optoacoustic signals'.
ANALYTICAL CHEMISTRY, 51,(4),(1979), 508.

3. Castleden, S.L., Kirkbright, G.F. and Menon, K.R., 'Quantitative Determination of Moisture in Single-cell Protein utilizing Photoacoustic Spectroscopy in the Near-Infrared Region'. (In Press).